In situ Surface Analysis of Novel Marine Foul-Release Coatings

Stephen Kenny MSc

Thesis submitted to the University of Nottingham
for the degree of Doctor of Philosophy

January 2017

Abstract

Exposure of artificial surfaces such as ship hulls to a marine environment leads to the attachment of assorted biomolecules, single celled organisms and marine invertebrates such as barnacles or mussels. Together, they form a structure known as a biofilm. These films lead to higher fuel consumption and add considerable expense to the operation of ships used by industrial and naval organisations. The work presented in this thesis describes the surface analysis of a novel poly(dimethylsiloxane) (PDMS) based foul-release coating. The coating also contains poly(ethylene glycol) groups (PEG). The differing chemical properties between these two domains led to an observed surface modification effect in water, whereby contact angle measurements decreased from ~110^{o} to ~65^{o} over a period of five minutes. This effect was rapidly reversible on drying. Time of Flight-Secondary Ion Mass Spectrometry cryogenic depth profiling experiments confirmed this change in surface chemistry where the frozen surface of the coating was shown to have a higher intensity of ions associated with PEG groups at the surface compared to that in the bulk. Water immersion also led to a swelling of the surface seen by a change in the surface topography by Atomic Force Microscopy investigations.

When applied to glass surfaces the coatings were flat and generally defect free regardless of the application method used. On exposure to *Pseudomonas aeruginosa* the coatings were found to be ten times more effective at preventing bacterial adhesion in the first instance than a PDMS standard. The mechanism of action was shown to be non-toxic by live/dead staining and did not appear to affect the way in which bacteria move on a surface. A flow adhesion assay demonstrated that a flow rate of almost two orders of magnitude lower was required to remove fifty percent of bacteria from a coated surface than on a glass standard, demonstrating the foul-release ability of the switching coating.

Sea trials in a French coastal region highlighted the importance of exposing candidate coatings to a true marine environment for a suitable duration in order

to determine their potential for use. Ultimately we show that the coating presented is a candidate for use as an effective coating for preventing marine biofouling and surface analysis was deemed to be an appropriate methodology to analyse coatings that have changing properties on exposure to water.

Acknowledgements

A body of work of this size cannot and should not be undertaken alone, collaboration is essential to the very nature of curious inquiry. Firstly, I would like to thank my supervisors Professor Clive Roberts, Professor Stephanie Allen and Professor Morgan Alexander for their diligence and patience. Their varied expertise has been invaluable and I feel privileged to have had access to such world-leading scientists.

The technical assistance from Dr Andrew Hook, Dr David Scurr, Dr Emily Smith, Dr Chris Parmenter and Professor Xinyong Chen has made my progression through this project easier and aided me in becoming a more skilled scientist. From the industrial end at Dow Corning David Pierre and Stuart Leadley must be thanked for their willingness to help with anything I might need and answer all my questions no matter how minor. Axl Rosenhahn and Kim Nolte from Ruhr-Universität Bochum have also been very generous with their time and effort on the sea trials.

My work was generously funded by the University of Nottingham, the Biotechnology and Biological Sciences Research Council and Dow Corning.

The group formerly known as the LBSA has made my time in Nottingham a delight, providing much more than scientific assistance and I would particularly like to thank Michael Taylor for his contribution to the depth profiles and Alessandro Carabelli for the bacterial adhesion assays.

For providing support and clarity throughout the last four years I send love to my parents and extended family as a whole, your encouragement has been unwavering. For variety and unparalleled enjoyment I would like to thank everyone at the university magazine, orchestra, radio station and tennis team.

Finally, this is to all those past and present in D20 who remind me every day it is more than an office, it is a way of life.

Table of Contents

Table of Figures

List of Tables

List of Abbreviations

The following abbreviations are used within this thesis

900c	Phosphorus-based cross-linking catalyst
AFM	Atomic Force Microscopy
AHL	*N*-Acyl Homoserine Lactone
ASW	Artificial Sea Water
BSA	Bovine Serum Albumin
DIC	Differential Interference Microscopy
DMT	Derjaagin, Muller and Toropov model
DNA	Deoxyribonucleic Acid
DOPA	Dihydroxyphenylalanine
HBFP	Hyperbranched Fluoropolymer
ICP MS	Inductively Coupled Plasma Mass Spectrometry
IMO	International Maritime Organisation
LB	Luria Bertani
MWNT	Multi-walled Carbon Nanotubes
PA01	*Pseudomonas aeruginosa*
PDMS	Polydimethyl Siloxane
PEG	Poly(ethylene glycol)
PPR	PDMS and PEG Containing Resin
QCM-D	Quartz Crystal Microbalance with Dissipation Monitoring
QNM	Quantum Nanomechanical Force Mapping
RMS	Root Mean Square
RPMI	Roswell Park Memorial Institute Medium-1640
SEM	Scanning Electron Microscopy
SiDA	Silicon based Drying Agent
SnO	Tin Octanoate
TnBT	Tetra-n-Butyl Titinate
ToF-SIMS	Time-of-Flight Mass Spectrometry
WCA	Water Contact Angle
XPS	X-Ray Photoelectron Spectroscopy

Chapter 1

Introduction

1.1. The Problem

The accumulation of biomolecules and marine organisms into films on a submerged surface has been a problem for as long as humanity has been seafaring. [1] This phenomenon has a number of consequences. The primary cost associated with the formation of such a structure on the hulls of vessels such as ships, yachts or submarines is increased fuel consumption due to incremental frictional drag. This was first demonstrated by Loeb *et al.* in 1984 where they simulated biofouling on propellers by applying microbial slime only a few hundred microns thick to rotating discs. [2] Even such a thin layer was shown to cause hydrodynamic problems. Other issues which arise as a result of fouling include the expense of purchasing coatings for the submerged entity as well as application, removal and cleaning of these films. This is before considering the cost of moving potentially very large aquatic vehicles into adequate facilities in order to apply the coatings. Also, the environmental cost of the burning of unnecessary fuel and increased time spent at sea due to the frictional drag adds to the already considerable expense.

The amount of excess carbon burnt purely as a consequence of biofouling could contribute to as much as 2% of the total amount of carbon that *can* be burnt between now and 2050 for the Earth's temperature to stay within 2^{o}C of warming. This temperature value is that recommended to accurately predict the resulting consequences of global warming and therefore to be able to plan appropriately. [3, 4]

Bohlander described studies on US marine ships that showed that after the cleaning of biofilms from their hulls, 18% less power was required for these ships to maintain a given speed. [5] The total cost for cleaning and prevention of biofouling is estimated to be $1 billion per year for the US Navy alone. [6]

Figure 1.1. (*Left*) Image of a fouled ship hull on the macroscale. (*Right*) Scanning electron micrograph image of a developed biofilm on a steel surface after 8-weeks immersion in an industrial water cooling system. [8]

Extensive biofouling can also lead to bacterial corrosion of a particular surface in shipping and other industrial operations such as water distribution and water cooling systems. This usually means that the entity in question must be entirely replaced. It is therefore of optimal importance to produce a coating that prevents biofouling sufficiently such that it prevents even the initial stages of biofilm formation including the attachment of proteins and other small, free-floating biomolecules. [7] Recently, popular and effective biocidal compounds have been found to be toxic to marine life, especially edible species such as shellfish, oysters and molluscs. This has led to a drive in the industry to find more environmentally friendly approaches.

1.2. Marine Biofilms

1.2.1. Biofilm Formation

Marine biofilms are formed when a large number of microorganisms coalesce on a submerged surface (**Figure 1.1**). These microorganisms can be bacteria, protazoa or a range of other single-celled species. These films are produced on a submerged surface in the following manner:

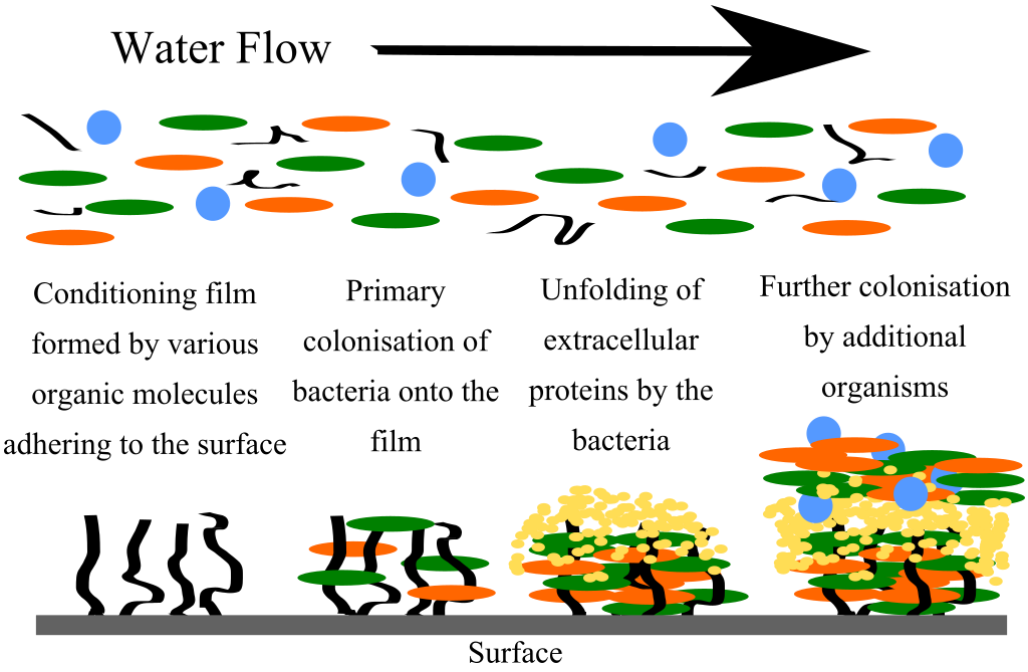

Figure 1.2. The process of biofilm formation on a substrate in a marine environment. Black lines represent biomacromolecules. Green, orange and blue circles are different bacterial species. The yellow colour represents extracellular proteins.

1) On exposure of a substrate to water that is constantly recycled mass transport of various organic biopolymers such as oleic acids and polysaccharides begins. This often causes them to become adsorbed to the surface. A large accumulation of these chemicals eventually forms a complete layer. This is known as a conditioning film. [9]
2) Within 2-3 hours, microorganisms including bacteria and protozoa are transported to the surface by diffusion, active transport and convection and adhere themselves to the conditioning film. [6, 10]
3) Unfolding of cell surface structures and exopolymer production by the adsorbed microorganisms strengthens their attachment. [11]
4) After a sufficient period of development of the biofilm, mass transfer of nutrients to the surface ensues with bacterial waste products being taken away. This stage also includes the recycling and potential removal of cells from the surface combined with secondary colonisation of microalgae and protozoa spores. [12]
5) Adhered cells metabolise, producing new cells and extracellular polymers. This is part of the maturation of the biofilm matrix that also

includes increased antimicrobial resistance in human based biofilms on the surface of medical devices. [13]

6) Finally, tertiary colonisers such as tunicates, molluscs and sessile cnidarians adhere to the biofilm. Sloughing of the biofilm occurs when the biofilm has obtained a critical thickness. This usually occurs post biofilm formation but there are notable exceptions such as polychaete larvae. [14-17]

This process is depicted in **Figure 1.2** and can occur on any submerged surface regardless of whether it is artificial or natural, as can be seen on the surface of rocks for example.

1.2.2. The Conditioning Film

Conditioning films that accumulate on the hulls of ships act as a platform for bacteria and other microorganisms to adhere themselves to a submerged surface. These preliminary films begin to form within seconds of the exposure of a surface to a marine environment. [18] It can be comprised of a variety of compounds such as glycoproteins, humic acids, proteins, nucleic acids, lipids, polysaccharides, and amino acids as well as various other unspecified macromolecules. [19, 20] Proteins are generally the first component to adhere to the surface. [21, 22] The chemical composition of the conditioning film can influence the physical and chemical characteristics of its surface such as: surface tension, interfacial free energy, hydrophobicity and surface roughness. [23, 24] This is especially true in the first four hours of immersion. The chemical composition and the quantity of adsorbed organic material also depends on the chemistry of the surface that they are adhering to.

Changes in the physical properties of a surface are likely to influence bacterial adhesion. They can also have a marked effect on the total amount of adsorbed material. The morphology of the conditioning film can vary depending on the prevailing conditions the surface is exposed to, including: nutrient availability, water flow rate, temperature and pH. [25, 26]

The structure of a biofilm changes depending on the composition and topography of the conditioning film. The availability of nutrients to constituent cells change and this has an effect on the thickness of the biofilm and the level of growth. [27] This in turn can affect the overall appearance of the biofilm and therefore the likelihood of specific macrofoulers being attracted towards the substrate.

Critical surface tension for wetting (known as wettability) is the substrate property that is most often correlated with primary film formation, with hydrophobic surfaces believed to be the more susceptible to protein attachment. This has been measured using liquid droplet contact angle experiments by Bott and Miller. [28] It has, however, not yet been conclusively proven whether a hydrophobic or hydrophilic surface is more attractive to such molecules. The surface charge of the submerged substrates can also affect the development of primary films. [29]

Using experimental custom-designed flow cell systems, Bar-Zeev *et al.* showed that the direct attachment of transparent exopolymer particles to a surface accelerated protobiofilm formation. They also demonstrated that this process begins within seconds of water exposure. [30] Therefore, the existence of polymers on the surface of the substrata increased the rate of biofilm formation. They analysed this process by visualising uncolonised exopolymers in coastal sea water via bright-field microscopy. Atomic force microscopy (AFM) was used to demonstrate that rapid conditioning of surfaces by organic polymers and colloids facilitates the attachment of bacterial cells. (**Figure 1.3**) The model presented showed that planktonic microgel particles are intimately involved in the initial stages of marine biofouling.

1.2.3. Marine Foulers and Their Organisation into Biofilms

After conditioning of the surface by biomolecules a variety of single celled species, followed by larger macrofoulers begin to colonise the submerged surface. These foulers have been studied in great depth in recent years in order to understand them and how they work and interact in a biofilm ecosystem.

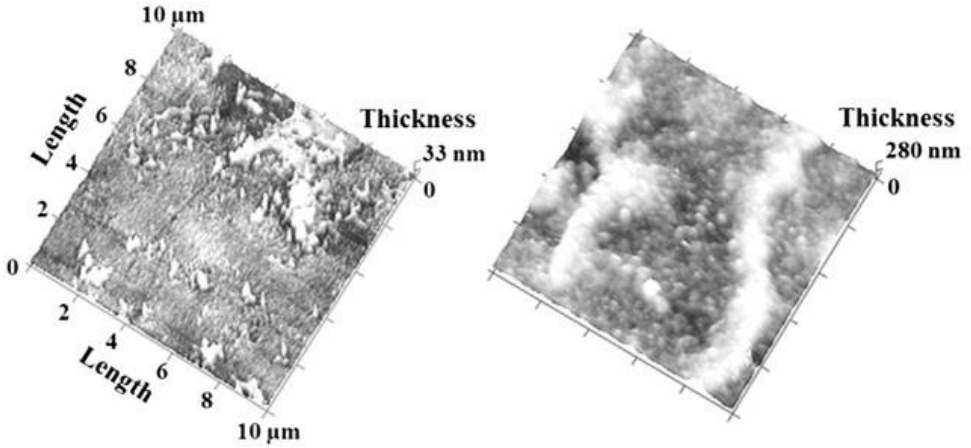

Figure 1.3. AFM tapping mode images of the surface topography of an organic conditioning layer on the surface of silicon inserts after 0.5 hours (*Left*) and 4 hours (*Right*). [30]

This is in order to devise innovative technologies to address the range of foulers that exist in and on marine biofilms. Foulers are split into two types, 'soft' and 'hard'. [31] Whilst soft foulers are generally slime layers containing diatoms, fungi, algae and bacteria, hard fouling involves organisms with siliceous structures such as tubeworms or barnacles. [32] Hard foulers are able to drastically decrease the effectiveness of a surface coating. For smaller foulers such as bacteria, bioinformatics of protein and DNA sequencing have been used in tandem with metabolomics to gain a better understanding of the identity of bacterial species that are prevalent in biofilms. [33-35] Similar methodologies have been used to understand the adhesive proteins and mechanics used by macrofoulers such as tunicates and molluscs to adhere to artificially manufactured substrata. [36, 37]

Study into the organisms that are present in biofilms is of particular interest currently as the complexity of the biofouling process means the make-up of a biofilm can vary drastically depending on the different conditions present. This makes the understanding of the mechanics of biofilm formation particularly important as marine biofilms can form on membrane bioreactors in sewage filtration, marine sensors and on industrial heat exchangers which use sea water as coolants. [38-40] For example, Doghri *et al*. analysed the species composition of bacterial communities on a carbon steel structure in a harbour in the French Atlantic coast. [41] This allowed for the identification of the four

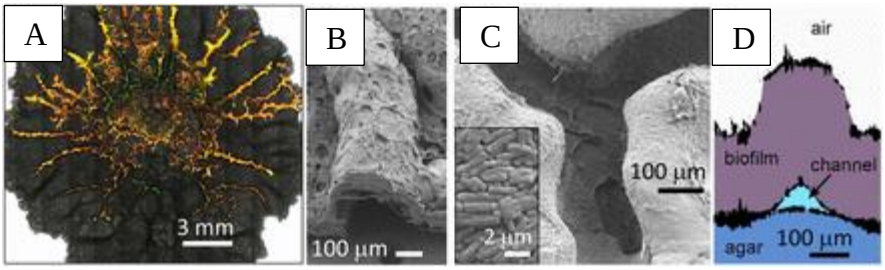

Figure 1.4. (A) Fluorescent microscopy image of a biofilm after fluorescent beads were injected via an aqueous solution. (B) Electron microscopy image of a cross section of a wrinkled channel inside a *Bacillus subtillis* biofilm. (C) Electron microscopy image of defined channels on the underside of the same biofilm. Inset shows the biofilm's microstructure. (D) Diagram of the side view of a biofilm wrinkle channel reconstructed from plastic moulds of the upper and lower surfaces of the biofilm and agar. [45]

most effective foulers for use as models in future work. These included *Flavobacterium* and *Roseobacter*. Dang and Lovell alternatively looked at the variety of species present after both a 24 and 72 hour period of exposure in an inlet salt marsh system near Georgetown Southern California. [42] They also found that *Roseobacter,* a subgroup of the bacterial division *Proteobacteria* was the most common group recovered in both periods of incubation. They are known to be fast and ubiquitous colonisers of surfaces and would therefore make useful models to test potential anti-bacterial products.

Biofilms have been shown to develop networks of clearly defined transport channels in the maturation phase, which are capable of facilitating the movement of liquid through the biofilm, moving nutrients towards bacteria whilst carrying away waste products. [43, 44] Wilking *et al*. used a monoculture of *Bacillus subtillis* to investigate the high permeability of these channels to liquid flow, facilitating the transport of liquid through the biofilm. [45] They found the channels enhanced the transport of liquid through the film. Depending on which bacterial species are present in a biofilm, the colonies can potentially be composed of ~20% cells and ~80% extracellular polymer cells. This process is now reasonably well studied with detailed mathematical models of the biofouling process having been developed that include multidimensional descriptions (**Figure 1.4**). [46, 47] Such simulations were used by Eberl *et al.* to determine the contribution of various physical processes to the mass transfer of water and nutrients. [48]

As well as producing channels, biofilms also develop compartmentalised zones as part of the overall matrix for specific biochemical and physiological reactions as a kind of defence mechanism. This is in order to prevent the destruction of the contained bacteria by harmful substances or rapid pH changes. [49] In work by Gieseke *et al*. biofilms in the nitrifying community were measured during a reactor cycle. During an aeration period they found that nitrification was oxygen limited and was reduced to just the top 200 μm of a biofilm's surface. [50] Alternatively Cobb and Bouwer used transformable chloro-compounds to show how biofilms develop sequential zones to isolate individual reactions, in this case aerobic respiration, denitrification and sulphate reduction. [51]

Understanding of macrofouling species and their attachment to submerged surfaces is equally important as those single-celled organisms, as often by this stage of fouling seafaring vessels are ruined and unusable. This is rendered a much simpler study due to the ability to just count individual foulers. Fonseca-Genevois *et al*. used aluminium surfaces at Farol Island, Brazil to look at meiofauna (marine invertebrates) formation over several weeks. [52] This work helped to understand the distinct stages in which meiofauna colonise a surface. Alternatively, the composition, dominance, diversity and spatial distribution of crustacean macrofoulers was analysed by Winfield *et al.*. [53] By submerging artificial clay panels in selected distinct reefs in the Gulf of Mexico, barnacles, amphipods and isopods were shown to be the dominant macrofoulers after three months in the ocean basin. They were also able to show that different areas in the Gulf had a lower diversity of species as well as a dominance of species that were resistant to organic matter pollution. This study highlighted the differences in the numbers of distinct species in areas that are comparatively close together. It is therefore of utmost importance to recognise the variety of biofouling that can occur depending on the specific environment. In developing biofilm prevention strategies it is best to ensure that the solutions are dynamic and flexible.

1.2.4. Attachment Forces and Communication Between Microorganisms

Charges on microorganisms, which may be different from that of the surface, can give rise to attraction between the two, aiding the adhesion process. Bacteria are able to sense they are at a surface due to membrane stresses arising from minor deformations from adhesion forces changing their phenotype from planktonic (free-floating) to sessile (anchored to a surface). [54] Generally environmental surfaces are net negatively charged electrostatically and produce repulsive forces against bacteria at a distance of 10-20 nm. [55] In the primary binding stage, the process of attachment is reversible. Over time the strengthening of the bonds via extracellular proteins and other molecules leads to substantial and irreversible bonding to the coating. The attachment is also dependent on van der Waals forces that act and attract at a distance of 10-100 nm on a particular bacterium suspended in a fluid stream close to the surface. [56] As bacterial cells and other microorganisms come within 5nm of the surface, the likelihood of physical contact by pilli and other cell adhesions greatly increases. Hydrophobic interactions are also important in the process. [57]

Increases in propellant kinetic energy may boost the probability of a bacterium overcoming the repulsive force between it and the surface. This is believed to be a particularly important function of bacterial flagellae in attachment. [58] Kogure *et al*. compared mutants of *Vibrio alginolyticus* that contained either solely polar flagellum or no flagellum at all. They showed that the swimming speed necessary to attach to glass surfaces was made possible by the polar flagellum.

In the small region close to the wall of the substratum, the hydrodynamic boundary layer, flow velocity is reduced which aids adhesion. Reversible attachment and its transition to irreversible attachment involves the workings of an array of short range forces such as covalent and hydrogen bonding as well as hydrophobic interactions. Bacteria often donate or accept electrons from the substratum. [59] This becomes particularly important where oxidative

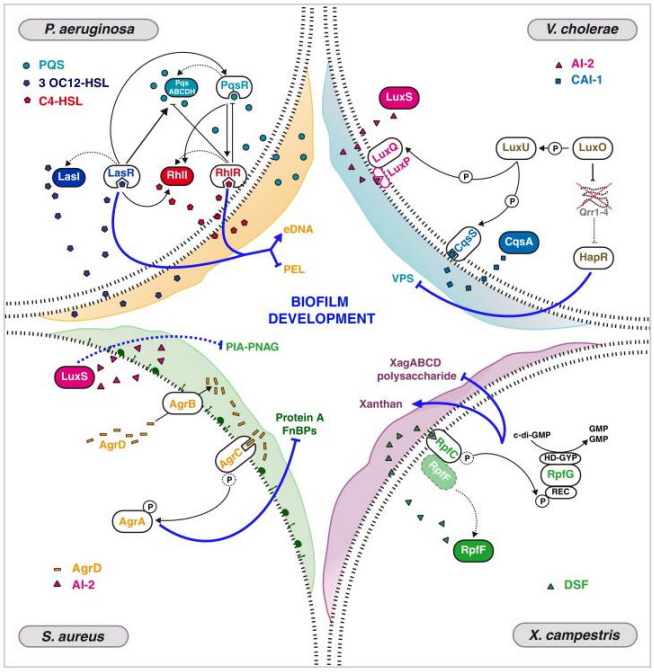

Figure 1.5. Schematic representation of quorum signalling regulatory cascades ending in the upregulation of biofilm matrix compounds in four selected bacterial pathogens. [62]

corrosion occurs. The processes described above all operate over a distance of roughly 20 nm.

Aside from using proteins to adhere to and sense surfaces, bacterial microorganisms also produce chemicals to communicate with other single celled species in order to form large scale biofilms. [60] This is known as quorum sensing and is how bacteria are able to communicate with each other. Examples of how this works in biofilm formation were demonstrated by Davies *et al.* who detailed how *Pseudomonas aeruginosa* utilises acyl-homoserine lactones (AHLs) to define the separation between bacterial pillars and the overall 3D structure of the biofilm. [61] They produced an a*lasI* mutant which formed flat undifferentiated biofilms, demonstrated by their sensitivity to sodium dodecyl sulfate biocides. This observation also explained how bacteria were able to become more resistant to chemicals that were damaging to them by collectively controlling gene expression. Hassett *et al.* showed that *Pseudomonas* uses two different transcriptional activator proteins LasR and RhlR and two autoinducers to reduce damage caused by oxidative stress from the chemicals hydrogen peroxide and phenazine methosulphate. [63]

Evolutionary constrains have also meant that this kind of communication is also possible between bacteria of different species. Recent work has suggested that there are universal signals that function in interspecies communication. [64] An AHL autoinducer, AI-2, is thought to be one such molecule. [65] An example of the chemical interconnectivity between different species of bacteria is shown in **Figure 1.5**.

1.2.5. Influence of Substratum Chemistry

How the differences in the chemistry of a surface affect its prevalence to be colonised by bacteria is a complex question. A wide array of organisms have therefore been studied, along with a variety of different materials in different conditions. Christensen *et al.* found that extracellular polymers in *Pseudomonas* change depending on the specific stage of the growth cycle. [66] For example, bacteria attached poorly to hydrophobic surfaces during exponential growth but this phenomenon was reversed when they entered stationary phase, where production of hydrophobic carbohydrate polymers occurred. Using other bacteria such as *Vibrio protelytica* and comparing both hydrophilic and hydrophobic surfaces, Paul and Jeffrey concluded that the attachment mechanisms utilised by the organism were unique depending on the surface. [67] This was demonstrated by the inhibition of adhesion of cells to hydrophobic polystyrene when proteolytic enzymes were used. This did not occur when using hydrophilic polystyrene. They therefore concluded that the adhesins were involved in cellular interactions with hydrophobic but not hydrophilic surfaces. These are currently speculations and previous evidence of how surface polarity affects bacterial adhesion has not necessarily been rendered moot by these findings.

Surface energy is an important factor in the potential for bacteria to adhere to a particular surface. The numbers of individual *Delaya marina* and a spontaneous mutant form of the bacteria were measured on different surfaces were measured by Shea *et al*. The wild type adhered to hydrophilic but not hydrophobic surfaces. The opposite was true with the mutant strain. [68] These

results suggested that the reduced ability to form extracellular polymers in non-mucoid forming mutants revealed a further type of adhesion mechanism present in the wild type. They go further to say those cells may potentially possess several adhesion mechanisms and utilize the mechanism most appropriate to the surface energy of the substratum. This information is important as it demonstrates the necessity of producing antifouling coatings with a wide range of critical surface energies.

Buchard *et al.* used surfaces of known surface energy to show that when motile bacterial species attach themselves to a surface, their motility is reduced or cut out entirely. [69] Gliding bacterium are bacterium which move under its own power without the use of the flagella, the more common method of motility in bacteria. For example, *Pseudomonas aeruginosa* use type IV pilli for this process. The research found that gliding was inhibited on surfaces of very low surface energy and was uncontrolled on hydrophilic surfaces. A further effect of surface chemistry therefore is that bacterial gliding is a function of the degree to which cells interact physicochemically with the surface. This interaction is therefore likely to be mediated by an extracellular polymer.

The strength of bacterial adhesion to surfaces has been analysed using AFM. Zhao *et al.* carried out surface selection studies of marine bacteria during adhesion events on substrates fabricated with self-assembled monolayers on gold. The test bacteria were *Shewanella* and *Pseudoalteromonas* (isolated from the German Wadden Sea). [70] AFM imaging allowed the observation of differences in the shape of the bacteria when adhering to surfaces and also looked at fingerprint morphologies of the initial adhesion processes. Fang *et al.* alternatively used AFM to show how the level of force that bacteria adhere to the surface of a substrate with increases after the accumulation of extracellular polymers produced at the surface of the bacteria. [71]

Motile strains of bacteria can place themselves easily at trenches and crevices in substratum materials. AFM images from Diaz *et al.* have been used to confirm that the initial distribution of bacteria on rough surfaces show

preferential directions as opposed to uneven distribution on smooth surfaces. [72]

Standard competitiveness between bacterial species is also prevalent in biofilm formation; McEldowney *et al.* determined that in mixed culture experimentation, adhesion of one organism interferes with that of another. This was independent of the nutritional status of the particular culture. [73] To corroborate this, Pedersen *et al.* found that adhesion of three marine isolates showed a difference in response to hydrophilic and hydrophobic surfaces, the population cell densities of the adhering bacteria and the nutrient concentrations present. [74] These experiments, whilst useful in determining various aspects of bacterial attachment to inorganic surfaces do not fully take into account that cellular metabolism is dynamic, so the results obtained do not give an all-encompassing picture of what is occurring. They do, however show that there are a number of factors to consider when developing strategies to prevent biofilm formation.

1.3. Biofouling Control Technologies

1.3.1. Considerations

Currently there is no known technique or product which is able to fully prevent or control the growth of biofilms without causing unwanted environmental or other assorted side effects. There are several strategies currently used for the treatment of biofilms. Biofilm prevention methods are divided into either ‘cleaning’ or ‘controlling’. The former consists of actively removing biological deposits whereas the latter aims to counteract and prevent the formation of these deposits. An example of such a cleaning strategy is using frequent and gentle wiping of hull surfaces using brushes which simultaneously spin whilst slowly moving up and down across the hull in order to prevent settlement of fouling organisms. [75, 76] Strategies can also be broken down into categories depending on whether they require external energy to carry out their functions or not. These are known as active or passive strategies respectively. An increased interest in sustainable environmentally-friendly solutions to this

problem has arisen in the wake of a ban on various undesirable compounds. [77, 78]

The desired characteristics of an antifouling coating presented by the Naval Sea Systems Commands are: a 12 year lifespan, durability, reparability and compatibility with existing cathodic protection systems. Furthermore they must have simple application and maintenance methods, be cost effective and smooth in port and at sea. Finally, the product must be commercially available and registered with the Environmental Protection Agency and potentially be compliant with current and future air emission regulations as well as significantly reducing copper emissions. [79]

One of the most common methods used to prevent biofilm formation is the use of biocides, chemical substances which deter or destroy the elements responsible for biofouling. An example of this was in work by Patil and Jagadeesan who found that biofouling development was decreased with an increase in exposure time to chlorine, a known biocide. [80] Tributyltin (TBT) which was a particularly effective biocidal anti-foulant had similar effects. TBT and a variety of other chemicals such as lead, arsenic and mercury have all been banned by the International Maritime Organisation in 2008 due to their detrimental environmental effects. [81-83]

Though there are currently still options being studied for using biocides as an anti-foulant technology, generally their potential for use has been discredited because of the aforementioned bans and also because of the rate at which bacteria can adapt to resist such chemicals. [84] The very evolutionary pressure that has caused bacteria to form biofilms on the surface of submerged inorganic surfaces has also caused them to adapt their genomes to include the ability of being able to resist antimicrobial compounds. [85, 86] Many gram-negative bacteria are adept at developing resistance as a stress-response in stationary phase by inducing the production of an RpoS sigma factor. Bacteria in a somewhat mature biofilm are considered to be physiologically similar to stationary-phase bacteria, with acyl HSL transcription activators becoming more prominent in cell clusters. [87] This adaptation is common in the field of

medicine where biofilms that form on implanted medical catheters can lead to unwanted additional infections and further resistance of the bacteria to drugs. This is particularly dangerous in hospitals where patients with compromised immune systems are particularly susceptible to such infections. [88]

Examples of current techniques designed to entirely bypass the issues associated with biocidal or ecologically damaging chemicals include the use of UV-LED lights at specific intensities and wavelengths to destroy DNA in the cells of potential foulants. [89, 90] Salta *et al.* devised a novel non-abrasive ultrasonic activated stream device to determine the cleaning capabilities of water flow across the surface of foul release coatings. [91] This was due to the limitations of coatings to entirely restrict biofilm formation. The ultrasound was able to excite endogenous bubbles in a flowing water stream. These bubbles were also capable of penetrating cracks in the hulls of ships. This method was found to be particularly successful, with no biofilm detectable on the coating's surface after 12 days immersion over in a marine environment. Similar results were seen in an isolated study with just the single species of *Staphylococcus epidermidis*. This process was non-damaging when comparing the surface roughness of the coatings to those that had not been exposed. New coating technologies have combined novel physical properties with more benign surface chemistries, which are discussed below

1.3.2. Paints and Foul-Release Coatings

Biofouling prevention strategies, creating barriers to ship hulls are as old as shipping itself. Copper plating was used by the Carthaginians in 1000BC. [92] Asphaltum and wax were also commonly used by the Greeks and Palestinian Fishermen. [93, 94] The current most popular method to remove slime coverage from boats is to frequently and systematically send machines or divers with scrapers or pressure washers underwater in a process known as 'hull husbandry'. [95, 96] This is neither the safest method nor the cheapest and can be logistically complex whilst the removed debris is impossible to collect effectively. Power washers can be damaging to ship hulls and any coating which may be attached to it. It is estimated the damage caused can cost

up to £5 per metre cleaned. [97] In dry dock conditions machine cleaners can also result in backsplash and redistribute the biofilm contaminants onto the cleaner, which can be breathed in and may be potentially harmful, particularly as there is likely a plethora of bacteria present. [98]

The traditional method that has lasted to the current day in preventing the accumulation of biofilms is the use of antifouling paints, which can be comprised of materials such as lacquers, sealers, surfacers and enamels. These paints can be produced with anti-bacterial compounds such as those used by Stupak *et al.* who applied sodium benzoate to soluble matrix paints. Trials in the Mar del Plata harbour confirmed successful prevention in barnacle attachment using such a paint. [99] In a similar vein, Hellio *et al*. conducted bioassays using a number of ethanolic and dichloromethane extracts from various marine algae from the Brittany coast and used them as a coating paint against marine bacteria. [100] High levels of inhibitory activity against bacteria combined with an absence of sea urchin larvae development toxicity suggests the products can potentially be combined with other antifouling preparations to act as environmentally friendly bacterial growth inhibitors.

Current trends in research to prevent biofouling has moved towards a class of coatings known as non-stick foul-release coatings. [101, 102] The difference between these coatings and the historically effective anti-fouling coatings which were the original gold standard is they do not rely on destructive mechanisms. These prevent fouling attachment by limiting the strength of bonding between foulers and the water exposed part of ships or industrial cooling systems. These bonds become limited so that the species attached are easily removed by the weight of fouling, the force of motion of the ship through the water or by the water current itself. [103]

As opposed to preventing growth chemically as demonstrated above, surface energies are important in determining the level of biofouling. Other research has attempted to develop surfaces with low surface free energies. Linder *et al.* showed that simulated perflourinated surfactant monolayers have good antifouling characteristics. [104] Tsibouklis *et al*. applied the recommendation

by Kobayashi that constituent low-surface energy anti-fouling polymers must have a flexible linear backbone. Side chains with low intermolecular interactions can be adhered to this via a pertinent linking group. [105] Two distinct compounds were tested: poly-(methylpropenoxyfluoroalkylsiloxane)s and poly(perfluoroacrylate)s and both were found to be successful adhesion inhibitors when applied as a smooth coating. [106]

1.3.3. Anti Quorum-Sensing Technology

Given quorum-sensing is the way that bacteria are able to communicate with each other, thus aiding in the formation of biofilms, developing ways to make this method of correspondence more difficult is a strategy currently being investigated.

Taking a simple model foulant in the form of *Pseudomonas aeruginosa*, Hentzer *et al.* used green fluorescent protein to detect gene expression in real-time, monitoring live cell to cell communication. [107] They then used Furanone 56 devised by Manny *et al.* which inhibited quorum-sensing transcription of the *lasB-gfp*(ASV) gene. [108] This compound had no impact on protein synthesis or the growth of the bacteria, not subjecting them to survival constraints. This made these bacteria less virulent. Manefield *et al.* similarly used furanone compounds though these were isolated from the marine macroalga *Delisea pulchra*. These were used to inhibit quorum sensing in *E. coli*. [109] In the presence of the furanone it was found that the LuxR involved in quorum sensing had a reduced half-life. It was concluded that the furanone acted to destabilise the homoserine lactone transcriptional activator, essential to quorum sensing. It is thought such chemicals could be included in the matrices of coatings to further aid the prevention of biofilm formation.

Synthetic compounds have been synthesised which have been found to regulate quorum sensing effectively. [110-112] Geske *et al*. produced a library of non-native AHLs which were particularly potent at inhibiting the quorum-sensing of *Pseudomonas*. [113] AHL analogues were synthesised by Rasch *et al.* and

compared with isolated compounds to see which ones inhibited protease activity of *Pectobacterium* A2JM. [114] This protein is regulated by quorum sensing. PenS-AHL was found to be the most effective chemical at preventing the communication. Janssens *et al.* modified furanones with bromine to look at how they may prevent *Salmonella enterica* biofilm formation. [115] They determined that this particular furanone interfered with the synthesis of flagella, preventing biofilm formation. It did as hypothesised interfere with quorum sensing systems but made the films more susceptible to antibiotic treatment. Conversely, Lönn-Stensrud *et al.*determined that a synthetic (Z)-5-bromomethylene-2(5H)-furanone inhibited autoinducer-2-mediated communication in various oral *Streptococci* bacteria, preventing biofilm formation. [116] This was found to be similar to results garnered for *E. Coli* quorum-sensing inhibition.

Natural products have been found to have quorum quenching properties. Vanillin has been isolated from vanilla beans and shown to inhibit violacein production (a product of quorum sensing) in *Chromobacterium violaceum*. [117] Similarly Ponnusamy *et al.* found a 46.3% reduction in biofilm formation when using vanillin against membrane biofilm bacteria *Aeromonas hydrophila* on a polystyrene surface as it inhibits AHL molecules. [118] Rasmussen *et al.* looked at the performance of garlic extracts on preventing quorum sensing in *Pseudomonas*. [119] It was concluded that the extract was able to reduce the expression of virulent genes such as those controlled by LasR and RhlR.

A variety of other natural products have been studied and found to be effective at limiting quorum sensing include cinnamaldehyde, AHL-lactonases from bacterial themselves and essential oils isolated from *Zingiber officinale* and *Melaleuca alternifolia*. [120-122] An alky-triphenylphosphonium salt was tested at different chain lengths against the mussel species *Mytilus galloprovincialis* whilst simultaneously analysing its ability at disrupting quorum sensing in *C. violaceum* and *V. harveyi*. [123] It was found to be repellent to the mussel and able to inhibit quorum sensing between the two bacterial species meaning that the chemicals were versatile in their ability to

prevent biofouling. The phosphonium salts were also found to be non-toxic, essential for the marine environment.

1.3.4. Biomimicry

The Dihydroxyphenylalanine (DOPA) section of a molecule developed by Statz was inspired by robust polymers found in a macrofouling organism *Mytilus edulis*. In recent years there has been a move towards isolating or mimicking chemical or physical properties found in nature in order to reduce biofouling. The benefits of such an approach are that these compounds are environmentally friendly due to their evolution within the defined ecosystem and they are also very well suited to preventing fouling due to their adaptation over millions of years.

Photoactive self-cleaning films break down foulants in the presence of visible or ultraviolet radiation due to reactive oxygen species production. Nakajima *et al.* attempted to prepare a thin, transparent superhydrophobic film with self-cleaning properties by including photocatalytic TiO_2 powders to the films. [124] This technology was inspired by water-repellent wax found on the innumerable projections on the surface of leaves. This particular solution satisfied the requirements of superhydrophobicity (water contact angle above 140^{o}), transparency and durability.

A further illustration of the concept of biomimicry being a popular area of research is current research in hydrogels. Hydrogels are substances which consist predominantly of water and a polymer network which holds it together. They are distinguishable from solid matter by their low elasticity and high water abundance (> 60% weight water). As opposed to solid materials previously used in fouling control, the surface of most marine creatures is soft and contains a high percentage of water. This makes them ideal candidates for the development of synthetic hydrogels or the isolation of their natural products. Most aquatic species have robust fouling defence due to evolution over millions of years. Intense study has been carried out to determine why the

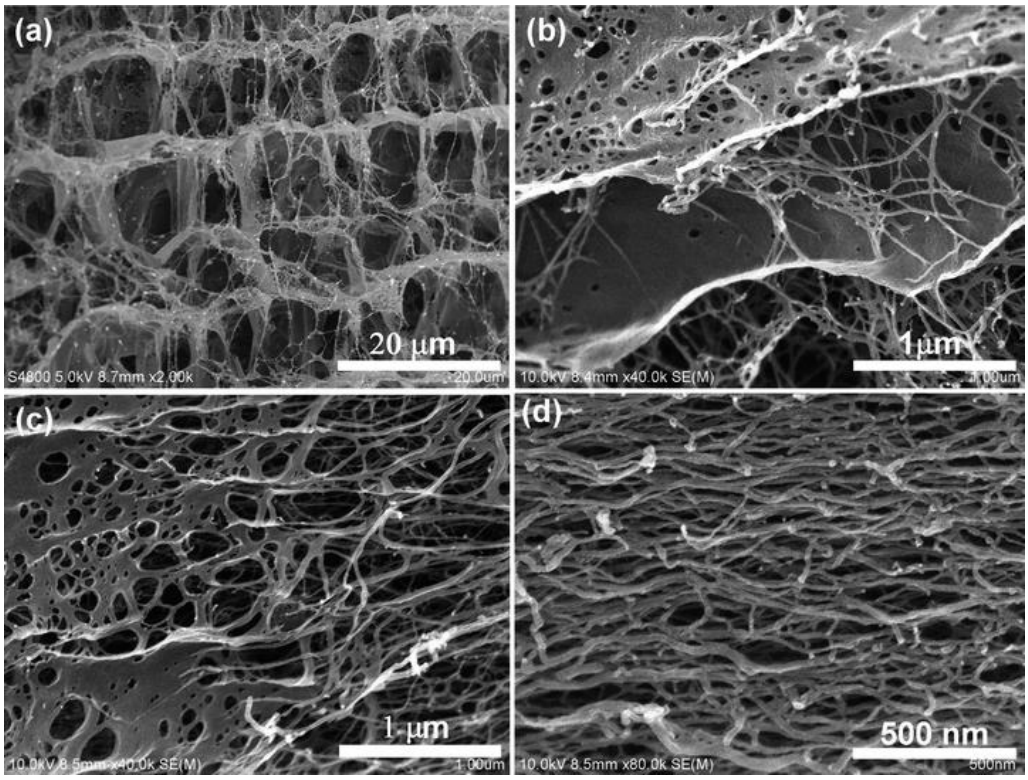

Figure 1.6. Scanning electron micrographs of mesoglea, a jellyfish isolated hydrogel with a high known mechanical strength. [127]

properties such natural products are so effective, whilst attempting to mimic these properties for use in anti-fouling technology. [125-127] They are found in the human body, as well as in seaweed and jellyfish (**Figure 1.6**). Katsuyama *et al.* devised poly (acryl amide), poly(vinyl alcohol) and polymethacrylic acid gels originating from *Laminaria angustata* which were all effective as germination and development inhibitors of zoospores. [128] This led them to conclude that they are useful as an environmentally benign novel surface coating for algal adhesion inhibition.

Yin *et al*. used a poly-zwitterionic material containing both cationic and anionic groups as part of a novel hydrogel coating. [129] These double network hydrogels using an *N*-(carboxymethyl)-*N*,*N*-dimethyl-2-(methacryloyloxy) ethanaminium, inner salt was characterised as a hydrophilic neutral hydrogel with a stable modulus which was insensitive to changes in pH and temperature.

The skin of fish and other aquatic species are often topographically, physically and chemically adapted to resist biofouling. [130, 131] Wang *et al.* imitated the

topography of yellowfin *Triacanthus blochii* by nanocasting onto a polydimethylsiloxane (PDMS) elastomer and they were able to refine the process to be easily controllable and replicable. [132] A novel surface technology based on micropatterns found on shark's skin was examined by Reddy *et al*. and shown to inhibit colonisation and migration of *E. coli*. [133] Though not proved conclusively, it has been hypothesised that the antifouling capability on shark skin is due to the flexing of denticles (tooth-like projections) against each other on a tractable surface. This occurs due to a regular pattern of ridges and grooves that run parallel to each other. [134, 135] Chung *et al.* showed a reduction in *Staphylococcus aureus* colony coverage over a period of 21 days on Sharklet AF^{TM}, a commercially available mimic of shark skin, compared to a smooth PDMS elastomer control. [137] Microscopy images of the surface topography of Sharklet can be seen in **Figure 1.7**. Dolphin and whales' skin has also been found to have similar properties to shark skin in their topographical nature and have been mimicked in laboratory conditions using nanoparticles (to simulate surface roughness) and also in the form of a gel-like coating layer. [138-140]

Another technique used by marine organisms is grooming of their surfaces that are susceptible to biofouling using brush-like appendages. An example of this inspired a brush engineered by Kohli *et al.* similar to the freshwater crab *Geothelphusa dehaani* which uses bristle brushes attached to a long stem in order to groom their gills. [141] These brushes have been shown to be somewhat ineffective however, even on smaller gill structures therefore it is unlikely to be the most effective single way of dealing with biofouling on a larger scale but could be applied in combination with other techniques.

1.3.5. Poly(ethylene glycol)

Poly(ethylene glycol) (PEG) is a heavily studied polymer and is the most prevalent anti-fouling material in use due to its weak basic ether linkages which give potential foulants limited opportunities to bind to it with their extracellular proteins. [142] There is steric repulsion of bacterial adhesion

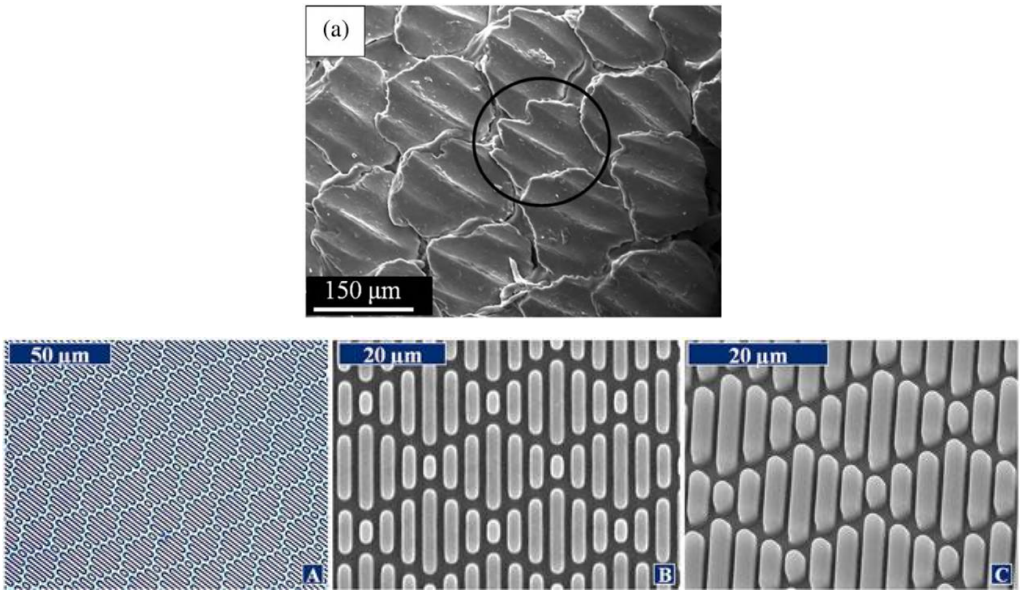

Figure 1.7. (*Top***)** Scanning Electron Micrograph of original shark skin. [136] (*Bottom Row)* Topography of a shark-skin inspired technology Sharklet AF^{TM} on a PDMS elastomer. Features are 2µm in width/spacing and 3µm in height. This spacing is thought to minimize bacterial accumulation by initially preventing expansion of small bacteria clusters. (*Left*) Top-down light microscope image. (*Middle*) Electron micrograph image. (*Right*) Electron micrograph image at a 35^{o} tilt. [137]

molecules due to the high exclusion volume on PEG provided by an osmotic and elastic component as well as high surface mobility of the groups. [143, 144] It also has a very low polymer-water interfacial energy value, further limiting the ability of bacteria and proteins to adhere. [145] It is nontoxic, water soluble and can easily be applied to other chemistries by being grafted onto their surface, providing the benefits of a range of materials as opposed to just one chemistry alone. [146] A drawback of PEG is that it can be easily degraded by either oxidation or by having its chain cleaved in a marine environment, meaning as a coating it may not last as long as would be desired. [147, 148] Covalently coupled PEG has been shown to improve the stability of compounds however. [149]

As opposed to the methods suggested above which largely involve relying on the inherent chemical and physical properties of the surface, Gudipati *et al.* attempted to take advantage of a strategy that involved the development of surfaces with topographical and compositional intricacies. [150] Coatings can be produced with desired heterogeneity on the nanoscale in terms of its composition, topography etc. It then theoretically becomes unfavourable

energetically for proteins or glycoproteins which form the conditioning film to adhere via either hydrophobic or hydrophilic interactions. The coating put forward was that of a cross-linked hyperbranched fluoropolymer (HBFP)-PEG-diamino terminated chemistry, which had an amphiphilic surface character. These coatings were asserted to be effective anti-foulants after examination using various surface energy analysis methods due to their high mechanical strength and even distribution of hydrophobic and hydrophilic domains.

Statz *et al*. used a PEG based polymer mPEG-$DOPA_3$ in which a mussel adhesive protein was conjugated to other antifouling polymers. The polymer was found to have similar settlement reduction capabilities to *Navicula* cells and *Ulva* zoospores as PDMS elastomers, one of the main candidates for anti-fouling research. [151] This was counter-intuitive given the adhesive nature of the protein so the authors concluded further study was required given that the results for *Navicula* and *Ulva* differed from each other. Krishnan *et al.* also looked at *Navicula* cells and *Ulva* coverage by using a dynamic surface active polymer which was a block copolymer containing PEG. [152] The block, which had been PEGylated was shown to migrate to the surface in water due to its hydrophilic properties. Combined with the low adhesive properties of fluoroalkyl groups they determined that it had good protein resistance properties, saw low adhesion of *Navicula* cells and *Ulva* and resulted in minimal settlement density amongst barnacle larvae.

As opposed to producing comb-like block copolymers, Zhao *et al*. developed hyperbranched polymers by grafting 12 PEG arms onto a- hydrophobic poly(vinylidene fluoride). [153] They were able to successfully lower the contact angle of the membrane to a desired hydrophilic chemistry. The greater the PEG content the lower likelihood of the adsorption of a small, stable protein Bovine Serum Albumin (BSA) onto the membranes. It was also shown that for effectiveness, brush density should be high enough to make the distance between PEG chains smaller than that of the dimension of the BSA molecules. The surfaces were also stable enough to potentially be considered as a candidate in hydrophilic filtration membranes.

PEG is a popular polymer for use in hydrogels, finding anti-fouling applications in medical devices, lab on a chip channels and marine fouling coatings. [154-156] Yeh *et al.* looked at how chain-length and cross-linking of PEG in hydrogels affected the ability of a surface to prevent biofouling. [157] In this case they demonstrated that the level of hydration depended directly on the molecular weight of the hydrogel. The chain lengths of the hydrogels were directly correlated with their hydration level. A 500 segment long chain was found to have the best resistance against *E. coli* and platelets. Lundberg *et al.* examined a library of similar PEG based hydrogel coatings. [158] The investigation also encompassed the system's curing, degrading and antifouling properties. They concluded that ester-free hydrogels were more hydrolytically stable though long PEG chains degraded more easily. Conversely, the longer the PEG chains, the better the antifouling properties against BSA, *Cobetia marina* and *Amphora coffeaeformis*, a marine diatom.

PEG is often used as a model to understand what features make marine foulants less likely to adhere to surfaces. Schlip *et al.* found that infiltration of water into an ethylene-glycol terminated self-assembled monolayer structure created hydration energy, preventing effective interaction of adhesives that species like *Ulva* zoospores used to attach themselves to surfaces. [159]

1.3.6. Silicones

Silicones and fluoropolymers are currently the two leading candidates for effective foul-release coatings. Silicones, or polydimethylsiloxane (**Figure 1.8**) and its importance has been ascertained by an awareness of its very low surface free energy and also its 'non-stick', simple-release characteristics. These characteristics make coatings that are made of PDMS easier to clean manually. They also have a low elasticity modulus. PDMS presents particularly low environmental hazards, which make it an ideal candidate material to comply with the guidelines set out by the International Maritime Organisation (IMO).

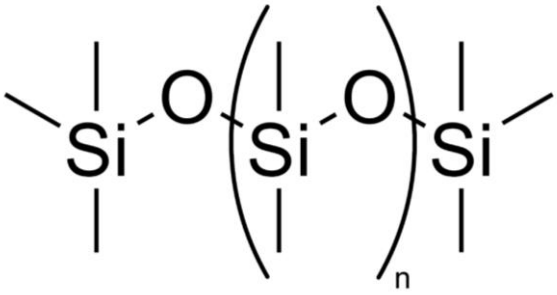

Figure 1.8. The chemical structure of polydimethyl siloxane.

Silicones are believed to be an ideal material for foul release. This has been attributed to it having an optimum range of critical surface tension related to its surface energy. [160] This foul release capability has been demonstrated against fluoropolymers and other coatings as well. [161-163] More energy is required to remove macrofouling from fluoropolymer coatings than silicones. However, fluoropolymer coatings have been seen to be harder and therefore more abrasion resistant, giving it the advantage of increased life-span. [164]

Examples of current work involving silicones is that of Beigbeder *et al.* who prepared a silicone-based coating with small amounts of either synthetic multi-walled carbon nanotubes (MWNT) or the clay mineral sepiolite. The ability of the coating to release *Ulva* sporelings was improved on addition of both the substances. Also recorded was the reduced adhesion strength of barnacles growing on the MWNT/silicone coating. The bulk properties of the coatings were unchanged on addition of the two materials. [165] Similarly, Beigbeder *et al*. carried out further experiments with a different sort of 'filled material' i.e. using montmorillonite (a soft phyllosilicate mineral) as the filler in a silicone matrix. On exposure to water, this particular coating was demonstrated using AFM to have a finer, smoother, less heterogenous surface. They concluded that, following on from the previous work, the increased reduction in adhesion strength of algae and barnacles demonstrated the potential benefits of nanocomposite materials in biofouling control. [166]

Truby *et al.* combined polydimethylphenylsilicone oil with a cured PDMS network in an attempt to improve the foul-release capabilities of PDMS based systems. [167] They found lower coverage of both hard and soft foulers at

various sites tested around North America as well as decreased adhesion strength of barnacles and certain oyster species. The addition of this particular oil made no difference to the toxicity of the formulation as it did not deplete and leech from the coating matrix.

Natural products have been applied to silicone coatings, such as zosteric acid (found in eelgrass) by Barrios *et al.* [168] Consistency of surface wettability and bulk modulus was achieved after the filled coating was immersed in freshwater. Also, bacterial populations were seen to decrease as the concentration of zosteric acid in the solution increased. The release rates were slower than other groups have reported, but the authors maintain that this could potentially ensure a longer service life.

There is an array of literature detailing the specific properties of silicone-based coatings themselves and how altering these properties affects their foul-release performance. For example, Stein *et al.* investigated how cross-linking density and filler loading affected the attachment strength of pseudobarnacles. [169] They found that whilst crosslinking density did not affect attachment strength of pseudobarnacles it did change the mechanism of coating failure, revealing a trade-off between mechanical integrity of the PDMS coating and their foul-release abilities. Holland *et al.* found that the motility of fouling diatoms changed when attached to elastomers. [170] Schumacher *et al.* looked at how feature size and geometry affected settlement of zoospores on engineered micro-topographies of the surface. They found that having evenly spaced features across the surface significantly reduced zoospore settlement in comparison to a smooth surface. [171]

The wealth of studies on PDMS as a foul-release coating demonstrates it is a very popular target for research in the field currently. This may further be explained by the fact that in order to study such a material it requires a multifaceted, interdisciplinary approach, combining analytical measurements and a variety of other considerations from nano-topographical details to bacterial genetics.

1.3.7. Amphiphilic Surfaces

Current predictions suggest that the ideal surfaces for biofilm prevention are chemically heterogeneous and have dynamic surface characteristics. [172] This is for several reasons. Firstly if a surface coating has unchanging chemistry, then even if it prevents bacteria adhesion to begin with, over time bacteria may develop biochemical solutions over evolutionary cycles. Secondly if a coating is comprised of several different chemistries, then it can exploit the benefits provided by them and have these drawbacks alleviated by the other components of the system. For example, whilst hydrophobic coatings are good at preventing the attachment of larger marine organisms they are not as effective at preventing bacterial attachment. [173] Or, as described above it could be used to increase the strength of a material that is already a good anti-foulant, providing it with the ideal characteristics for its practical use. Inspiration has been taken from nature for this surface tuning such as self-assembling surfactants and phospholipid bilayers. [174, 175] The ability to create desired morphologies down to the nanoscale was applied to amphiphilic coatings.

These kinds of surfaces can be formed in a number of ways. For example, block copolymers are often used. [176-178] These are made up of several different chemical blocks of which the polymerised monomers are distinct from each other. This can take the form of a number of blocks, e.g. diblock, triblock. [179, 180] Alternatively, graft copolymers can also be used, an alternative form of branched copolymers where the side chains which are attached to the main chain are structurally or chemically distinct. [181, 182] There can be overlap with block copolymers, e.g. if two side chain groups are alternating an A-B block copolymer. The change in the surface of amphiphilic coatings has been reported by Weinman *et al*. who used AFM to show how water can affect surface topography of such coatings via swelling, due to the altered surface chemistry (**Figure 1.9**). [183] Cho *et al.* combined polystyrene block copolymers with grafted hydrophobic and fluorine-free hydrophilic side chains to develop an amphiphilic surface which changed character in water (**Figure 1.10**). [238]

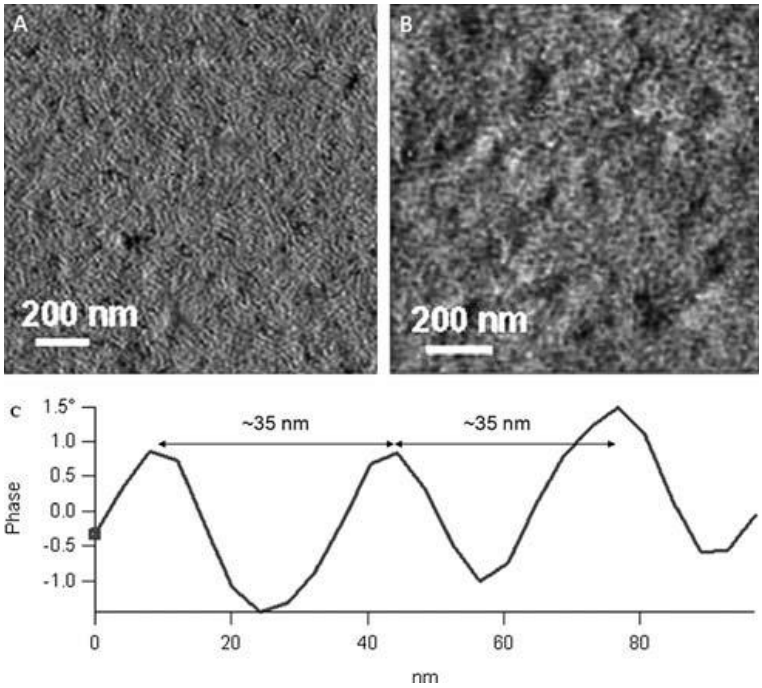

Figure 1.9. (*Top Left*) AFM phase image of polystyrene block copolymer containing ethoxylated fluoroalkyl groups in air. (*Top Right*) Phase image of the same copolymer in water which demonstrates a more swollen surface with cylindrical type morphology. (*Bottom*) Line scan from the water image which demonstrates a domain size of 35 nm after swelling in water. [183]

Long chain fluorinated compounds have been shown to accumulate in mammalian blood cells, meaning they could be potentially damaging to the environment. These were replaced with polypropylene glycol and mixtures of assorted alkyl groups and alcohols. [184] Kim *et al.* took a higher throughput methodology (looking at a large number of materials simultaneously) whilst developing random copolymers with a base of hydrophobic styrene and hydrophilic 2-hydroxyethyl methacrylate/ethylene glycol methacrylate. [185] These were synthesized using an assortment of different monomer ratios and cross-linked by radical polymerisation. BSA was used as the model foulant to determine protein adsorption and assays showed that the coatings in general had promising anti-biofouling properties. This high-throughput approach was also used by Majumdar *et al.* who considered four different variables of polymer composition. These included alkoxysilane functionality, chain length of alkyl groups attached to quaternary ammonium salt moieties and the molecular weight of added PDMS chains. [186] This resulted in 24 unique

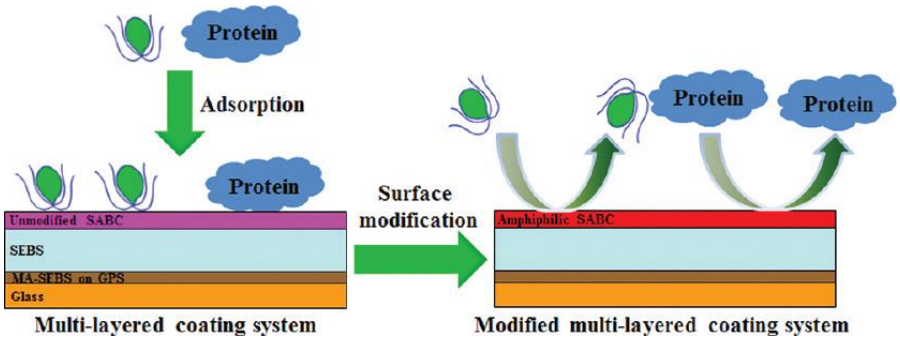

Figure 1.10. Diagram representing the work carried out by Cho *et al.* who modified polystyrene block copolymers by grafting hydrophobic and hydrophilic chains onto the copolymer. The additions of such side chains reduced the adhesion of proteins and diatoms. [238]

coatings. They were all subjected to two species of marine bacteria and *Navicula incerta*, a diatom. The authors observed in this work that compositional variables did make a difference to a coating's foul release behaviour toward specific marine organisms as higher concentrations of ammonium salts enhanced anti-fouling character.

The first published example of an amphiphilic coating used specifically as a marine anti-biofouling coating was by Gudipati *et al*. who synthesised a hyperbranched pentafluorostyrene cross-linked with PEG and PDMS. [187] Surface analysis using AFM and X-Ray Photoelectron Spectroscopy (XPS) confirmed a complex chemistry and topography that underwent reconstruction when incubated in both pure and artificial seawater. The coatings were able to reduce surface attachment of a BSA by 60% and also produced a 45% reduction in the fouling of a green alga compared to commercially available coatings. [188]

Kumar *et al*. used a free plasma process to produce nanostructured amphiphilic coating by co-polymerising fluorodecyl acrylate and diethylneglycol dimethyl ether precursors. [189] They noticed a switching effect, with the water contact angle values of the coatings decreasing from 120^{o} to 60^{o} over a period of five hours. The authors believed this suggested a reorientation of hydrophilic segments to the coating-water interface due to polar interactions between PEG and water molecules. This phenomenon was rapidly reversible when the sample was blow-dried. This switching effect in polymer brushes has also been

observed in tissue engineering applications. [190] For example thermoresponsive coatings designed for cell cultures which are based predominantly on poly(N-isopropylacrylamide) have been investigated. [191] Temperature was seen to switch the surface from a hydrophilic to a hydrophobic state. Goswami *et al.* also reported a large reduction in Water Contact Angle (WCA) of Nafion due to chemical reorientation of sulfonate groups on a Teflon backbone. [192] Surface wettability has been tuned to alter to a variety of different conditions including optical, magnetic and mechanical changes on superhydrophobic surfaces such as PDMS and specifically arranged carbon nanotubes. [193]

The studies presented above and a wealth of other work currently being undertaken demonstrates why amphiphilic coatings are thought to be a promising solution to the problem of biofouling. [194-196]

1.4. Aims

The general aim of this project was to (in collaboration with *Dow Corning*) develop and characterise potentially eco-friendly novel foul-release coatings for marine applications which are cost effective. This was in an attempt to limit the necessity of removing nautical vessels from the sea in order to manually clean them, restricting damage of the hull in the long term. This involved firstly assessing the surface chemical and physical characteristics of the PDMS based coatings and determining the best method for the deposition of them onto substrate surfaces (Chapter 3). Next their stability and character in water was analysed to ensure that they maintained their integrity over a sufficient period of time and do not damage the environment through the leeching of chemicals from their cross-linked matrix (Chapter 4). The potential for these coatings to prevent initial bacterial attachment was tested using model bacteria strains (*Pseudomonas aeruginosa*). Total coverage of the bacteria across the surface of the coatings was analysed as well as if the bacterial species were compromised on adhesion to the coating (Chapter 5). The foul-release potential of the coatings were assessed by looking at the force required to remove the same bacterial species from their surfaces. Exposure to a true marine environment

over a period of one week and quantification of the resultant biofilm coverage via biological assays and microscopy was the final stage of experimentation (Chapter 6).

Chapter 2

Materials and Methods

2.1. Chemicals

Resin, cross-linking catalysts and drying agents for the formation of the coating films were supplied by *Dow Corning*. The Polydimethyl siloxane (PDMS) based Resin (PPR) containing Polyethylene glycol (PEG) domains exists in a viscous liquid form (**Figure 2.1**). A phosphorus containing catalyst known as 900c and Tyzor® tetra-n-butyl titinate (TnBT), a titanium containing catalyst were used to promote the following cross-linking reactions:

1. $SiOR + H_2O \dashrightarrow SiOH + ROH$ (Equation 1)
2. $SiOH + SiOH \dashrightarrow Si\text{-}O\text{-}Si + H_2O$ (Equation 2)

Tin(II)-ethylhexanoate (SnO) and an alkoxysilane (SiDA) acted as drying agents. Solvents were obtained from VWR Chemicals (Pennsylvania, US).

2.2. Preparation of Polymer Films

Six sample types were devised using different catalysts and concentrations: **1** 1% 900c w:w (with resin) **2** 1% 900c / 5% SiDA **3** 5% TnBT **4** 5% TnBT / 5% SiDA **5** 4% TnBT / 1% SnO and **6** 4% TnBT / 1% SnO / 5% SiDA. The coating mixture was blended using an over-the-top stirrer at 800RPM for 3 minutes causing the polymer to interact with the moisture in the air and cross-link. Samples were then applied to glass slides using a *BYK* drawdown paint applicator frame (Wesel, Germany) to deposit a 100 μM thick coating (**Figure 2.2 (***Left*). The glass slides were pre-cleaned using methylethyl ketone for standardization purposes. This solvent was also used to clean the Badger Model 200™ (Illinois, US) airbrush to prevent blockages. For Scanning Electron Microscopy (SEM) analysis coatings were sprayed onto 12.5 mm plastic stubs using the Air-Brush (**Figure 2.2 (***Right*)). For bacterial movement and adhesion

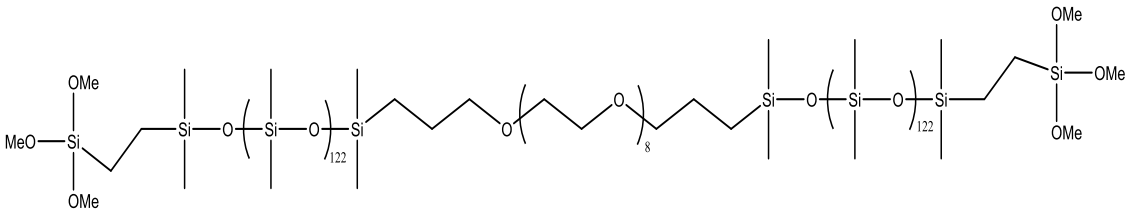

Figure 2.1. Chemical structure of the PDMS containing resin. 122 PDMS groups frame smaller PEG domains in the centre.

Figure 2.2. (*Left*) Image of BYK paint applicator for applying coatings to glass slides (*Right*) Badger airbrush used to apply coating to SEM stubs and glass coverslips.

analysis, coatings were sprayed onto 22 mm glass cover slips. The samples were left to dry for 24 hours before analysis.

2.3. Atomic Force Microscopy (AFM)

The atomic force microscope and was first developed at IBM in 1986. [197] AFM is able to investigate at nanoscale resolution the surfaces of a wide range of samples, including insulators, in both ambient and aqueous environments. This is particularly beneficial in analysing biological samples. The resolution of AFM is up to 1000 times greater than the optical diffraction limit meaning it has the potential to differentiate details on the order of fractions of nanometres. AFM operates by a running a nanoscale tip mounted at the end of a flexible cantilever over a surface. This is opposed to using light or electrons to irradiate a surface. The force microscope therefore acts as a kind of ‘feeling’ microscopy. This tip can either be rastered across or near to the surface or intermittently tapped onto it. These are known as contact, non-contact and tapping mode respectively. [198]

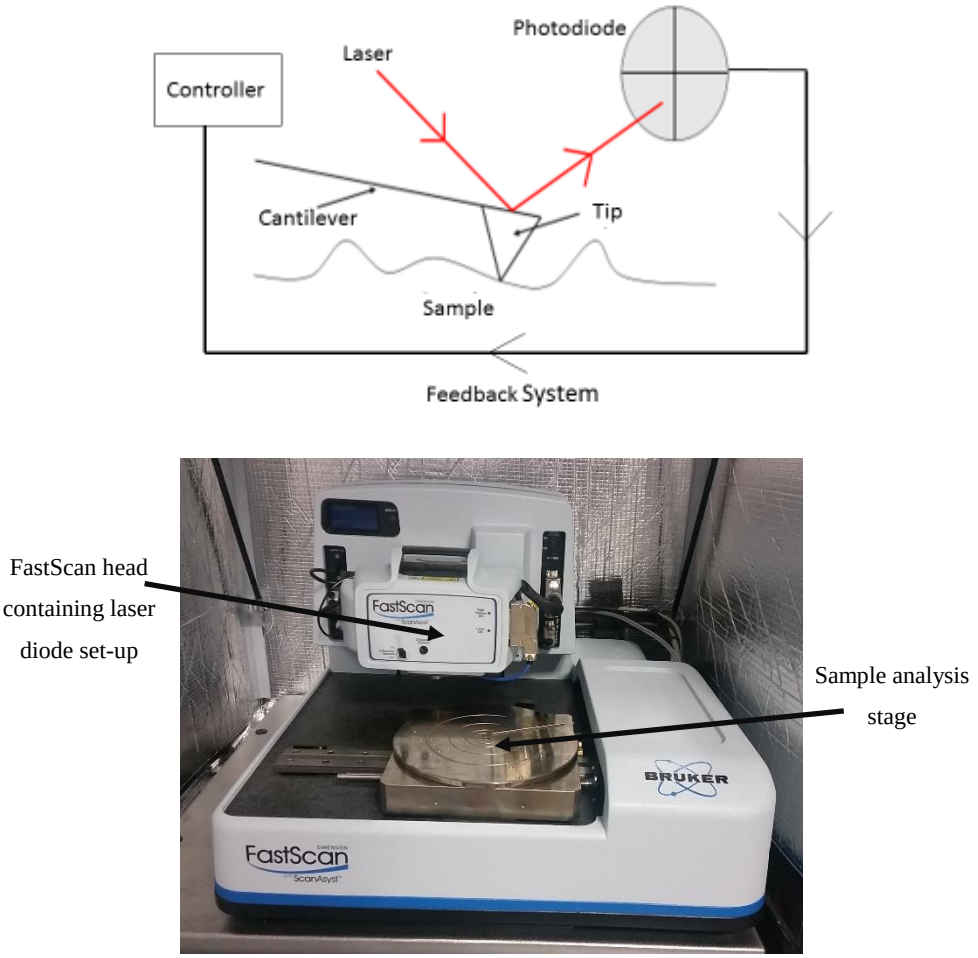

Figure 2.3. (*Top*) Schematic of the basic set-up of an atomic force microscope. The movement of the tip across the surface is detected by a laser deflected onto the top of the cantilever. (*Bottom*) Photograph of the Bruker Icon FastScan AFM.

The AFM tip is usually manufactured from silicon based material using lithographic techniques. A laser is applied to the back of the cantilever in order to detect movement of the tip in the vertical direction via an optical lever effect. (**Figure 2.3**) This change in height across a surface is captured by a photodiode which detects the movement of the laser light. This information is then processed into an image of the surface. These images can provide surface characteristics such as roughness and topography. The nature of direct physical interaction between the probe and the surface also allows surface properties such as hardness and adhesion to be determined at the same spatial resolution. [199, 200]

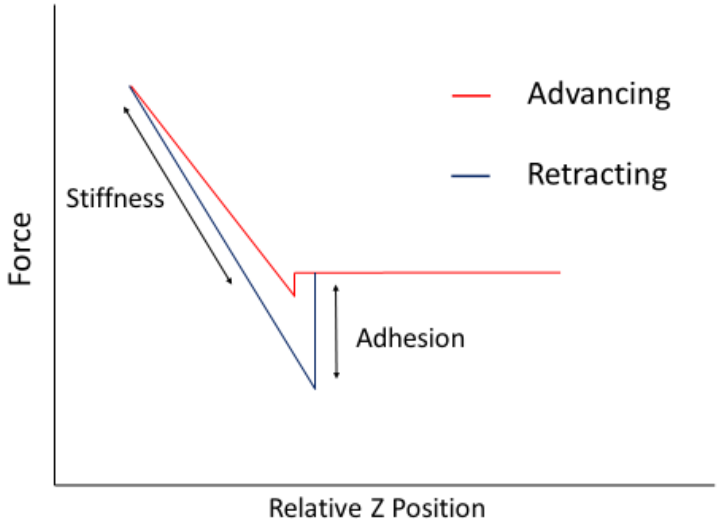

Figure 2.4. Diagram of a standard force vs distance curve showing the regions from which the mechanical properties of the surface are derived.

Polymers and biological samples tend to be softer than other materials and hence can be damaged by the AFM probe during analysis, particularly in contact mode where the tip is in continuous physical contact with the surface. Tapping mode was developed to circumvent this particular problem and enable such surfaces to be imaged with a reduced chance of permanent damage. In this mode the cantilever resonates at or near to its resonant frequency – this method of excitation often being termed 'acoustic' tapping mode. The amplitude of this oscillation is kept constant. As the tip approaches the surface, the amplitude of oscillation is dampened and a feedback loop is used to maintain tip-sample average separation such that the oscillation reaches a target amplitude (the so-called 'set point'). In tapping mode, the tip tends to touch the surface only at the bottom of each oscillation cycle. In recent years Bruker has developed the PeakForce Quantum Nanomechanical Force Mapping® mode (QNM), whereby the tip oscillation is under more direct and continuous control. This allows the quantitative determination of other surface properties than simple tapping allowed such as modulus, adhesion, deformation and dissipation, whilst maintaining a very low force on the probe making it less destructive on soft and fragile samples. [201]

As stated AFM is also capable of providing quantitative information of the surface such as that of stiffness and adhesion. This can be achieved by recording force-distance curves by driving the tip towards and into the sample surface whilst measuring the cantilever deflection. As the tip gets close enough to the sample the tip comes into the range where interacting forces begin to occur and the cantilever bends towards the surface and eventually jumps into contact when the attractive forces exceed the stiffness of the lever. [202] As the tip is driven further into the surface the cantilever straightens until repulsive forces cause further deflection. The cantilever is then removed from the surface, in retraction adhesion may hold the tip onto the surface until the energy stored in the flexed cantilever exceeds this force and the tip jumps away from the surface.

The vertical position of the tip against its deflection throughout the process can be plotted as a force vs distance curve (**Figure 2.4**). The force is determined by the magnitude of the deflection of the cantilever, quantified using Hooke's law (Equation 3).

$$F = -kd \quad \text{(Equation 3)}$$

F equates to force, k is the cantilever's force constant and d is the deflection of the cantilever. This information is then used to determine other mechanical properties. Using the portion of the curve where the tip is driven into the sample, Young's modulus can be calculated. The deflection of the cantilever as it is drawn away from the surface can be converted into force using Equation 3. This provides the adhesive force. The spring constant of the cantilever is determined using its resonant frequency and the 'Q factor' or the number of oscillations for the energy of the oscillating cantilever to fall to 0.2% of its original energy (Equation 4). [203] The sensor response is recorded prior to analysis using a known hard surface, usually glass, measuring deflection using the linear part of the curve. [204]

$$k = 2\pi^3 l^3 w \sqrt{(\rho^3 / E)} \; f_0{}^3 \quad \text{(Equation 4)}$$

2.4. Time of Flight Secondary Ion Mass Spectrometry (ToF-SIMS)

SIMS allows the recording of mass spectra of surfaces in a vacuum environment, providing detailed chemical analysis. This information can be used to ascertain details of the orientation of groups within polymer structures. This information is obtained by analysing emitted fragments from the top 1-2 nm of a surface after it has been bombarded with primary ions. (**Figure 2.5**). [205] The fragmentation process occurs by the transferring of kinetic energy from the primary ions to the surface atoms via a collision cascade breaking the bonds between these atoms at the surface. Secondary molecules and fragments are liberated from the surface including neutral species, electrons and charged ions which make up around 1% of the total that are detected and analysed by the mass spectrometer.

Secondary ions formed by the collision cascade are accelerated through a flight tube and energy corrected using an ion mirror such that they reach the detector at a time corresponding to their molecular weight.The heavier they are, the longer the travel time to the detector. These ions exist initially as packets of surface ions by virtue of the pulsing of the primary ion beams.

These packets are withdrawn into a drift tube. It is upon acceleration in the drift tube that the ions separate into their respective masses. Since development of the earliest forms of the mass analyser in the 1940s the use of the instrument as a whole has widened in its use and become more advanced. It is now commonly used to analyse surface contaminants, cells, metabolites and other biological samples culminating in improved systems with lateral resolution of 100 nm. [206- 208]

SIMS has two major operation modes: static and dynamic. Dynamic SIMS, whilst effective at depth profiling through samples by using a high ion dose, can cause significant damage to surfaces. Dynamic SIMS is useful in the analysis of semiconductor materials. *Static* SIMS is the mode of choice for more sensitive surfaces. *Static* mode uses very low ion doses (1×10^{12} ions/cm^2) to obtain intact molecular ions and fragments which closely represent

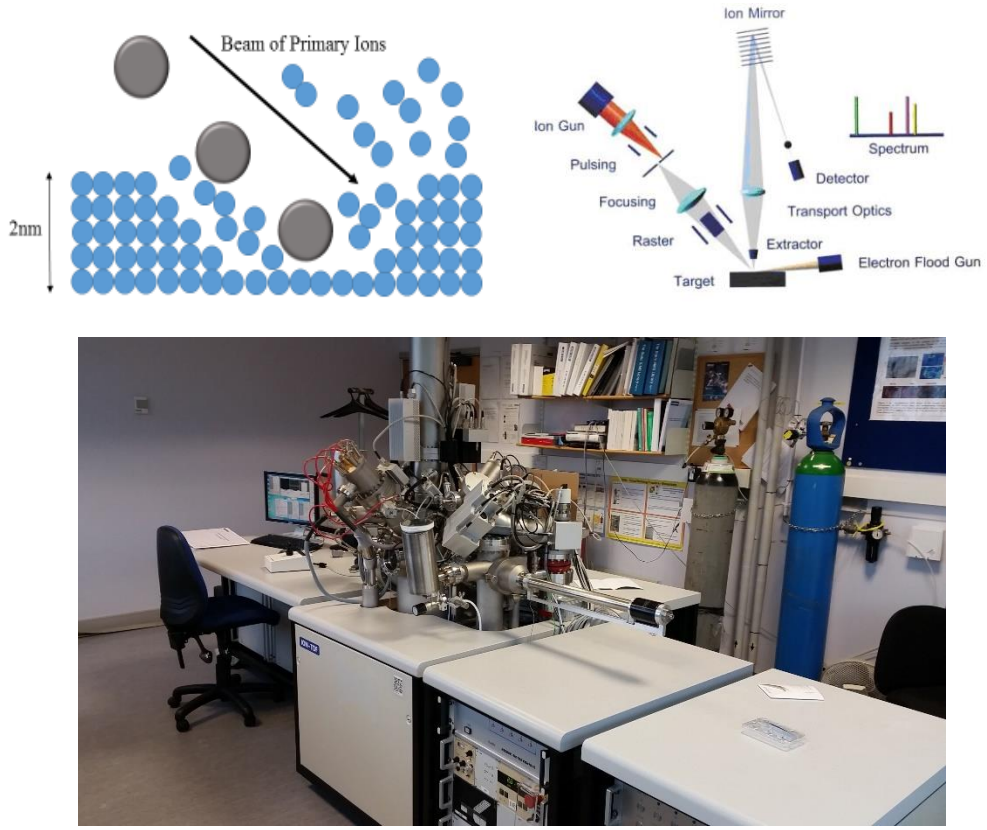

Figure 2.5. (*Top Left*) Schematic of primary ions hitting a surface and releasing secondary ions (*Top Right*) ©IONTOF schematic of a SIMS instrument. (*Bottom*) Image of the ToF-SIMS IV instrument.

the structure of the sample by ensuring limited damage by reducing the chance of analysing in the same area as a previous primary ion impact. ToF-SIMS can be operated in positive and negative modes to obtain specta of the surface with oppositely charged ions.

A variety of primary ions are used in ToF-SIMS. They include liquid metals Ga^+ and In^+, polyatomic clusters such as C_{60}^+ and Ar_{5000}^+, surface ionisation sources like Cs^+ or other liquid metal ion sources such as Bi_n^+ (n = 1-7). Using larger clusters offers a wealth of advantages over the monatomic ion sources such as improved mass resolution, secondary ion yields and surface sensitivity. Large clusters also reduce surface damage. This is particularly important when analysing complex samples and those that are easily deteriorated such as silicones, DNA and other biological structures. Bi_3^+ primary ion sources were used throughout this work.

When an insulator such as a polymer surface is bombarded with positively charged ions it gains a net positive charge. This is exacerbated by the emission of secondary electrons. This unwanted accumulation of positive charge can affect the function of ToF-SIMS by influencing secondary ion formation and therefore requires neutralising. This is achieved via an electron flood gun which provides the surface with a supply of low energy electrons.

ToF-SIMS is capable of providing spatial resolution of the data collected in the form of a chemical map. On selecting specific ions obtained from the analysis, the distribution of those ions across the surface can be seen. The size of the image depends on the size of the area analysed and each pixel of each image provides individual chemical information. This allows for regions of interest to be analysed. In this work 500 x 500 µm ToF-SIMS images of the coatings were acquired with 100 pixels/mm resolution. (**Figure 2.6**)

3D sample information can also be obtained using ToF-SIMS. This is achieved by obtaining spectra as the surface is eroded via an incident etching beam in a process known as depth profiling. [209] Each layer can be analysed separately allowing for the relative intensity of ions throughout the bulk to be analysed. 3D changes in chemistry through a larger section of the sample can be determined this way.

2.5. X-Ray Photoelectron Spectroscopy (XPS)

Electron spectroscopy for chemical analysis (ESCA) or as it is more commonly known XPS is a strongly surface sensitive technique which measures elemental composition and bonding environments of a given sample. XPS provides information on all elements aside from hydrogen and helium from approximately the top 10 nm of a surface. [210]

After the discovery of the photoelectric effect in 1887, which described electron emission from material after absorbing energy in the form of X-rays, it was applied to analysis in 1907. [211] X-rays are used to irradiate the sample and are generated by bombarding an anode with high energy electrons from a

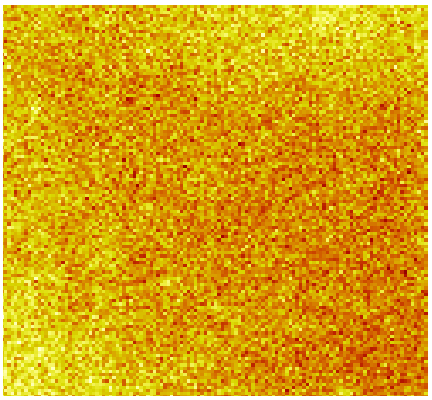

Figure 2.6. 500 x 500 µm ToF-SIMS total ion image of the surface of a silicone based polymer film obtained using an IONTOF IV instrument and SurfaceLab6 software.

heated filament. The anode is usually made of aluminium or magnesium. The X-rays penetrate through the sample and cause electrons to be ejected from core energy levels in near-surface atoms (**Figure 2.7**). It is necessary that the energy of the X- rays are sufficient to overcome the electron's binding energy (E_B) holding it towards the nucleus. Only a small number of electrons that are released from an atom lose no energy and this number decreases the further away from the surface the atom is. Despite the capability of X-rays to penetrate up to a distance of microns through the sample, this loss of energy of electrons through collisions means that only electrons from the top 10 nm are detected.

The energy of the X-ray source is known, therefore the binding energy of emitted electrons can be determined by measuring the kinetic energy of electrons that reach the detector using Einstein's equation:

$$E_B = h\nu - E_{bind} - \Phi \quad \text{(Equation 5)}$$

hν is the energy of the X-rays used and Φ is the spectrometer's work function. [208] According to the laws of quantum mechanics, binding energies for core electrons of any given atom are unique. Therefore XPS spectra can be used to determine the atoms present at the surface of a sample.

The constant removal of electrons from the surface of an insulating material naturally leads to charging effects. This causes the sample to gain a net positive charge. This in turn affects the spectra causing the binding energy of the

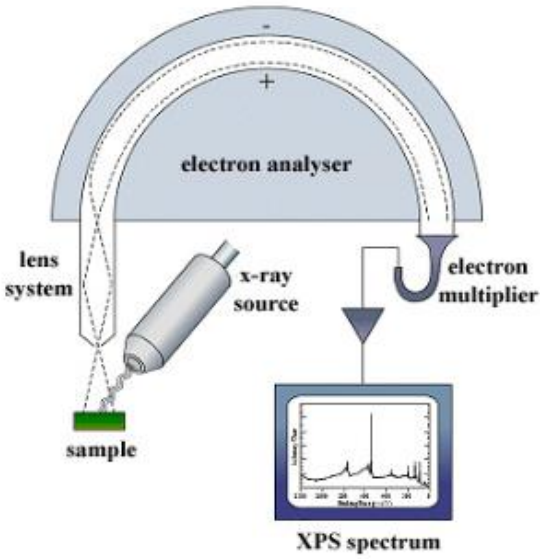

Figure 2.7. Diagrammatic representation of the process of analysis inside an XPS instrument.

electrons to shift. As in ToF-SIMS an electron flood gun is utilised to minimise surface charging. In the data process stage charge correction is also carried out, commonly shifting the data such that carbon atoms bonded to other carbon atoms are seen in a spectrum with energy of 285eV.

XPS spectra are usually acquired in two forms, a survey scan (or 'wide scan') (**Figure 2.8**) covering the entire energy range of 0 to 1000eV and high resolution scans (**Figure 2.9**) which normally concentrate on a range of energies corresponding to one specific element. These energies are plotted against the detected electron count per second of that particular energy (CPS). The area under the curve provides the relative quantities of each atom at the surface. High resolution scans are useful as they can be used to detect the specific local chemical environment of a particular photoelectron.

Minor shifts in binding energy are seen if an atom from a particular element is bound to a different type of atom. This is known as a chemical shift. (**Figure 2.9**) Carbon 1s core levels for example contain a number of component peaks due to carbon atoms existing in several different chemical states. If a carbon atom has a single bond to an oxygen a peak exists at a shifted 286.5eV as opposed to the standard C-C 285eV, a chemical short of 1.5 eV.

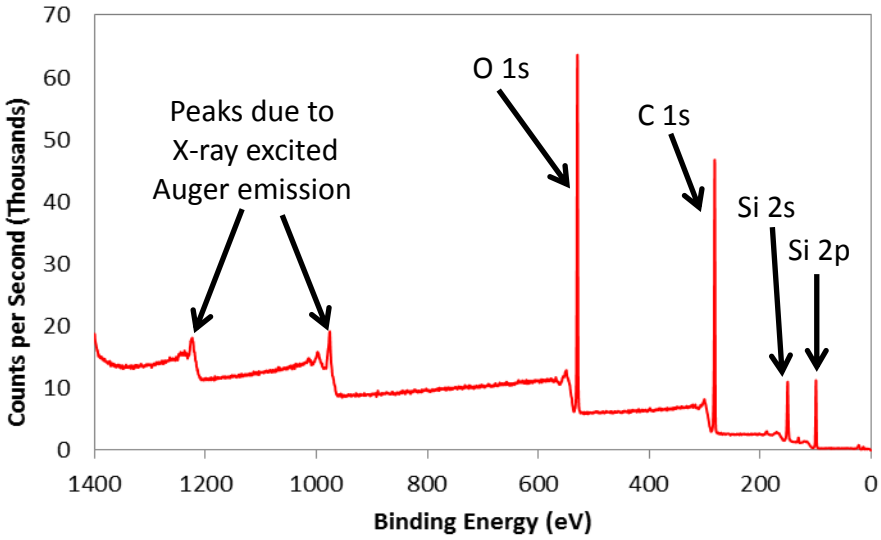

Figure 2.8 Survey spectrum or wide scan of a PDMS containing polymer material obtained via XPS.

These also provide quantitative information as to the total number of specific functional groups that exist at the surface of a sample. Therefore, a wide variety of information can be gleaned from closer study of particular elements. Adventitious hydrocarbons and surface oxidation products are common contaminants and therefore are often visible in XPS survey spectra so it is of utmost importance to handle samples for analysis with care. XPS like ToF-SIMS is also capable of taking measurements of the chemical make-up of the bulk of a sample. In this case Argon clusters from a Gas Cluster Ion Source (GCIB) can be used to etch through the sample. Changes in chemistry through the bulk can then be detected by producing a depth profile.

XPS analysis presented herein was undertaken using a Kratos Axis Ultra spectrometer (Manchester, UK). A monochromated aluminium X-ray gun was used (Al Kα = 1486.6eV). Survey spectra or wide scans were carried out at pass

energy 80eV (the energy allowed for given electrons to reach the detector slits). For high resolution scans 20eV pass energy was used for Si 2p, O 1s, C 1s and 80eV pass energy for P 2p, Ti 2p and Sn 3d.

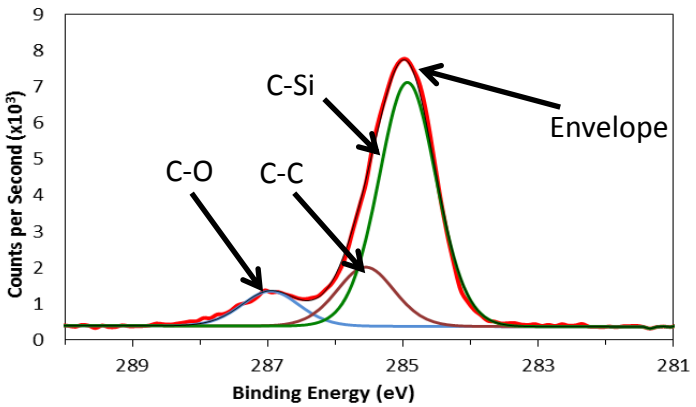

Figure 2.9. Example of a high resolution Carbon 1s XPS spectrum including fitted peaks for specific atomic environments.

Acquisition time for core levels was 10 minutes. All samples considered required charge compensation using default settings for polymeric materials. A charge neutraliser filament provided a flux of low energy electrons for uniform neutralisation. All measurements were carried out with a take-off angle of 90^{o} relative to the sample plane. Three different positions within the $1cm^2$ area were analysed for each sample. CasaXPS (UK) software version 2.3.16 was used to process the XPS data. Peak fit assignments were modelled with reference to a database of components related to the material components analysed.

2.6. Water Contact Angle Measurements (WCA)

WCA measurements provides a quantitative measurement of the wettability of a surface. This hydrophobicity or hydrophilicity information (if water is the solvent used) has been used in an attempt to determine the relationship between biological properties of a surface. [212, 213] Contact angle measurements for each sample were taken using 18.2Ω·cm miliQ water. A KSV CAM 200 computer controlled Optical Contact Angle Meter was used (Helsinki, Finland). The sessile drop method was employed using 2µL droplets of water. (**Figure 2.10**)

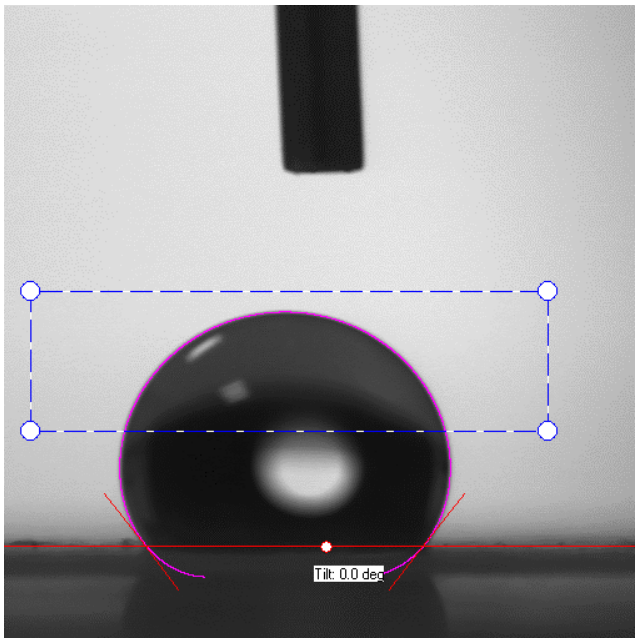

Figure 2.10. Circle fit of a profile of a 2µL droplet of water on PTFE tape. The circle fit displays a high contact angle of ~120^{o} indicating the surface is hydrophobic. The blue box is used by the software to calculate curvature of the droplet.

The side profile of the droplet extracted from the image was used to determine the contact angle. The profile is curve fitted to the Young-Laplace equation (Equation 6). The angle taken from each side of the droplet is averaged.

$$\sigma_{sg} = \sigma_{sl} + \sigma_{lg} \cdot \cos\theta \quad \text{(Equation 6)}$$

The contact is considered at the thermodynamics equilibrium of the three phases: solid, liquid and gas. This equation assumes a flat, rigid surface

2.7. Bacterial Incubation and Attachment Assay

Bacterial work was carried out using a *Pseudomonas aeruginosa* strain PA01-Nottingham containing plasmid pME6032ΔlaclQ::MCherry Tc resistant for constitutive expression of mCherry fluorescent tag. mCherry plasmids were expressed in these bacteria. This was selected over green fluorescent protein as there is less autofluorescence observed. These transformed strains of bacteria were streaked onto Luria Bertani (LB) agar plates (Oxford, UK) and grown overnight in a 37^{o}C oven. Sterile plastic loops were then used to remove a

single colony of bacteria and this was placed into 10mL of LB broth. This was then cultured at 37^{o}C 200RPM overnight. This overnight culture was then centrifuged at 9995RPM for 10 minutes at 22^{o}C. This separated the media from the bacteria allowing it to be removed and replaced with 10mL of RPMI-1640 (Sigma, UK). These bacteria were then resuspended in this RPMI by vortexing the mixture. The centrifugation and resuspension steps were repeated to entirely remove the LB media from the bacterial culture.

All samples were UV-sterilised for 10 minutes prior to exposure to bacteria. The slides were then incubated in 15 ml of RPMI-1640 containing diluted bacteria suspended in the RPMI medium (OD^{600} = 0.01). The samples were left for bacteria to grow at 37 ^{o}C and shaken at 60RPM for 72 hours. After this time period the slides were removed and rinsed two times using sterile phosphate-buffered silane (PBS) and once in sterile deionised water. Confocal microscopy was then used to image the samples.

2.8. Fluorescence Confocal Microscopy

Fluorescence confocal microscopy is used to look at chemical compounds which fluoresce when they are illuminated at specific wavelengths of light. These chemicals are known as fluorophores. High energy light is used to excite the fluorophore which then absorbs the energy and emits a lower energy light. [214] This longer wavelength light is then identified by the detector and an image can be formed. Confocal microscopy allows for high resolution and contrast imaging by improving the signal to noise ratio. [215]

Initially a laser light source of a certain wavelength illuminates the sample and a dichromatic mirror reflects the laser light towards the sample (**Figure 2.11**). This mirror allows longer wavelength emitted light to pass through to the detector. The objective lens focusses the excitation light onto the sample and the emitted light onto the detector. In order to stop scattered light potentiall causing unwanted photo-bleaching, confocal microscopes use pinholes to block the scattered light from above and below the focal planes. [214] If the pinholes

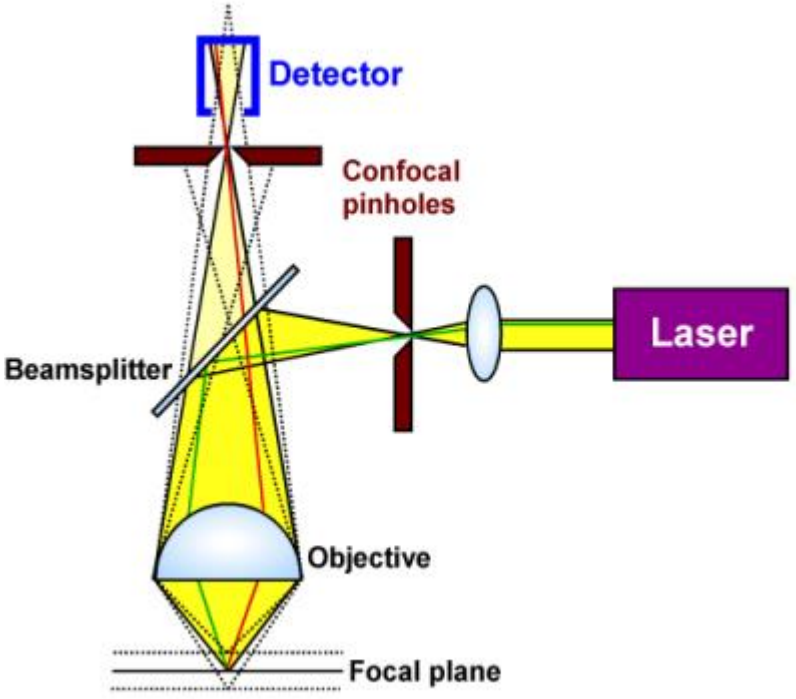

Figure 2.11 Schematic of the basic components of a confocal microscope [216]

are too small a large portion of the total fluorescence signal may be blocked, too large and the resolution decreases. Therefore a photomultiplier is used to amplify the total amount of fluorescence signal from the sample. At this point gain and exposure time must be used wisely in order to increase sensitivity sufficiently without increasing background noise. Cross sections of a sample can be taken and combined in the z axis to construct 3D images of the total sample.

A Zeiss LSM 700 fluorescent confocal microscope (Carl Zeiss, Germany). A 555 nm laser was used as the excitation source to detect mCherry labelled PA01 bacteria with ZEN 2009 imaging software.

2.9. Differential Interference Contrast Microscopy (DIC)

Transparent, unstained biological specimens are difficult to observe using classical phase contrast microscopy due to the presence of halo artifacts. Differential Interference Contrast Microscopy or Nomarski Interference Contrast microscopy is an optical microscopy technique able to distinguish

features in biological samples by exploiting differences in the refractive index of the components that comprise it. This variation is detected by using a specimen and a reference light ray and determining the phase difference between the two. [217]

This method ensures that clear images can be produced when analysing thick samples as well as improved overall resolution as compared to phase microscopy. The fact that the samples do not need to be stained or prepared in any particular way means that biological processes are less impeded than if they were to be altered in such a way prior to analysis.

Initially unpolarised light from a 100W tungsten-halogen lamp enters the microscope and is polarised at 45^{o}. It then enters the first prism a 'Normaski-modified Wollaston Prism' made of quartz and the two rays of light are separated polarised perpendicular to each other (**Figure 2.12**). These are the specimen and reference lights. The condenser focusses these two points onto the sample such that they pass through points adjacent to each other, one through the sample and one through the background. The separation of these two points is usually similar to the resolution of the microscope's objective lens (~0.2μm). This alters the optical path length of the sample if there are differences in sample thickness or refractive index. These rays then travel through an objective lens and are focussed onto a second prism. This combines the two light rays into a single polarised beam at 135^{o}. This is known as differential interference.

After polarisation, the beams of light can interfere with each other. The rays of light have different phases with each other due to the differences in optical path lengths from the different sample points. Recombining this light generates the observed image which displays a contrast between the optical path lengths. This is usually displayed as differences in brightness between different points with the sample appearing brighter than the background. The image often presents a 3D appearance but this does not necessarily represent the true

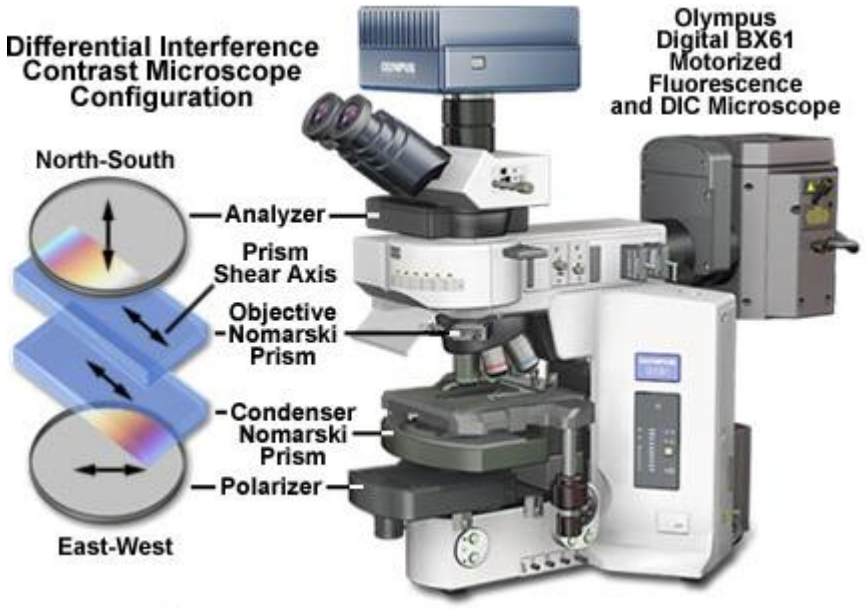

Figure 2.12 Diagram of a Differential Interference Contrast Microscope. [218]

situation, it is more an optical feature than true geometric relief.

DIC is capable of investigating biofilm formation as an imaging technique by taking individual stills and also tracking real time changes in bacterial movement through videos. [219, 220]

The work presented in this thesis was carried out using a Nikon Eclipse Ti 2000 (Tokyo, Japan) inverted DIC at 40x magnification in bright field mode operating at 50Hz. 620 x 620 µm areas were taken.

Chapter 3

Surface Characterisation of Polymer Films

3.1. Introduction

Poly(dimethyl Siloxane) based polymers have shown potential for use as foul-release coatings due to their low surface energy. The coating devised by *Dow Corning* is a PDMS-Polyether block copolymer (**Fig 2.1.**) that is trimethoxysilyl-terminated and can be cross-linked by a range of catalysts and drying agents. The surface of the polymer is where interactions with bacteria occur therefore it is essential that the surface chemical and physical details are known. These can then be corroborated with biological data. Further necessary information to determine includes how the concentration of the catalysts affects the speed of drying of the coating and whether this alters the surface properties. The temperature of the drying conditions used may also change the appearance of the coating's surface. In order to comply with the desired characteristics of a marine anti-fouling coating put forth by the Naval Sea Systems Command it is necessary that the coating is smooth, durable and has a simple application method. [81] If coatings are not smooth then there is an increased surface area for bacteria to adhere to. Lab-based techniques can be used to apply the coatings to glass, and the surface characterised to give an indication as to whether these application methods can be scaled for use in industrial environments.

3.1.1. Aims

The aim of this work was to use a reproducible method for applying coatings to a surface and to analyse their chemical and mechanical properties. It was the objective to create featureless coatings and analyse them using optical observation and imaging techniques such as SEM and AFM to confirm the suitability of these deposition methods. The consistency of the coating across the surface was also to be analysed chemically by determining the uniformity

of the chemistry across the surface using ToF-SIMS and XPS and whether changes in catalyst affected the surface chemistry.

3.2. Methods

3.2.1. Coating Preparation

ThermoFisher scientific glass slides (Massachusetts, US) were cleaned using a methylethyl ketone solvent. Each of the six coatings described above (**Methods 2.2.**) were then applied to these glass slides using a draw-down paint applicator to create uniform 100µm thick coatings. This thickness was chosen to allow for a range of tests to be done on them. These coatings were devised by mixing the relative amounts of the PPR with a catalyst using an over the top stirrer to enable moisture in the air to aid with cross-linking in a condensation reaction. For SEM analysis the coatings were sprayed onto plastic stubs using an airbrush on a high flow setting for five seconds. For ToF-SIMS analysis the spray-gun was used to apply the coatings to glass cover slips.

3.2.2. Scanning Electron Microscopy

Imaging was carried out using an FEI Quanta 200 3D Dual Beam FIB-SEM operated at either 15 or 20kV. The electron beam was rastered over the sample surface and the resulting backscattered electrons and secondary electrons were collected. All the samples were initially coated with carbon for 25 seconds using an Agar Turbo Carbon coater to prevent charging in the instrument chamber.

3.2.3. Atomic Force Microscopy

The surface of the coatings were analysed using a Bruker Dimension Icon® AFM (BruckerNano, Santa Barbara, US) using PeakForce QNM® mode. Bruker MSNL-F tips were used for imaging experimentation (silicon tip/nitride lever) with a 0.97 N/m spring constant (calculated via the Sader method) and a

resonant frequency of 116.29 kHz. [219, 220] Three different areas were scanned on each sample with the field of view ranging from 50 nm to 20 µm. All images were flattened to remove curvature and slope using *Gwyddion – SPM Data Analysis* software. Root-mean-square (rms) values for roughness were calculated using an average of at least five measurements over areas of 1 µm x 1 µm. For force measurements, an RTESPA tip with a 27.7 N/m spring constant and 314.47 kHz resonant frequency functionalised with a 21µm diameter glass bead was used. 2 x 156 force curves were taken over two separate 60 µm areas with an Asylum MFP-3D AFM. Nanomechanical attributes were calculated using a Microsoft Excel macro designed by Xinyong Chen (Nottingham, UK). [221] The DMT model was used to calculate Young's modulus via the slope from the retract curve.

3.2.4. Pendulum Hardness

A Sheen (Cambridge, UK) pendulum hardness rocker was used to evaluate the strength of the coatings resistance to changes in its shape. The rocker determines relative hardness between samples by measuring the number of swings required to damp the triangular pendulum oscillating over the surface.

3.2.5. Water Contact Angle

A KSV CAM 200 computer controlled Optical Contact Angle Meter was used to determine the wettability of the surface of the coatings (Helsinki, Finland). A 2 µL 18.2 Ω·cm miliQ water droplet was placed onto the surface using the sessile drop method. 3 images 3 seconds apart were captured per 2 µL water droplet applied to the surface. The second image of the set was analysed computationally using the CAM 200 software via the Young equation which is able to calculate the contact angle using the three phase boundary values: γ_{lg}, γ_{sg} and γ_{sl} where s is solid, l is liquid and g is gas. The second image was selected to obtain the most accurate results when the droplet had settled on the surface. This was repeated across five different areas of the sample with five

repeats taken (n=25). The temperature and humidity remained stable for the entire run, between 21.7-22.7 ^{o}C and 33.5-36.5% RH respectively.

3.2.6. X-Ray Photoelectron Spectroscopy

XPS was carried in a Kratos Analytical Ultra photoelectron spectrometer with a mono-chromated Al Kα X-ray source (1486.6eV) (Manchester, UK). Survey spectra or wide scans were carried out at pass energy 80eV. Core level (high resolution scans) were carried out at 20eV pass energy for Si 2p, O 1s, C 1s and 80eV pass energy for P 2p, Ti 2p and Sn 3d. Acquisition time for core levels was 10 minutes. All samples considered required charge compensation using default settings for polymeric materials. A charge neutralizer filament provided a flux of low energy electrons for uniform neutralisation.

All measurements were carried out with a take-off angle of 90^{o} compared to the sample. Three different positions within a 1cm^2 area were analysed for each sample. CasaXPS (UK) software version 2.3.16 was used to process the XPS data. Peak fit assignments were modelled with reference to a database of components related to the material components analysed. [223, 224] High resolution carbon scans were used to charge correct the entire spectrum to C-C at 285.0eV. For quantification the relative sensitivity factor was set at 0.278. Dr Emily Smith helped to run the equipment for this experiment.

3.2.7. Time-of-Flight Mass Spectrometry

ToF-SIMS was conducted using an ION-TOF IV (Münster, Germany) instrument operated using a Bi_3^+ primary ion source at 25keV. This was carried out in bunched mode. A 1pA primary ion beam was rastered across the sample, collecting positive and negative secondary ions from a 100x100 μm area of each slide for a 10s acquisition duration. This was repeated three times in both positive and negative polarities. Static SIMS conditions were established by maintaining the primary ion dose below 10^{12} ions/cm^2. Charge compensation was applied using a low energy electron flood gun due to the polymeric,

insulating nature of the sample. Accurate mass assignment was carried out using a high resolution ToF analyser. ION-TOF's software SURFACELAB6 was employed for data process. Assignments of secondary ions were made with reference to a database of secondary ions related to the material components analysed. [225, 226] Dr David Scurr helped to run the equipment for this experiment.

3.3. Results

3.3.1. Macroscale Appearance and Optical Microscopy

After the coatings were left to dry overnight it was necessary to assess their appearance by inspection. Obvious defects or issues with applying coatings are likely to decrease the coating's ability to act as an effective anti-foulant. [22] This is particularly true considering the complications of applying the coating to a larger sea-faring vessel in a scaled up process. **Figure 3.1** (*Upper*) displays an example of the coating (formulation **1**) after being applied to a glass slide by either a paint applicator (*Left*) or spray gun (*Right*). These samples were representative of all the six formulations on their respective substrates. The applicator deposited coatings appeared transparent and relatively smooth with no air bubbles or visible defects. For the coatings applied using the spray gun there were visible air bubbles and though the coating had limited defects, they were less homogenous across the surface. Again, all of the samples deposited in this manner were similar in this respect. All coatings were dry at the point of inspection. The entire process from weighing of the reactants to their application onto substrates took five minutes. Cleaning of the applicators and mixing vessels had to take place immediately as all of the coatings dried quickly.

Most of the coatings could be applied to the glass relatively easily aside from coating formulation **3** (cross-linked using TnBT) which cross-linked at such a rapid rate that it became difficult to apply physically using the applicator. It was also more viscous at the point of application than the other coatings which often blocked the spray gun and therefore took repeated attempts to achieve a desirable layer on the glass.

Optical microscopy (**Figure 3.1** (*Lower*)) was used to corroborate visual inspection of the coatings. In the combined image the majority of the coatings

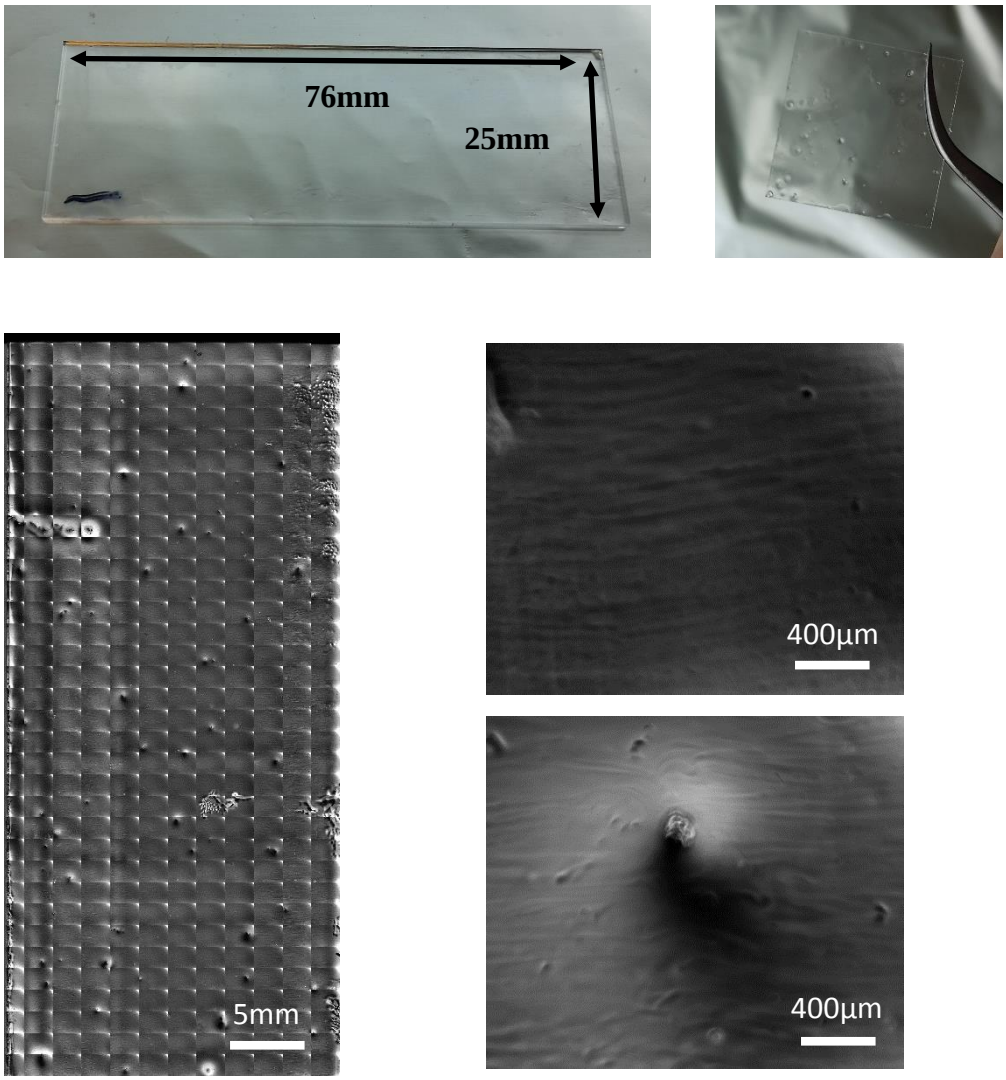

Figure 3.1. (*Top Left*) Photo of a glass slide after having PPR coating applied using a paint applicator. (*Top Right*) Photo of a glass cover slip after PPR resin has been applied using an airbrush. (*Bottom Left*) Optical microscope images stitched together to demonstrate coverage across an entire glass slide of PPR. (*Middle Right*) Individual image of a less featured region of the same coating. (*Lower Right*) Different area of the same sample featuring aggregations, lumps and other coating inhomogeneity.

were seen to be comprised of a flat, featureless surface. Some ‘bumps’ were present on the surface of the sample. Other minor defects included surface aggregates of amorphous appearance and small perforations. The defects were most prominent at the edges of the slide. Also, in the defect-free images there were some clear lateral grooves which were not straight and extended across the whole sample.

3.3.2. Scanning Electron Microscopy

SEM was used to confirm the details gleaned by optical microscopy. SEM offers superior magnification and resolution to optical microscopy making it well suited to this task. It was also better able to analyse the samples which were sprayed onto the surface as opposed to physically applied. **Figure 3.2** displays electron micrographs of these coatings which were sprayed onto plastic SEM stubs. The images in the left hand column of **Figure 3.2** are characteristic of all the coatings aside from formulation **3** which are displayed on the right. The coatings appeared flat and homogenous across the surface. The majority of the coating was defect free though there were examples of imperfections similar to the bumps seen in the optical microscopy images (**Figure 3.2 (***Bottom Left)*). There was also some cracking of the coating at the edge of the stub. For formulation **3** the coating appeared incomplete with many imperfections across the surface such as folding over and under itself. Large cracks and creases could be seen as well as the appearance of other assorted amorphous shapes (**Appendix 9.1**)

3.3.3. Atomic Force Microscopy

AFM was used due to its ability to discern differences in topography at the nanoscale as well as providing mechanical detail of the materials. In **Figure 3.3** (*Top Left*) an AFM image depicts a perforated network structure which was not seen in SEM. The majority of images in lower magnifications (5µm image size and above) showed a flat, homogenous surface with limited detail (**Figure 3.3** (*Top Right*)). Some images of those coatings using higher concentrations of catalyst however did demonstrate the presence of similar defects to those seen in the other forms of microscopy (**Appendix 9.2**). The changes in height across the surface were extracted as a map of quantitative results to show the range of

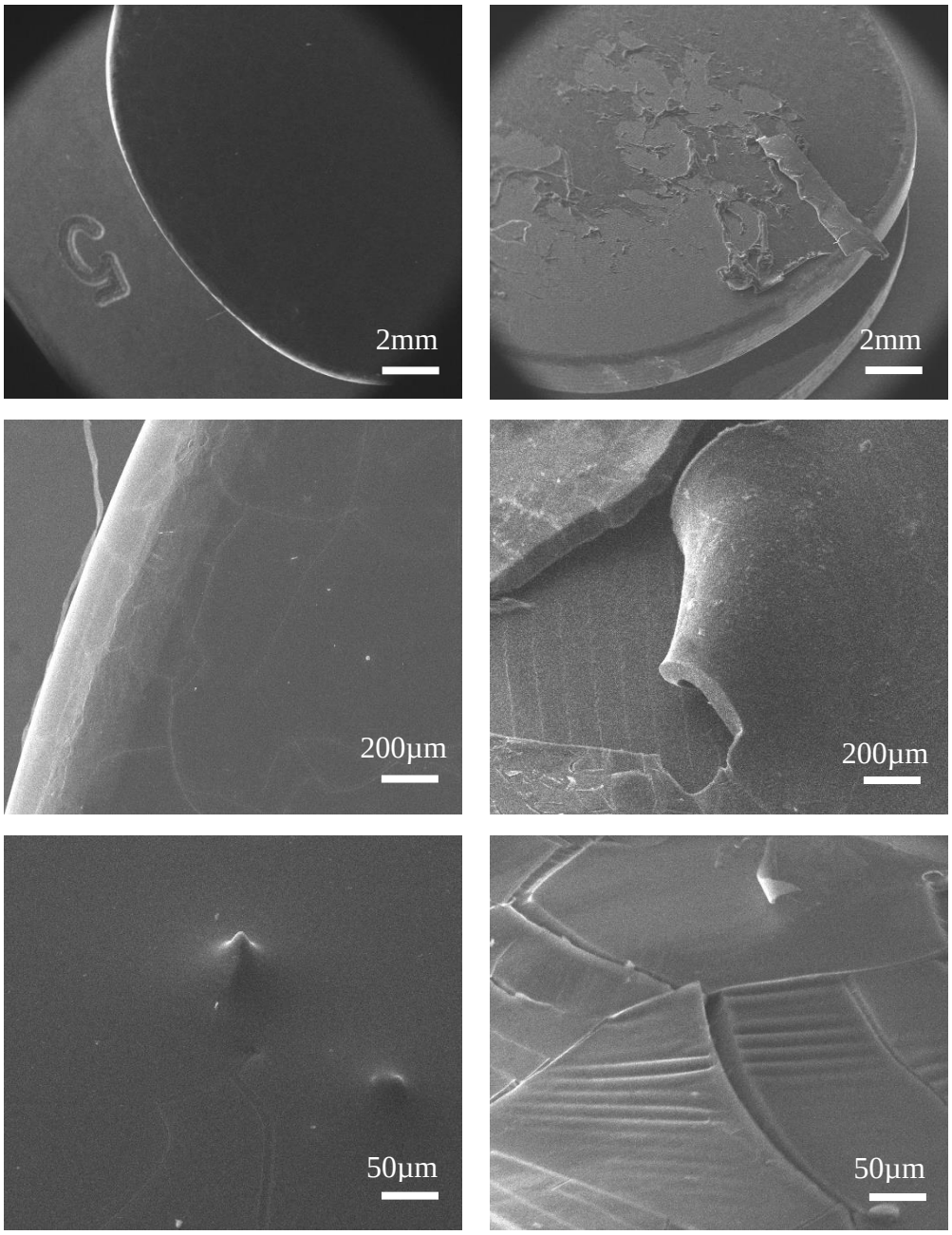

Figure 3.2. Scanning electron micrograph images of PDMS based coatings sprayed onto a plastic stub. (*Left Hand Column*) Representative images of all coatings aside from the resin which was cross-linked using only the TnBT catalyst. The images show a homogenous, smooth, relatively defect free coating across the surface of the stub. Minor defects may be due to the difficulty in controlling the rate of coating deposition with the spray gun. (*Right Hand Column*) Representative images of the coating cross linked using just the TnBT catalyst. The coating is incomplete across the stub with major imperfections such as cracking and folding.

heights across the sample (**Figure 3.3** (*Bottom Right*)). This was translated into root mean square (RMS) roughness data (RMS = 4.56 nm).

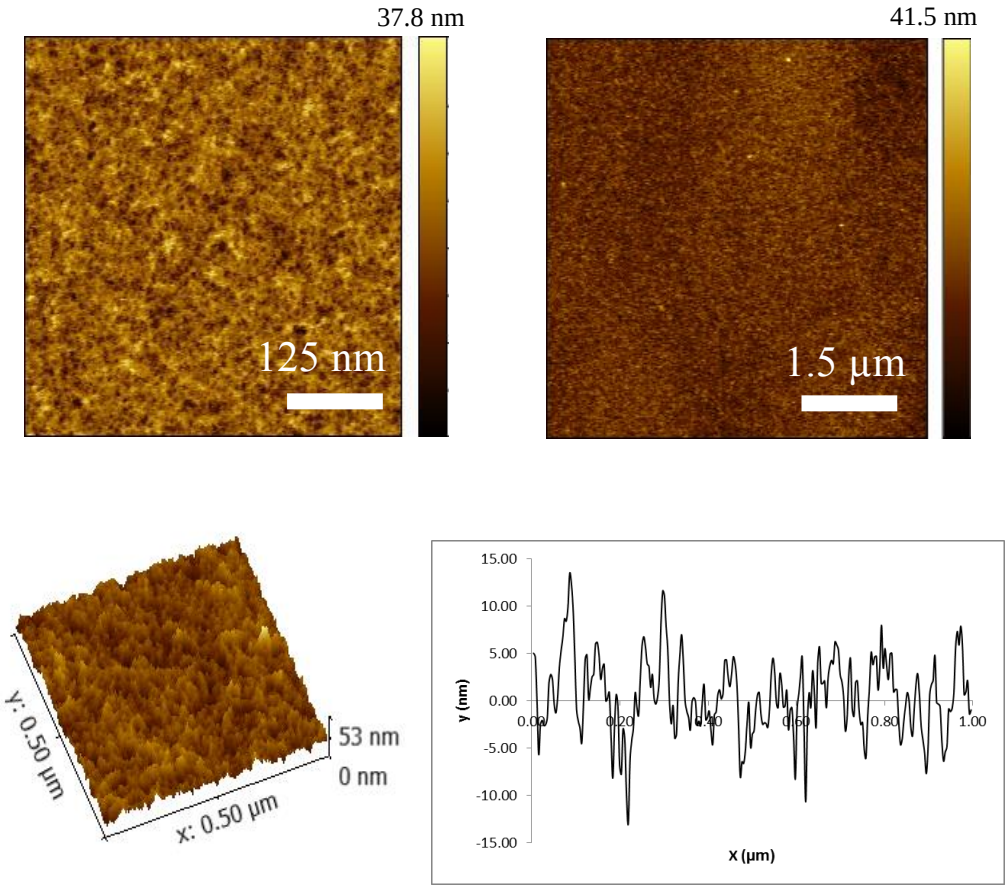

Figure 3.3. (*Top Left*) 500 x 500 nm AFM height image of PDMS coating cross-linked using octylsilyl phosphonate. Depicts a fine, pore-like network surface structure at the nanoscale. (*Top Right*) 5 x 5 µm of the same surface in a different area. Demonstrates a flat, defect free homogenous surface. (*Bottom Left*) 3D visualisation of the 500 nm image. (*Bottom Right*) Height profile extracted from a 1 x 1 µm image. Shows limited variation in height across the surface (RMS = 4.56 nm).

Mechanical data was also obtained in the form of force curves (**Figure 3.4** (*Top*)). These curves, which detail the forces experienced by the AFM probe as it approaches, indents and then retracts from the coating were not linear and the pull off region at the base of the curve suggests that the surface has adhesive properties. The entire length of the ramp, or the total distance moved forward and backward by the tip was six microns. Extracting the quantitative data from the curves showed that the Young's Modulus of the coatings range from 35 to 60kPa with the titanium catalysed coatings being generally harder, between 50 and 60 kPa and the phosphorus coatings between 30 and 40. The work of adhesion to pull the tip from the surface was between 155.3 and 204.23 $pJ.m^{-2}$. The contact area was estimated using the bespoke macro. QNM mode was used

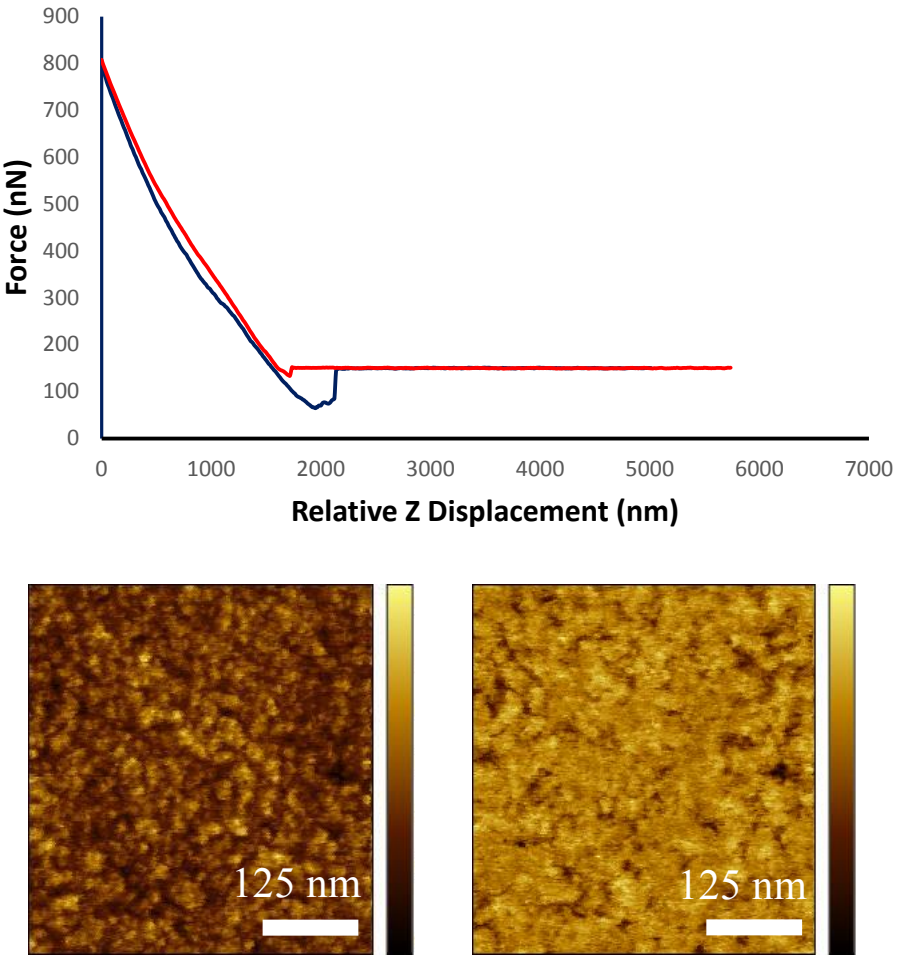

Figure 3.4. (*Top*) Characteristic force vs displacement curve of each of the coatings demonstrated by the 900c cross-linked coating (red tip approach and blue tip retract). (*Bottom Left*) 500 x 500 nm adhesion map of the same coating using force mapping. Limited variation across the sample can be observed (*Bottom Right*) 500 x 500 nm stiffness map of the same coating using force mapping. Again the properties are consistent across the surface.

Table 3.1. Comparison between each coating of the number of swings required before the pendulum on the hardness rocker was fully damped. Coatings containing SiDA were likely harder due to the preference of dense 3D networking when using such a drying agent.

Number	Formulation	Swings
1	900c	8
2	900c / SiDA	37
3	TnBT	18
4	TnBT / SiDA	27
5	TnBT / Sn Octate	18
6	TnBT / Sn Octate / SiDA	36

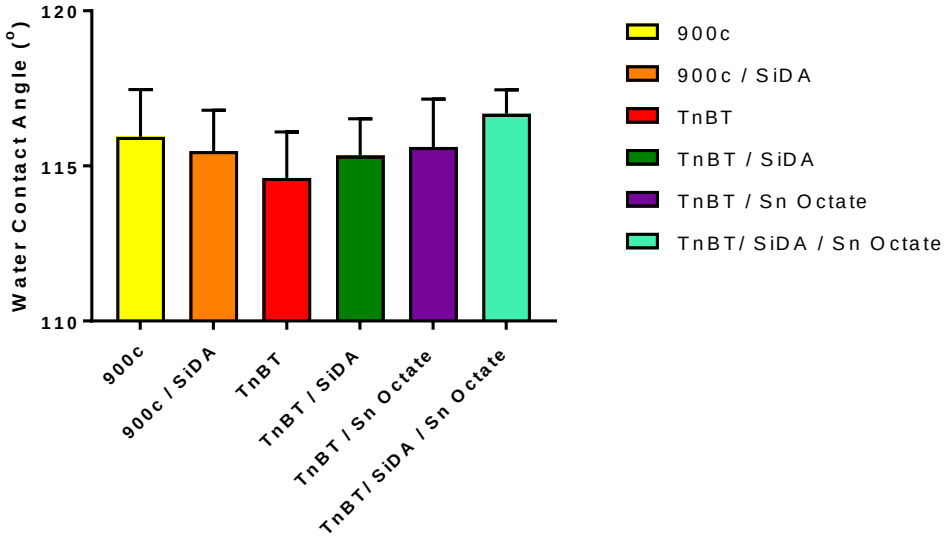

Figure 3.5. Water contact angles of each coating formulation (n=25). All six coatings demonstrated high water contact angles above 110° but there are no significant differences in contact angle discernible between the samples. Error bars were calculated using the standard deviation of the values recorded.

to determine the consistency of the mechanical properties across the surface (**Figure 3.4** (*Bottom*)). For both the stiffness and adhesion maps of the coatings, these properties appeared to be uniform with limited variation. The minor differences between individual regions correspond to those changes seen in the topography of the surface.

3.3.4. Pendulum Hardness

To compare macroscale mechanical properties to that on the nanoscale a pendulum hardness rocker was used. The number of swings taken to damp the pendulum are displayed in **Table 3.1**. The coatings which were cross-linked using the SiDA took the longest to fully stop the pendulum rocking. The coating containing just 900c took the shortest amount of time to damp the pendulum, indicating it is the softest coating. The coating which had TnBT as its cross linking catalyst was harder than the 900c coating alone. The addition of SnO as a drying agent with or without SiDA made no difference to the number of swings taken to damp the pendulum.

3.3.5. Water Contact Angle

To determine the surface wettability of the coatings, WCA was used. After applying a 2μL drop of water to the coatings, an average contact angle of above 110^{o} was observed for all of the coatings. The values for each of the coatings can be seen in **Figure 3.5**. Coating formulation **6** demonstrated the highest WCA on average (~117^{o}). However, the error of the samples overlap such that there is no significant difference between the coatings, all having their mean values within one standard deviation of each other.

3.3.6. X-Ray Photoelectron Spectroscopy

To understand the chemistry of the surface and to attempt to correlate it with the physical data obtained, XPS was used. **Figure 3.6** (*Lower*) compares the relative elemental composition of each element at the surface. Carbon is seen to be the most abundant element at around 58% of the total surface composition. Oxygen contributed a 23% atomic percentage with silicon making up the rest of the total. The contribution of tin, phosphorus and titanium core levels could not be detected. In comparison to the bulk composition, predicted by the elemental composition of the polymer as a whole, more carbon was seen at the surface at the expense of silicon. This bulk measurement was calculated by determining the relative concentrations (atomic percentage) of the resin from its structure (**Figure 2.1**) as well as the contribution from the cross-linking catalysts. Oxygen content was similar to its predicted level (~25%).

High resolution spectroscopy was used to identify the functional composition of the surface. **Figure 3.7** depicts a carbon peak which has been fitted with additional regions under the main curve. The synthetic peaks under this curve at 284.5, 285.5 and 287eV represent the contribution to the carbon peak of C-Si, C-C and C-O electron environments respectively. The large area under the C-Si curve demonstrates that the majority of carbon atoms detected are bonded

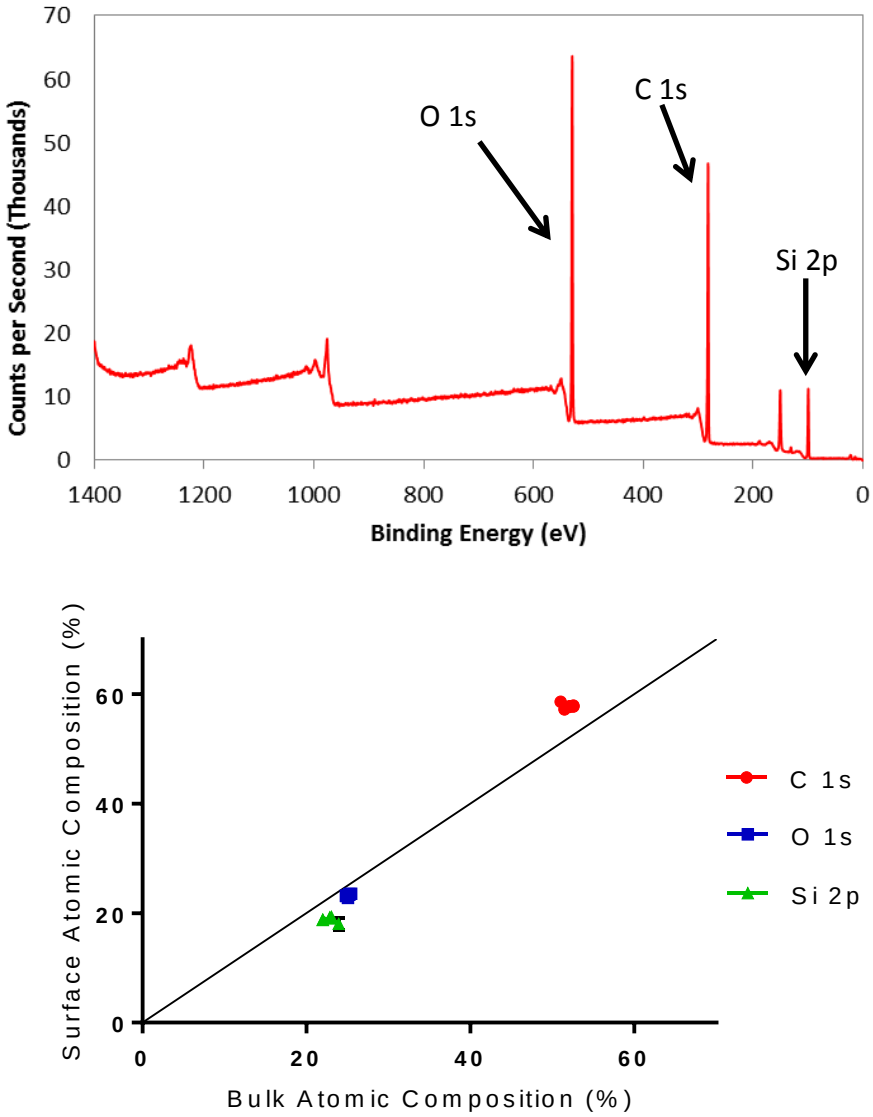

Figure 3.6. (*Upper*) Representative wide scan of the PDMS based coating. Prominent carbon 1s, silicon 2p and oxygen 1s peaks are present. No discernible peaks for Ti, P or Sn are seen. (*Lower*) Graph displaying measured surface elemental composition vs predicted bulk concentration for all six of the coatings. C 1s concentration higher than predicted likely due to increased presence of methyl groups in PDMS at the surface.

Table 3.2. Elemental composition of each coating formulation determined via XPS.

Atomic Percentage	O 1s	C 1s	Si 2p
Sample			
900c	22.95	57.37	19.68
900c/Z6040	23.19	58.01	18.80
TnBT	23.18	57.70	19.12
TnBT/Z6040	23.81	57.48	18.72
TnBT/SnO	23.02	57.80	19.17
TnBT/SnO/Z6040	23.33	57.72	18.94

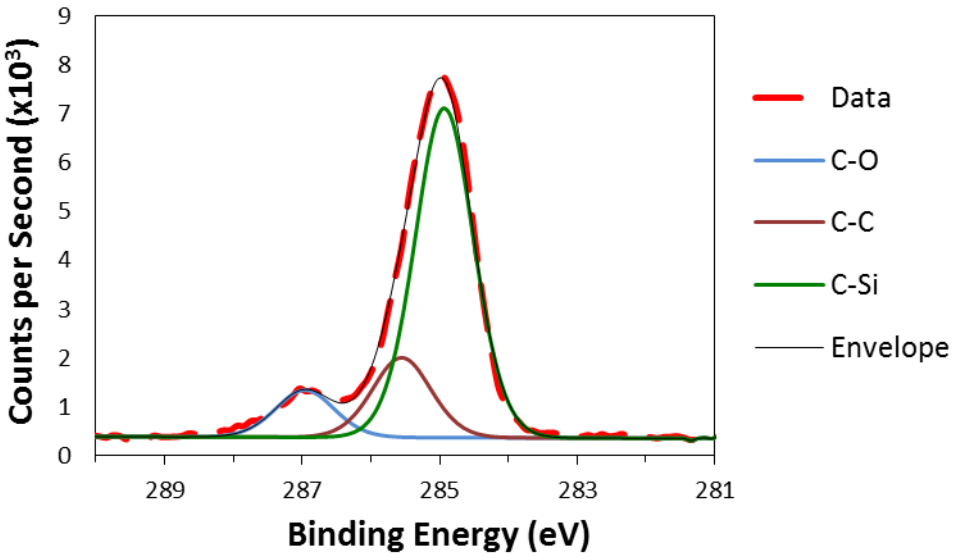

Figure 3.7. Component fitting of a Carbon 1s XPS high resolution scan of the amphiphilic coating formulation **1** cross-linked using a phosphorus based catalysed. The scan was taken at a 90^{o} electron emission angle. Scan representative of each of the carbon peaks from the core levels of each coating formulation. The most common atom identity is that of C-Si, demonstrating predominantly PDMS at the surface. C-O shoulder peak at ~287 likely due to the contribution of PEG.

to silicon atoms. The presence of a shoulder at 287eV demonstrates the significant presence of carbon bonded to oxygen.

3.3.7. Time-of-Flight Mass Spectrometry

To complement and compare the chemical data obtained using XPS, chemical fragment information of the coatings was collected using ToF-SIMS. **Figure 3.8** (*Top*) is a representative mass spectrum of the coating cross-linked using TnBT, highlighting particularly intense peaks at 73^{+} and 147^{+} m/z which are indicative of PDMS. [225] There are also clear peaks at 45^{+} and 133^{+} m/z which imply a presence of PEG. [226] Peaks at 63^{-} and 79^{-} were seen in the coatings cross-linked using 900c indicating the presence of PO_2^{-} and PO_3^{-} respectively as their catalyst due to the presence of phosphorus and phosphoric acid as a product of the cross-linking process. (**Figure 3.8** (*Middle*)). These peaks were absent in the TnBT catalysed coating. Conversely for the coatings cross-linked using TnBT, peaks which are associated with Ti^{+} ions such as those at 48^{+} m/z were not be seen in their respective spectra.

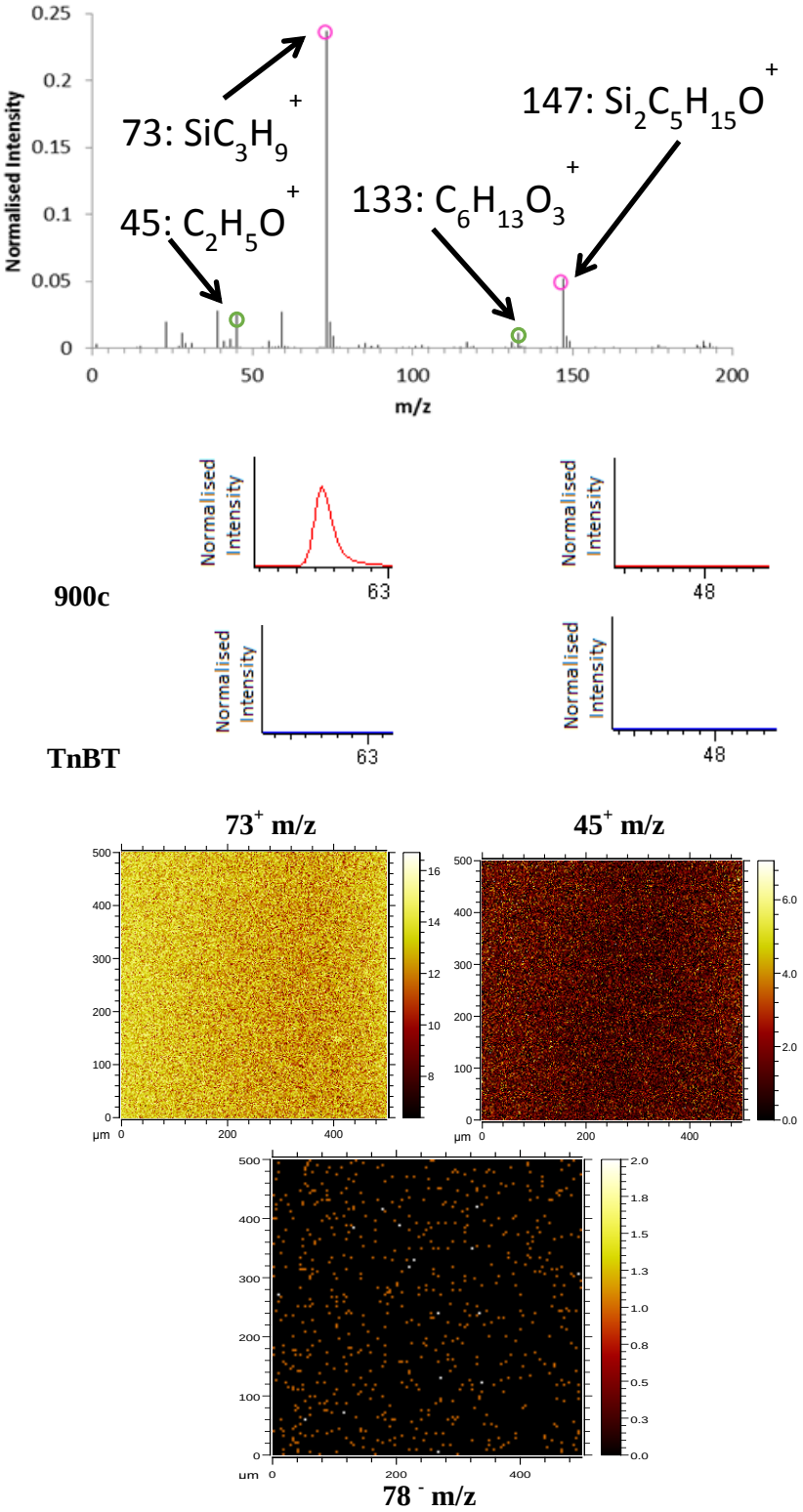

Figure 3.8. (*Top*) ToF-SIMS spectrum of TnBT catalysed coating. Major peaks due predominantly to PDMS influence. PEG presence can also be seen clearly. (*Middle*) Comparison of isolated peaks which denote presence of the phosphorus catalyst (PO_2^- at 63 m/z) and the titanium catalyst (Ti^+ at 48 m/z) between the different samples. Phosphorus does not appear in the coating which is cross-linked using a Ti-based catalysed. Titanium does not appear in either coating, likely due to the inherent problems of ToF-SIMS in detecting heavy metals. (*Bottom*) from top left to bottom, ToF-SIMS images of representative ions for PDMS (73^+), PEG (45^+) and phosphorus-based 900c (79^-) for the coating formulation containing 900c. The images demonstrate homogenous chemistry across the surface.

The coverage of the chemistry across the surface was analysed using ToF-SIMS imaging. **Figure 3.8** (*Bottom*) demonstrates homogenous coverage of representative PDMS, PEG and 900c ions respectively. The PDMS image is the most saturated image, with the highest intensity of that particular ion across the surface. Phosphorus ions are the lowest in overall intensity across the surface of the three major chemical components.

3.4. Discussion

3.4.1. Application and Appearance

Initial inspection of the coatings suggested that using a paint applicator to deposit the films onto glass slides led to a smoother, more defect-free coating being produced in comparison with using an air gun. Most defects viewed in optical microscopy were at the edges of the slides, likely just artefacts of the drying process as the edge is perpendicular to the coating plane. In the higher magnification images, bumps in the surface were apparent. This could be for one of two reasons. Firstly the applicator must be used manually so drawing down the coating across the glass slides may not have been as consistent as would have been required to create a fully flat surface on the microscale. The presence of irregular grooves across the surface also supports this theory. Secondly, there may not have been consistency of distribution of the catalyst with the resin in the stirring process which would mean some areas may have catalysed and hardened at a less controlled rate. This suggests the deposition process using the applicator is not necessarily as accurate down to a scale that would be desired.

For the coatings that were applied to a glass cover slip to using an air-gun there were air bubbles seen across the dry coating. This may have occurred as the spray gun requires a pressurised air propellant to be applied to the coating in order to discharge it from the gun. It was also difficult to control the thickness of the coating as the air gun offered limited control other than the speed of propulsion of the ejected mixture. As the spraying had to be done manually it was difficult to create a totally uniform coating. Bubbles were less prevalent in

the coating applied to the plastic stubs as seen in the SEM images. This could either be due to the difference in hardness of the surface of each substrate or that the glass cover slip is double the size of the plastic SEM stub. This may have allowed the propellant to further affect the physical deposition process. The SEM images also showed the presence of lumps, again likely to be consequences of the drying process. Given their presence in coatings regardless of their application method it suggests that the most likely explanation for such defects is the lack of homogenous distribution of the catalyst in the reaction mixture. This can further be asserted by the comparison of the stiffness of these features in AFM compared to the surface as a whole. These features are seen as being significantly stiffer in the QNM images.

The coatings which were cross-linked using TnBT alone at 5% (w:w) produced the least consistent coatings across the surface of substrates. The faster speed at which these coatings dried made their application using a spray gun more difficult as they became viscous and blocked up the nozzle. Even when they were applied before drying they produced incomplete coatings containing numerous defects as seen in **Figure 3.2** (*Right*). The cracking was mostly at the edge of the sample where the sharp perpendicular curves makes applying a consistent coating a particular challenge. Given this occurred on several samples it is more likely that the higher concentration of the catalyst caused these inconsistencies. The other coatings using TnBT as a cross-linker produced just as consistent coatings as those using 900c so it is more likely that the concentration of this particular catalyst being too high in formulation **3**. Increasing the concentration of a catalyst whether 900c or TnBT increased the number of these aggregate features so this would suggest that this is the most likely explanation for the presence of such features.

In higher magnification AFM imaging, all the coating's surfaces showed a fine somewhat porous networked structure, likely resulting from the cross-linking process. This nanostructure did not change when the different coatings were dried at 4 and 50^{o}C. Therefore the catalyst used to develop the films is likely to be the most important variable with regards to the final properties of these coatings.

3.4.2. Physical Properties of the Coatings

Biofouling is exacerbated with increasing surface area which increases as a result of roughness, so limiting the value of this parameter to nanometres is desirable for an effective coating. Roughness can also affect WCA measurements. Surfaces are generally not 'ideal' so it is necessary to understand whether a coating fits the Wenzel or the Cassie-Baxter models in order to correct for roughness artefacts affecting surface contact angle. Non-ideal surfaces do not fit the Young equation which assumes a flat smooth surface and therefore the surface character can affect the contact angle in ways that can make the WCA results difficult to interpret. The fact that the droplet size used (2μL) was two to three orders of magnitude greater than the roughness ratio of this surface (≥ 1) means that roughness did not affect the WCA measurements significantly. Therefore the measured contact angles can be assumed to be reasonably accurate and consistent with their Young's values.

The reported coatings fit into Wenzel model given the length of the size of the base of the droplet for the WCA measurements was 1.5 mm and the roughness scale on the order of nms (determined via AFM), a substantial difference in magnitude. [229] Though chemically heterogeneous surfaces often fit the Cassie-Baxter model, the surfaces need to be specifically engineered to prevent penetration of liquid into the grooves of the surface and this was not carried out on these coatings. Though it is likely that these particular coatings fit the Wenzel model, it is not totally clear due to the lack of completeness of the work in this area as swelling of the surface can also affect the contact angle. [230]

The minimal contact of water droplets with the surface as seen in **Figure 2.10** implies that the surface in question was hydrophobic. The WCA of the formulations developed were all between 110^{o} and 120^{o} which is considered hydrophobic. [231, 232] This is expected due to the presence of hydrophobic methyl groups attached to silicon atoms in the long PDMS regions of the

polymer chain. [233] This is corroborated by chemical analysis via XPS and ToF-SIMS which both detected PDMS strongly at the surface.

Physical surface properties can also be related to the function of the coating. In developing a good coating two particular aspects must be considered, its durability and its flexibility. Marine vessels must be able to withstand strong forces from the waves and potentially high pressures at lower depths. If a coating is not durable enough to withstand these events it will not be fit for purpose. If the surface is harder it is less likely to get scratched. Conversely, flexibility is required as the ship hull that the coating is adhering to is not totally straight and water seeping into the coating will lead it to swell substantially. For coatings that are hard this can lead to delamination and cracking. [234]

Pure PDMS silicone rubber requires 20 swings before the pendulum is damped. Silicone cross-linked using harder binders such as phenyls tend to increase to over 100 swings. For more flexible coatings which are used on string, only five swings may be required. For the coatings devised herein the range of results was between 8 and 37. The coatings that used SiDA as a drying agent had an increased hardness likely due to this particular drying agent participating in dense 3D networking. The coatings cross-linked with the two catalysts alone also differed. TnBT cross-linking led to a harder coating though Sn Octanoate did not appear to affect the hardness of the coating at all. This suggests that either the higher concentration of catalyst or the catalyst itself leads to denser cross-linking. This was not able to be determined via AFM imaging, with the networks at the nanoscale appearing identical. It remains a question as to exactly how this increased density of cross-linking manifests itself aside from these macroscale hardness measurements.

Nanomechanical measurements of the surface using AFM agreed somewhat with the macroscale measurements. TnBT cross-linked coatings were generally harder than those using 900c though the inclusion of SiDA as part of the reaction mixture did not appear to affect the hardness properties on the nanoscale. The TnBT catalyst can be assumed in this case to act as a harder

binder. These combined properties of the surface show that the surface has been devised such that it is not too hard and potentially flexible. The success of these coatings in a marine environment are discussed in later chapters.

For the mechanical properties, several repeats were used on different areas of the sample. For the AFM force measurements, ramps were used which took force curves from over an area of 50 x 50 μm. These values did not significantly vary from point to point and region to region. The QNM imaging (**Figure 3.4**) also demonstrated that the mechanical properties (stiffness and adhesion in this case) of the coating were consistent across the whole surface. The chemical make-up across the surface was also uniform. Using ToF-SIMS imaging, representative fragments for PDMS, PEG and the 900c catalyst were seen to be spread evenly across the scan area. Dimethyl siloxane associated ions were the most intense ions in both the spectra and the images. Given the number of PDMS groups in the polymer chain this is expected. Despite this, the sensitivity of the technique meant that the less prevalent PEG could also be detected at the surface.

3.4.3. Coating Chemistry

XPS detected a higher abundance of carbon at the surface than expected which theoretically could be attributed to either PEG or PDMS. For PDMS the ratio of C:Si:O would be expected to be 2:1:1 respectively. For PEG this ratio would be 2:1 C:O. Given that the elemental composition at the surface of the sample is similar to the theoretical ratio of PDMS (~60:20:20) it could be assumed that PDMS is the dominant unit at the surface. This would give a 3:1:1 ratio. This increase in carbon at the slight expense of silicon as seen in **Figure 3.6** suggests that there is a detectable contribution of PEG to the surface chemistry. The high resolution scans agree with this hypothesis as the largest synthetic peak under the carbon peak corresponds to C-Si environments. The shoulder at 287eV of the carbon peak is assumed to relate to C-O bonds. In a standard PDMS high resolution scan of carbon, this shoulder is absent. [235] It is therefore clear that though the surface is dominated by PDMS, PEG is present in detectible amounts at the surface of these coatings (10% of the total carbon

atoms). ToF-SIMS with its superior sensitivity in comparison to XPS confirms that PDMS is preferentially present at the surface in comparison to the PEG.

Despite the inclusion of catalysts and drying agents in the reaction mixture, titanium and tin were not detected in either ToF-SIMS or XPS. Phosphorus was detected in ToF-SIMS but not XPS. For XPS this is not surprising as the limit of detection is only in the parts per hundred/thousand. The two elements are on the limit of this hence are not detected. ToF-SIMS is more complex in its interpretation. The technique has an inherent problem with analysing titanium as it is generally more difficult to ionise in the system. This is due to their larger ionization cross section, which may explain the lack of detectability of Ti^+ ions in the spectra of those coatings which were catalyzed using TnBT. Alternatively, it may be a result of the cross-linking process, in that the titanium and tin atoms are preferentially kept in the bulk. This is less likely than the instrumental deficiencies as there are clear peaks associated with phosphorus in the 900c catalyzed coatings. This cannot however be firmly concluded from the data.

3.5. Conclusions

Five of the six formulations of the PPR coating were able to form predominantly flat, featureless coatings across a surface when deposited by either a paint applicator or a spray-gun. The process from mixing to final application is relatively quick, taking less than five minutes and is not strenuous or intricate. Minor defects were likely either drying artefacts or a result of the coatings being catalysed with an excessive concentration of catalyst, particularly in the case of formulation **3** which used TnBT alone at 5% (w:w) to cross-link the coating. The coatings were shown to all be reasonably hydrophobic and demonstrated properties associated with being flexible yet durable. The chemical and mechanical properties were uniform across the coating, with PDMS dominating the surface and PEG contributing to a lesser extent to the chemistry of the surface. Phosphorus was only subtly detectable and titanium was absent in both XPS and ToF-SIMS meaning it was difficult to characterise their contribution to the overall surface character.

Chapter 4

The Effect of Simulated Marine Environments on PDMS Based Polymer Films

4.1. Introduction

In order to evaluate the potential for the use of PDMS based coatings devised by *Dow Corning* as an anti-fouling technology, it is essential to understand the effects that a marine environment would have on them and whether it alters their surface properties. Attributes desired for an effective foul-release coating are a low elastic modulus and surface energy as well as having stability in sea water. [236] Using surface sensitive techniques to analyse the effect of pure water and sea water on foul release coatings can assist this understanding. This form of analysis is especially important considering the complexity that sea water has in comparison with millipure water. [237, 238] The presence of various chains of oleic acids and polysaccharides as well as the ionic species present in such a complex environment are very likely to have an effect on the surface and its properties over time. Whereas techniques like AFM have proved popular in analysing such surface changes, working just as well in water as in air, vacuum chemical analysis techniques such as ToF-SIMS and XPS require more complex procedures. This is especially true if changes at the surface are time dependent in an aqueous environment. These changes whether rapid (due to surface chemistry alterations) or longer term effects of the environment on physical integrity may alter their ability to act as effective fouling deterrents.

Surface techniques such as AFM have been used to determine adhesion of cypris larvae and the foul release characteristics of fluoropolymeric coatings. [239, 240] It has also been used to evaluate the changes in surface topography when anti-fouling coatings are exposed to water. [241] XPS has also been used to similar ends, analysing changes in the surface chemistry of amphiphilic biomimetic polymer coatings when water immersed. [242, 243] These chemical details are often corroborated with WCA measurements that allow for

changes in surface kinetics to be quantified in combination with the observed chemical changes. [244] ToF-SIMS has been used to analyse mobile groups in pentafluorostyrene films that vary at the surface depending on the temperature. [245]

Equally important in assessing a coatings effectiveness is determining whether the catalysts used in the cross-linking process leech into water when exposed. This can potentially be a problem if the catalysts used are toxic to particular species in the marine ecosystem.

4.1.1. Aims

In this work surface analytical techniques were used to analyse changes in the coating formulations after contact with water. Depending on the technique used the samples were immersed in either ultrapure water or seawater from the Pembrokeshire coast in the UK. The work focussed on changes in surface chemistry, topography and physical properties. The potential for catalytic leeching was also investigated in order to analyse the environmental inertness of the coatings.

4.2. Methods

4.2.1. Coating Development

The six coating formulations described above (**Methods 2.2.**) were applied to glass slides using a draw-down paint applicator depositing uniform 100µm thick coatings. For XPS, SEM and ToF-SIMS these slides were cut using a diamond cutter in order to fit into the respective chambers on small plastic stubs.

4.2.2. Water Contact Angle

A KSV CAM 200 computer controlled Optical Contact Angle Meter was used to determine the wettability of the surface of the coatings. The sessile drop method was employed. 60 frames 5 seconds apart were recorded of a 2µL 18.2Ω·cm miliQ water droplet placed onto the surface. Each image was analysed computationally on the CAM 200 software using the Young equation which requires the three phase boundary values: γ_{lg}, γ_{sg} and γ_{sl} with l denoting liquid, s solid and g for gas. This was recorded 5 times across the glass slide. Polytetrafluoroethylene (PTFE) tape was used as a hydrophobic control. The temperature and humidity remained stable for the ambient run, between 21.7-22.7 ^{o}C and 33.5-36.5% respectively. For the experiments in which temperatures were varied a Fisher Isotemp stage temperature controller was used.

4.2.3. Atomic Force Microscopy

The surface of the coatings were analysed using a Bruker Dimension Icon® AFM using PeakForce QNM® mode. Bruker MSNL-F tips were used (silicon tip/nitride lever) with a 0.97 N/m spring constant (calculated via the Sader method) and resonant frequency of 116.29 kHz. 1µm x 1µm areas were recorded. All images were flattened to remove curvature and slope using *Gwyddion – SPM Data Analysis* software. Images were then carried out in liquid PeakForce mode after immersing the sample in Artificial Sea Water

(ASW) standard D1141 (2003) for at least 5 minutes. Root-mean-square (rms) values for roughness were calculated using an average of > five measurements over areas of 1µm x 1 µm .

For force measurements, an RTESPA tip with a 30.6 N/m spring constant and 314.47 kHz resonant frequency functionalised with a 21µM diameter glass bead was used. 2 x 169 force curves were taken over two separate 60 µM areas with an Asylum MFP-3D AFM. Nanomechanical attributes were calculated using a Microsoft Excel macro designed by Xinyong Chen (Nottingham, UK). The DMT model was used to calculate Young's modulus via the slope from the retract curve in order to remove contributions by plasticity. The sea water used for this experiment was from Dale Harbour, Pembrokshire (Wales, UK).

4.2.4. Scanning Electron Microscopy

Imaging was carried out using a JEOL JSM 6060 LV FIB-SEM operated at either 15 or 20kV. The electron beam was rastered over the sample surface and the resulting backscattered electrons and secondary electrons were scanned simultaneously using the beam. All the samples were initially coated with gold for 100 seconds using a Leica EM SCD005 Sputter coater to prevent charging in the instrument chamber. The coatings were left in Pembrokshire sea water for 1 month, with images taking after one week and at the end of the month.

4.2.5. Time-of-Flight Mass Spectrometry

ToF-SIMS data were taken using a ToF-SIMS IV instrument fitted with a bismuth liquid metal ion gun and an argon cluster sputter gun. 40µL of milliQ water was placed on formulation **2** for 5 mins before being plunged into liquid nitrogen. The methodology was modelled on that from M. Taylor *et al.* [246] The analysis beam was a 25keV bismuth source using Bi_3^{++} ions. This was rastered over a 100 x 100 µm area with 128 x 128 pixel resolutions. The target current was recorded as 0.29 pA with a total primary ion dose of 8.98 x 10^{10} ions/cm^2. A 5 keV Ar_{1455} cluster source at 5.1 nA current etched through the sample over a 400 x 400µM area. The beam rastering was carried out in a non-

interlaced mode with 1 frame of analysis and 2 seconds for sputtering per cycle. The corresponding beam dose was 6.72 $\times 10^{12}$ ions/cm^2. An argon beam target current of 9 nA was employed for all samples. The sample temperature did not exceed −70°C in the entry chamber, maintained at -110°C under a 2 x 10^{-6} T vacuum so the water did not affect the vacuum pressure. Analysis was carried out in the main chamber at -120°C. To prevent the possibility of surface ice crystallisation, samples were maintained at this temperature during depth profiling. The total transfer time of samples from the liquid nitrogen to the entry chamber was kept to a minimum to prevent frost formation on the sample surface. Charge neutralisation of the surface was carried out utilising a low energy electron flood gun. ION-TOF's software SURFACELAB6 was employed for data process.

For samples analysed over a period of immersion a control glass slide and the six formulations were left in Pembrokeshire sea water at approximately 4°C for three months. These were then rinsed using ultrapure water and were spray dried in an attempt to prevent salt deposits from forming. Dr Michael Taylor helped to run the equipment for this experiment.

4.2.6. X-Ray Photoelectron Spectroscopy

XPS was carried out on a Kratos Analytical Ultra photoelectron spectrometer with a mono-chromated Al kα X-ray source (1486.6eV) operated at 120W in FoV1, 110 µm aperture mode. For the hydrated samples, as above 40µL of miliQ water was left to wet formulation **2** (1 x 1 cm) for five minutes mounted on an XPS sample stub and pinned by a copper bar. This prepared sample was then dunked into liquid nitrogen. The stub was then removed from the liquid nitrogen and placed onto the pre-cooled sample transfer arm in the entry chamber under nitrogen flow at a temperature ~ -70°C. The chamber was left to reach a pressure of 5 x 10^{-9} T at which point the entry door to the main chamber was opened and the sample was introduced for analysis. The sample did not exceed a temperature of -70°C in the entry chamber, maintaining -

160^{o}C under a 5 x 10^{-9} T vacuum. Occasionally the argon flux from the gas cluster ion source caused the pressure to increase to ~1 x 10^{-8} T. Analysis was performed in the main chamber at -160^{o}C, the sample was maintained below this temperature when depth profiled to reduce the possibility of surface ice crystallization.

Survey spectra or wide scans were carried out at pass energy 80eV. Core levels (high resolution scans) were carried out at 20eV pass energy for Si 2p, O 1s and C 1s. Acquisition time for core levels was 10 minutes. All samples considered required charge compensation using default settings for polymeric materials. A charge neutralizer filament provided a flux of low energy electrons for uniform neutralisation. All measurements were carried out with a take-off angle of 90^{o} compared to the sample. For depth profiling a 10 kV, $^{1000}Ar^{+}$ cluster source at a rate of ~0.1 nm and current operated at 0.3 pA etched through the sample over a 3 x 3 mm area. The cycle between etching and analysis was 30 seconds analysis followed by 120 seconds of etching with the argon cluster sources. CasaXPS (UK) software version 2.3.16 was used to process the XPS data. Dr Emily Smith helped to run the equipment for this experiment.

4.2.7. Inductively-Coupled Plasma Mass Spectrometry (ICP MS)

Elemental concentrations of leeched catalyst into week-long coating-exposed miliQ water samples were determined using a Thermo Fischer (Bremen, Germany) X Series ICP mass spectrometer. The instrument employed three operational modes, (i) a collision-cell (Q cell) using He with kinetic energy discrimination in order to remove polyatomic interferences, (ii) standard mode, where the collision cell was evacuated and (iii) hydrogen mode in which H_2 gas was used as the cell gas. Samples were introduced from an autosampler (Cetac ASX-520) incorporating an ASXpress™ rapid uptake module through a PEEK nebulizer (Burgener Mira Mist). For titanium detection semi-quantitative mode was used whereby Finnigan™ ELEMENT2 software generated a rate response curve of mass against isotopic sensitivity. An in-

house standard solution for KH_2PO_4 was used as an internal calibration standard for phosphorus. Each sample was diluted into a matrix of 2% (v/v) nitric acid. Peak dwell times were 10 ms for both elements using 150 scans per sample. Sample processing was undertaken using Qtegra™ software (Thermo-Fisher Scientific) utilizing external cross-calibration between pulse-counting and analogue detector modes when required. Saul Vazquez helped to run the equipment for this experiment.

4.3. Results

4.3.1. Water Contact Angle

WCA measurements were used to determine how the different chemical groups that make up the PPR may alter the surface character in water. The change in WCA of the surface of each coating compared to a hydrophobic control over time is displayed in **Figure 4.1** (*Top*). The initial contact angle was ~110 ^{o} for each formulation with the wettability of the surface increasing on immersion over time as shown by the gradual decrease in contact angle over a period of five minutes before levelling off at ~65^{o}. This is compared to the hydrophobic control PTFE tape which remained at ~120^{o}. The rate of the decrease in contact angle over time was the same for all of the formulations. The volume of the water droplet decreased slightly over the period of the run whilst the length of the base of the droplet increased markedly (**Appendix 3**). These changes can be seen visually in **Figure 4.1** (*Middle*). After removal of the water from the surface, the contact angle returned to its original state within 3 seconds, or the length of time taken to reapply a droplet and image the surface.

In the temperature controlled WCA measurements the rate that the contact angle decreased was faster at 50^{o}C (**Figure 4.2**) reaching a sub 60^{o} contact angle within one minute. The lowest contact angle value was also markedly lower than that seen when the coating was in either the ambient conditions or at low temperatures. This value was ~20^{o}. The surface area of the droplet also decreased more substantially than in the other experiments at different temperatures. The 5^{o}C experiment differed from the other temperatures tested as the overall decrease in contact angle was very small (~6^{o}). The value at t = ~0 was significantly lower at the beginning of the experiment (~70^{o}) than seen at higher temperatures.

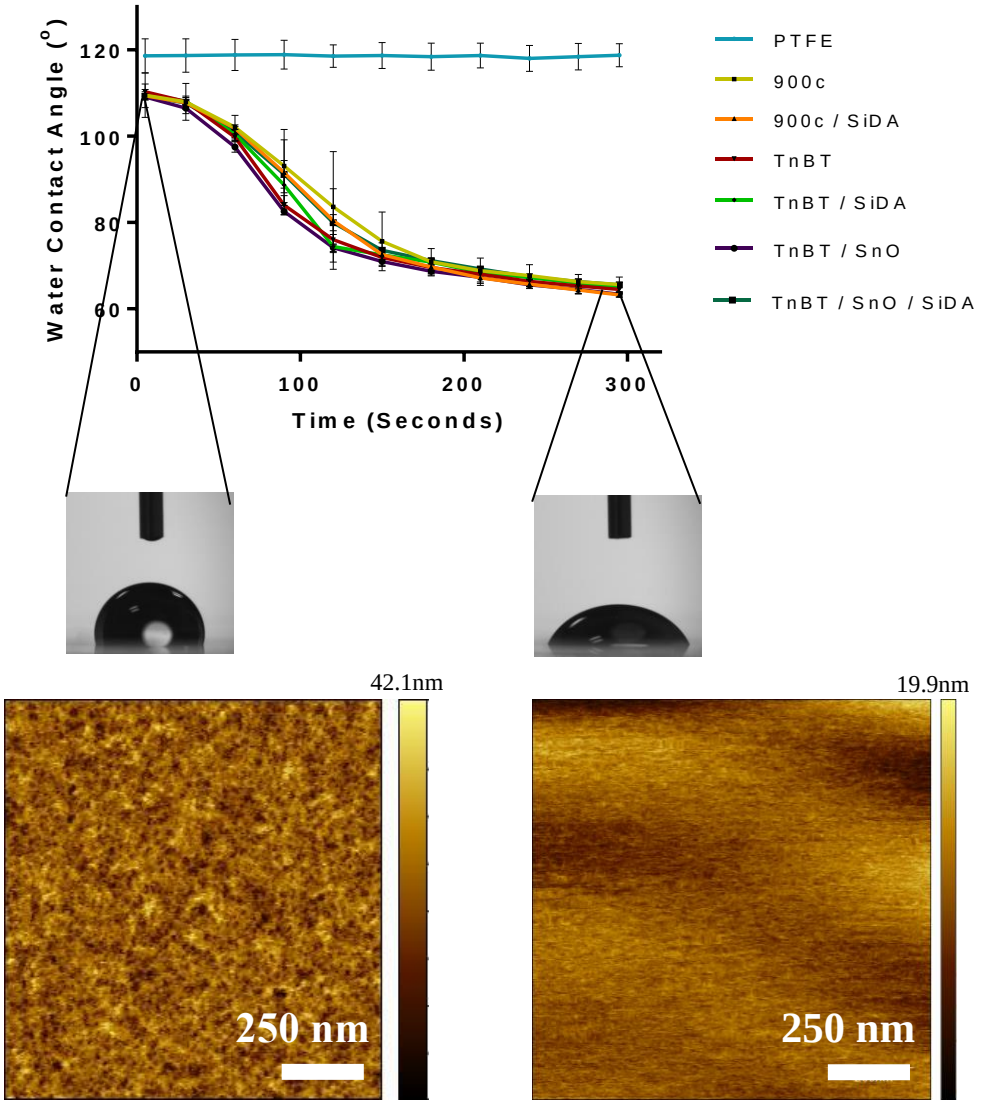

Figure 4.1. (*Top*) Graph depicting decrease in water contact angle of each coating with time. The graph shows a trend of each coating having a high initial WCA at ~110°, decreasing until ~200s before levelling at a significantly lower value than at the start (~60°). Polytetrafluoroethylene tape was used as a hydrophobic control whose contact angle remained consistent through the course of the experiment. (*Middle Left*) Water droplet on the surface of the 900c catalysed coating after 5 seconds demonstrated a strongly hydrophobic surface (~100°). (*Middle Right*) Water droplet on the surface of the 900c catalysed coating after 300 seconds which implies a more hydrophilic surface (~65°). (*Bottom Left*) 1 µm x 1 µm AFM height image depicting a fine, pore riddled network surface structure at the nanoscale. RMS = 4.56 nm (*Bottom Right*) Image after the coating was immersed in artificial sea-water for five minutes. The surface is less featured and this difference in topography suggests changes in the surface due to swelling and molecular reorientation. RMS = 1.97 nm, ($p < 0.005$). Images representative of all of the coating formulations.

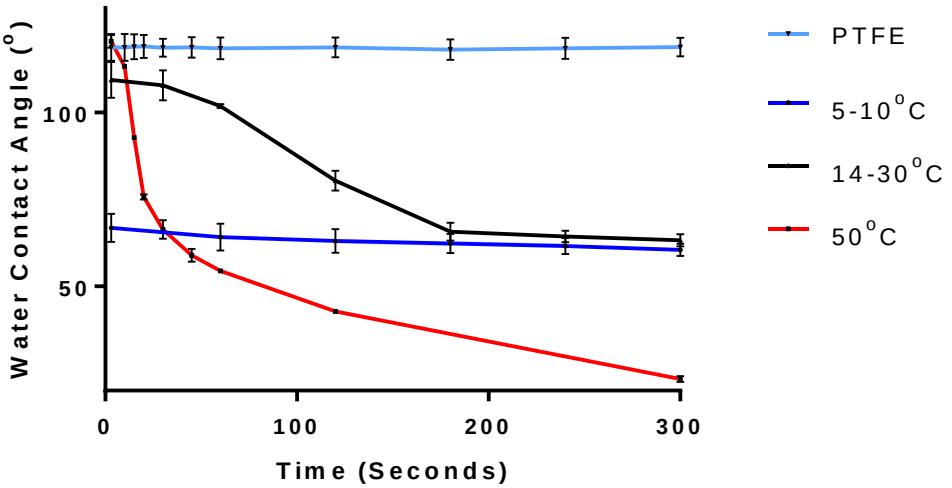

Figure 4.2. Graph depicting the change in water contact angle with time dependent on temperature using coating formulation **1** as a representative example. At 5-10°C a consistent contact angle is seen throughout the time lapse. The coating at 50 °C decreases in contact angle rapidly, faster than the sample at room temperature and finishing at a lower overall contact angle than any of the other samples. It suggests a more rapid reorientation of surface chemistry or an artefact of evaporation.

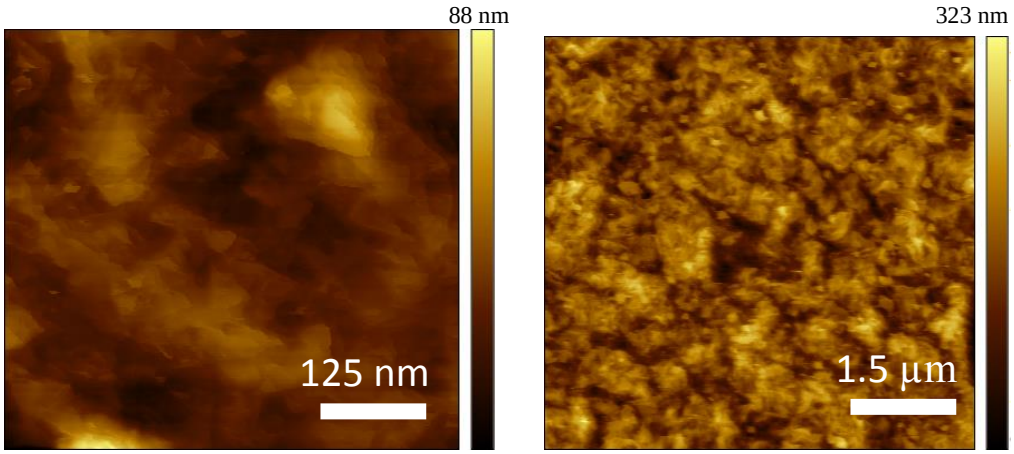

Figure 4.3 (*Left*) 500 nm AFM image of the surface of coating formulation 4 after being left in sea water for three months. The network structure is no longer visible. (*Right*) A 5 micron AFM image of the same coating. The surface is far less flat and has more of a featured surface than when analysed in a non-aqueous environment.

4.3.2. Atomic Force Microscopy

Figure 4.1 (*Lower*) shows a comparison of the topographic details of coating formulation **2** in an ambient state when analysed by AFM as opposed to that when immersed in artificial sea water. In ambient conditions the coating was

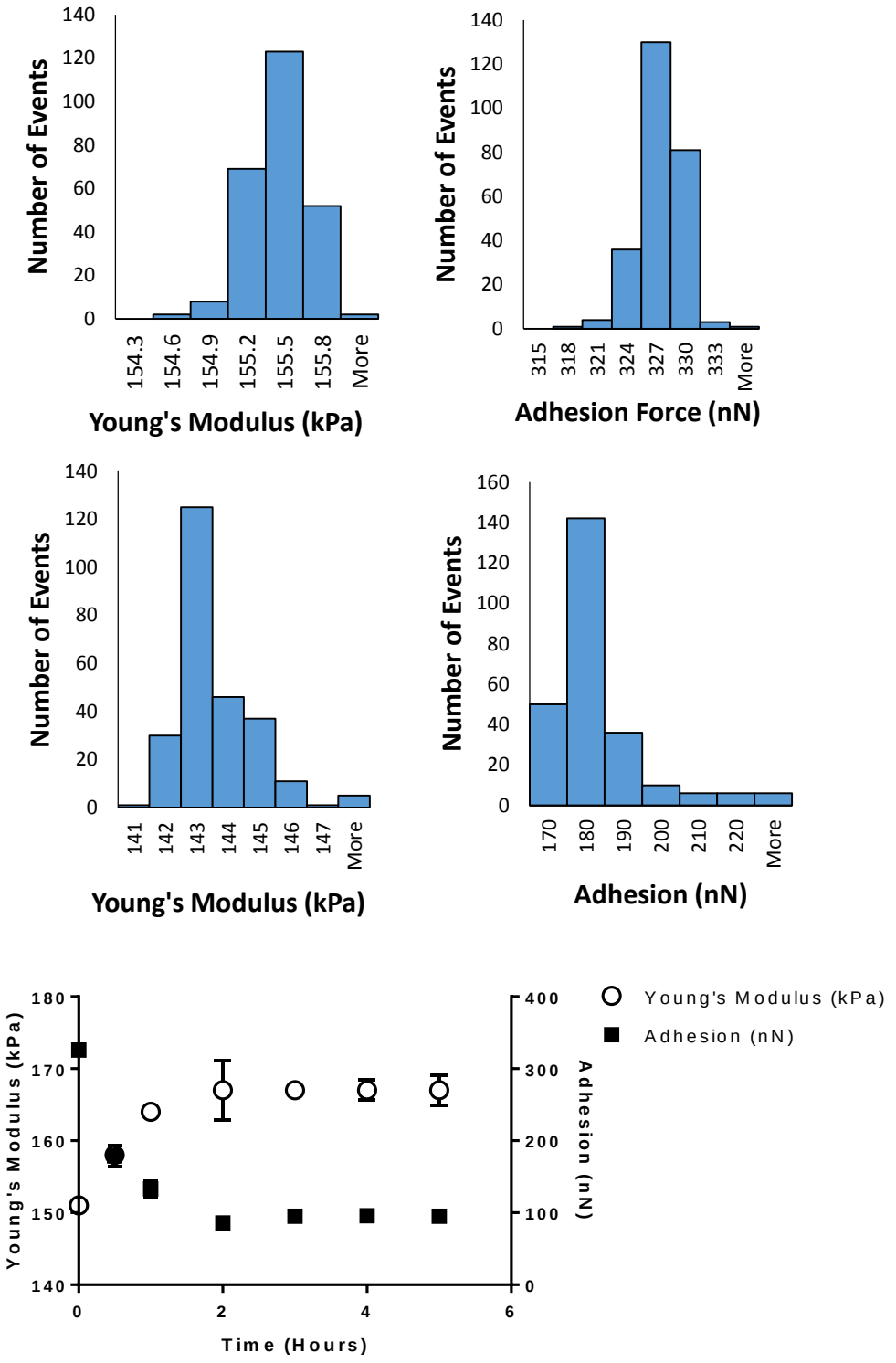

Figure 4.4. (*Top Left*) Histogram of the statistical distribution of the Young's Modulus of coating formulation **2** after collection of 450 force curves over 2 60 x 60µm regions in air. (*Top Right*) Histogram of the statistical distribution of the adhesion taken from the same curves. (*Middle Left and Right*) Histograms of Young's modulus and adhesion of two areas of the same sample in Pembrokeshire sea water. (*Bottom*) Measurements of elastic modulus (O) and Adhesion (■) in sea water over 5 hours. Modulus appears to increase in the first hour or two whereas adhesion decreases due to the aqueous environment. A glass bead was used for all measurements.

depicted as having a fine network structure. This detail is lost when imaged in sea water. After being immersed in sea water the sample appears to have swelled regions. The roughness is significantly lower after immersion in sea water (a reduction from 5 nm RMS to 2 nm).

After immersion in sea water for a period of three months, some of the surface topography changed significantly (**Figure 4.3**). This was seen at a range of magnifications. As opposed to the flat surface common in the non-hydrated coatings when viewed at higher magnifications, there are clear height deviations and an unstructured aggregate-like formation across the surface as well as a distinct lack of an ordered network structure.

The average Young's Modulus values were 155 ± 0.33 and 151 ± 1.6 kPa in air and in Pembrokeshire sea water respectively. There was a distinct difference in adhesion values, 326nN in air and 179nN in sea water.

Over a period of 5 hours immersion in sea water the modulus of the surface increased by roughly 15kPa and the adhesion strength was reduced by 20nN. The change occurred predominantly in the first two hours of immersion.

4.3.3. Scanning Electron Microscopy

Pre immersion the coating appeared flat and featureless with low roughness values and only the occassional minor defects as shown in the previous chapter and in **Figure 4.5** (*Upper)*. Over a period of three weeks the coating itself did not appear to change greatly with the majority of the coating containing little detail. However, in some regions crystalline like features were visible (**Figure 4.5** (*Bottom*)). These varied in size from nanometres up to almost 100µm. These crystalline features affected the coating itself. For example, in **Figure 4.5** (*Middle Right*) rings were present around the amorphously shaped aggregations. The longer the coatings were kept in the sea water, the larger these aggregations became, taking up more of the surface of the coating as seen

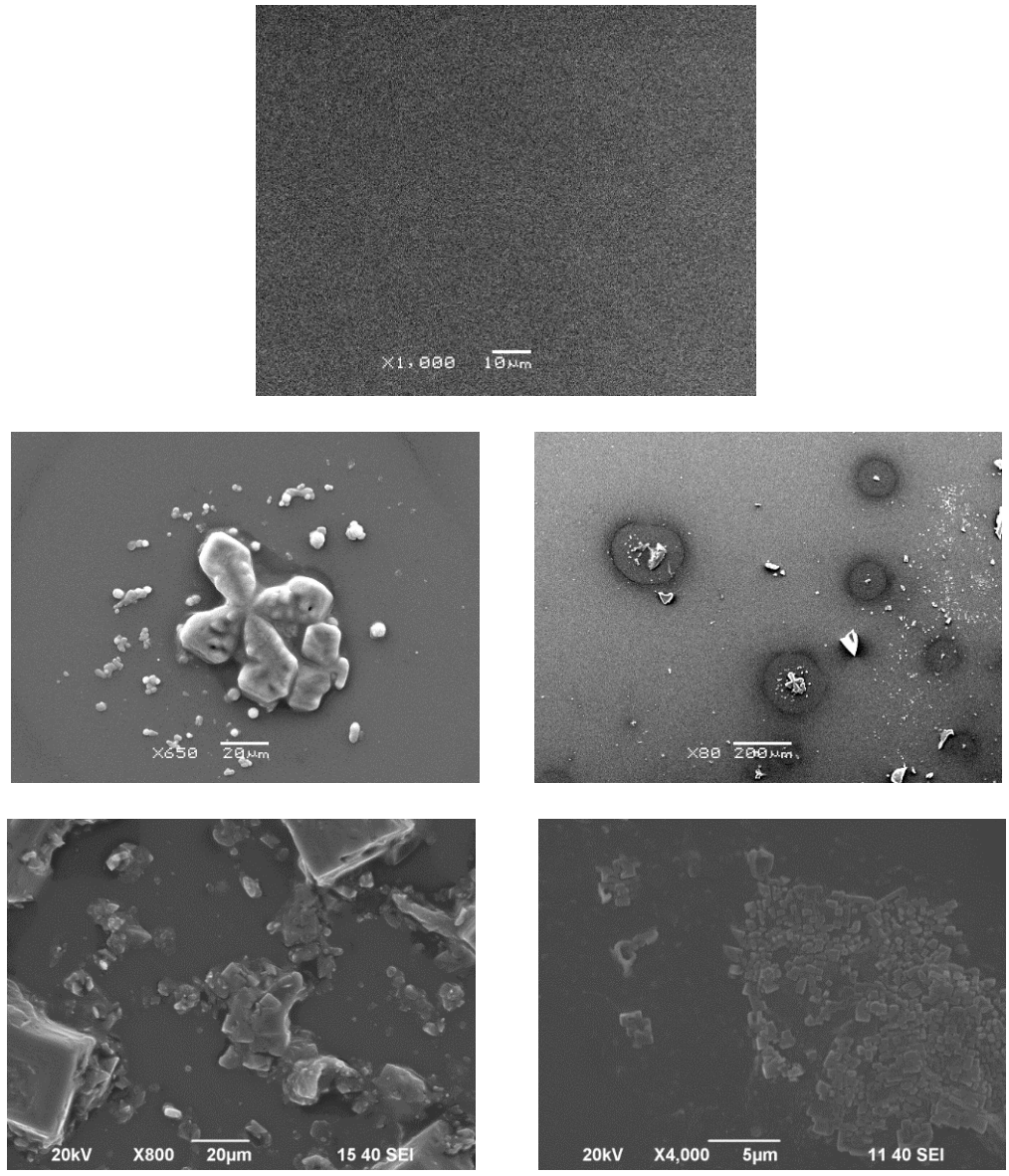

Figure 4.5. (*Top*) SEM image of a non-immersed control of the coating cross-linked using 900c and SiDA. (*Middle*) Images of coating formulation 5 after exposure to sea water for one week. Salt crystals were visible at the surface despite rinsing. (*Bottom*) Images of the same coating after 3 weeks exposure. Further salt aggregates in a very crystalline state can be seen across the sample.

at the bottom of **Figure 4.4**. The shapes of these aggregations also became more square in shape and obviously crystalline than in the samples that had only been immersed for one week. The coating did not suffer from delamination or have an increase in the number of surface defects after exposure for a greater amount of time.

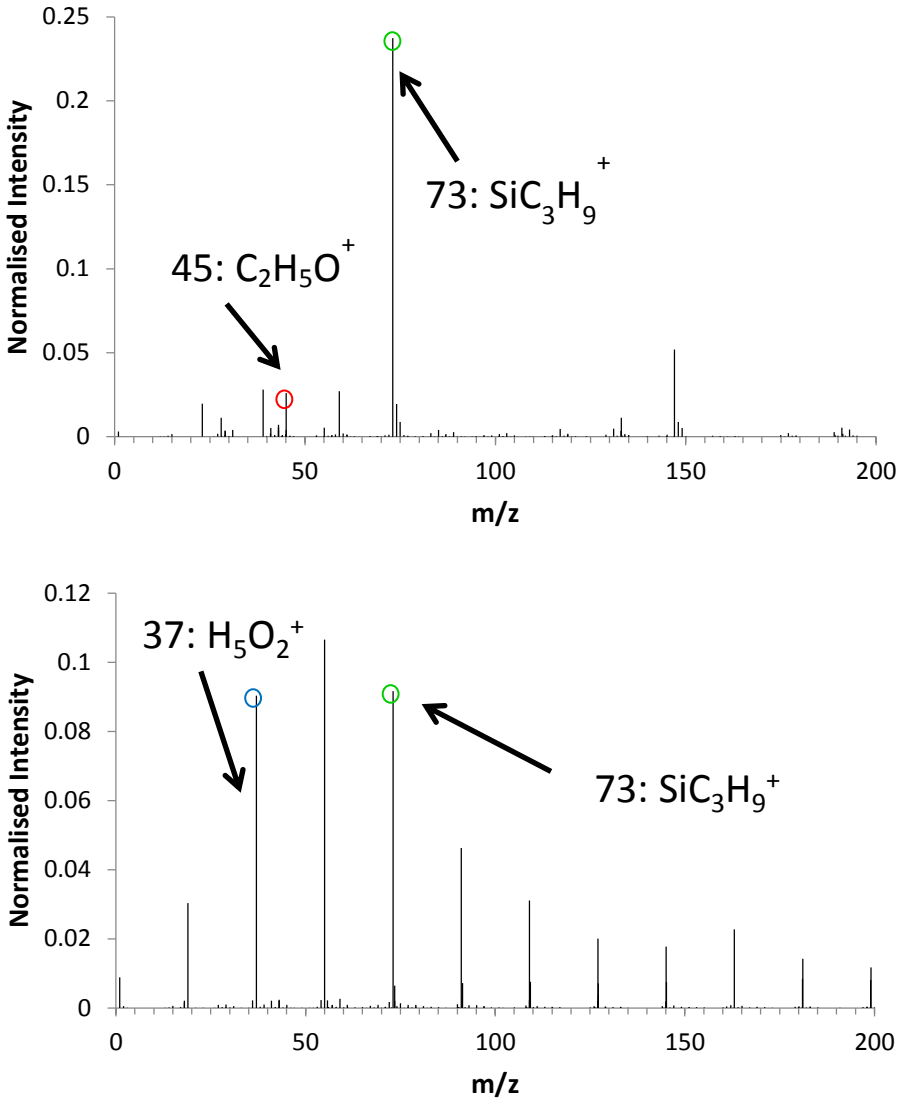

Figure 4.6. (*Upper*) Positive polarity mass spectrum of coating formulation **2** (900c & SiDA) with indicative peaks for PEG and PDMS highlighted in red and green respectively. (*Lower*) Mass spectrum of coating in a hydrated state as demonstrated by the presence of polyatomic water cluster ions at 37 m/z. Indicative peaks for water (ice) and PDMS are highlighted in blue and green respectively.

4.3.4. Time-of-Flight Mass Spectroscopy

Cryo ToF-SIMS was used to determine chemical changes at the surface of the coating when frozen, as this can provide information on the coating's surface chemistry in a representation of the marine environment. Previous analysis demonstrated that the mass spectra of all of the coating formulations displayed intense peaks at 45^+, 73^+ and 147^+.

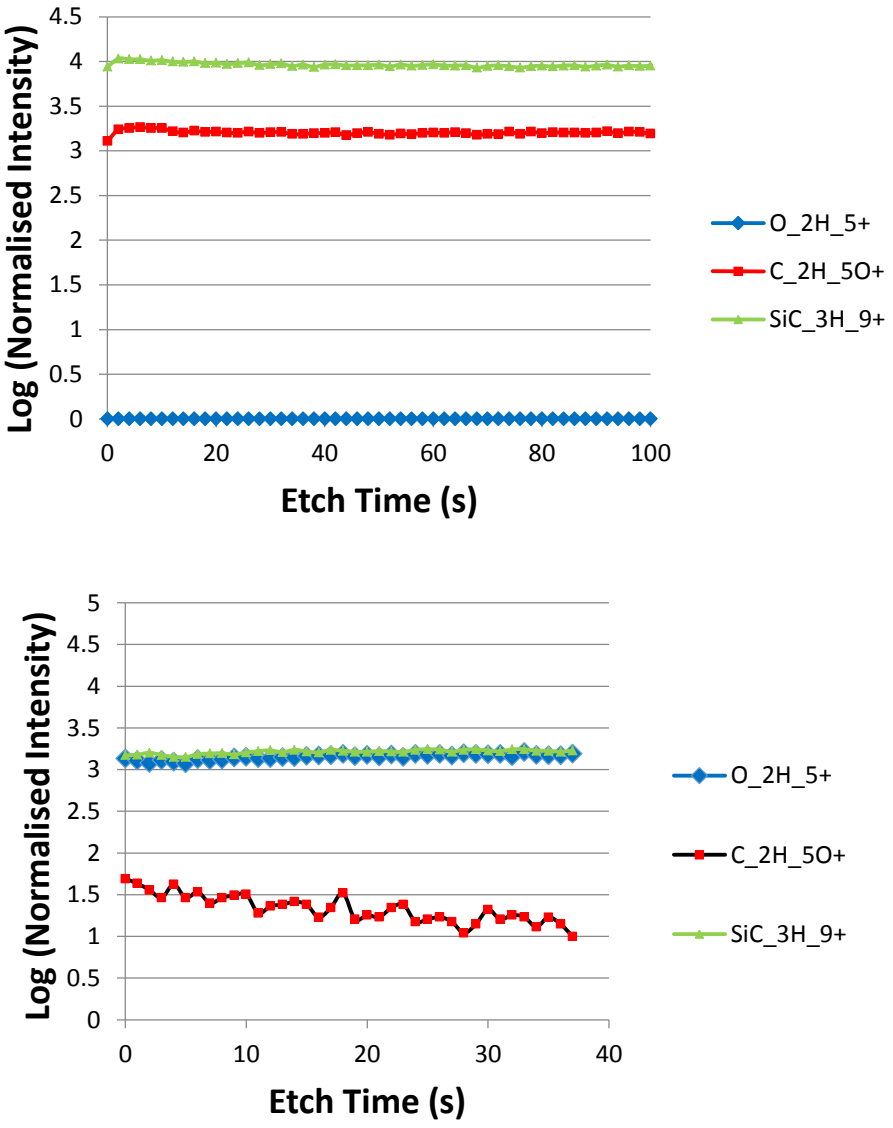

Figure 4.7. (*Upper*) Depth profile through a non-hydrated coating formulation 2. Uniform intensitities of representative ions of PDMS and PEG groups seen throughout the profile. (*Lower*) Depth profile of the same coating after application of deionised water on the surface for at least 5 minutes. Spectra were recorded in cryogenic conditions in order to maintain hydrated state. Demonstrates increased intensity of PEG groups at the surface than through the bulk in a hydrated state.

For comparison this is displayed in **Figure 4.6** (*Top*). Formulation **2** was also analysed cryogenically (**Figure 4.6** (*Lower*)). Surface spectra displayed intense peaks at 37^{+} and 55^{+} m/z. These were not as clearly visible in the ambient spectra. However, the strong peak at 73 m/z, similar to that in the ambient spectra was also present in the surface spectrum of the coating when in a frozen state.

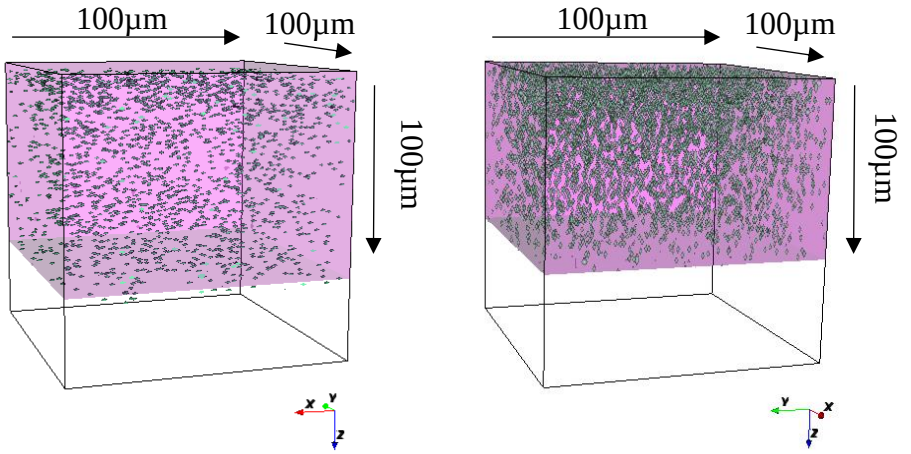

Figure 4.8. Three-dimensional renders of the coating formulation 2 (*Left*) Dry state render with uniform $SiC_3H_9^+$ to $C_2H_5O^+$ ion distributions (green points and saturated pink colour respectively). (*Right*) Hydrated state render with increased amounts of the PEG seen at the surface displayed than through the bulk.

To further confirm the differences that occur at the surface in a marine environment, depth profiling was carried out. This comparison between these two environments is shown in **Figure 4.7**. Profiles are represented in logarithmic scale due to the relative differences in ion intensities rather than simply normalising due to the low intensities of the hydrophilic groups. In the ambient spectra the ratio of $SiC_3H_9^+$ to $C_2H_5O^+$ was consistent throughout the bulk of the coating. The $H_5O_2^+$ ion was not present at the surface or in the bulk but is prominent in the sample that had water frozen within it. There was a change in the intensity of $C_2H_5O^+$ in the hydrated sample, with the intensity of the ion decreasing through the bulk compared with that seen at the surface. The $SiC_3H_9^+$ ion conversely slightly increased. This change is seen more clearly in the 3D renders displayed in **Figure 4.8**. The consistency of $C_2H_5O^+$ ions through the bulk of the ambient sample is contrasted with the clear difference in the number of these ions seen at the surface. The surface region is more densely populated with PEG ions than towards the base of the bulk in which there are markedly less. Complementary results in the negative polarity mode can be seen in **Appendix 5**.

When the coatings were left in Pembrokeshire sea water over a period of three months, there was a marked increase in the surface levels of salt. **Figure 4.9** shows the levels and distribution of particular ion species across 500µm of the

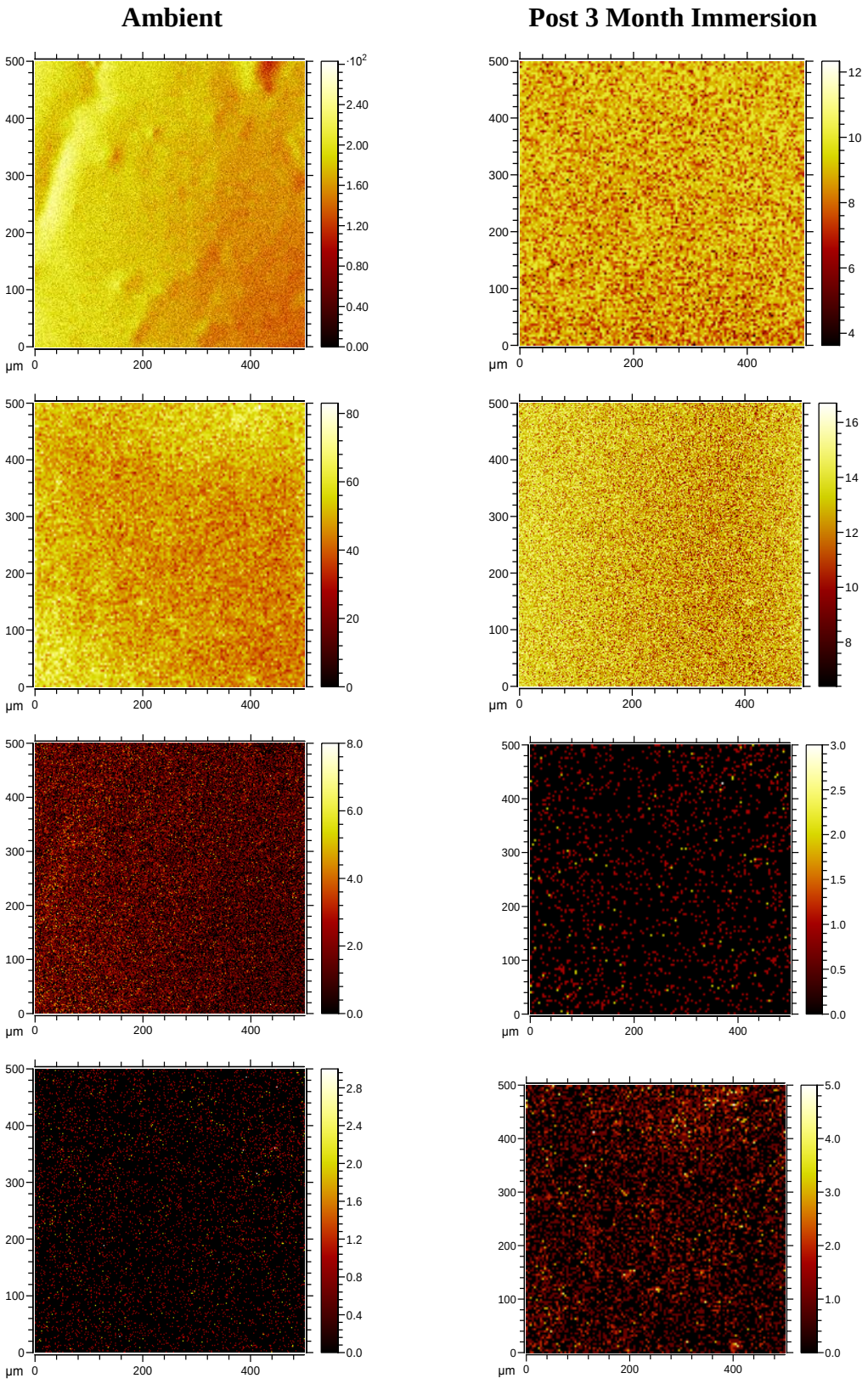

Figure 4.9. 500 x 500µm ToF-SIMS images of the surface of the coating cross-linked using TnBT after immersion in sea water for 3 months. They are representative of results seen for all coating formulations From top to bottom the images are for total positive ion count, $SiC_3H_9^+$, $C_4H_9O_2^+$ and Na^+ respectively. Displays increased intensity of salts at the surface after water immersion.

surface, including those indicative of PDMS, PEG and Sodium (though also similar for other ion salts).

The distribution of ions was consistent across the surface regardless of their identities or whether the samples had been exposed to sea water. However, the normalized intensity of the ions did have some variation between samples. In the images for sodium, the number and intensity of Na^+ ions appear qualitatively greater in number. The intensity of the PEG associated ions were lower when the sample was exposed to sea water.

4.3.5. X-Ray Photoelectron Spectroscopy

XPS was used to provide respective surface chemical detail after coating to compare with the results seen in ToF-SIMS. After sample formulation **2** was hydrated, exposed to liquid nitrogen and analysed, the wide scan showed a predomenant peak at 560eV implying a large presence of oxygen (**Figure 4.10** (*Top*). There was also a minor peak at 285eV related to carbon.

Depth profiles of the surface with water on were either difficult to obtain or the profiles were unchanged throughout the bulk, with the spectra remaining similar to that seen in **Figure 4.10** in that the peak at 560eV remained the most intense and other chemistries didn't contribute to the total. This elemental composition through the bulk is also displayed in **Fig 4.10** (*Bottom*).

In an effort to determine the extent of changes in surface chemistry of the coatings in a simulated marine environment, ambient depth profiles were also carried out. The percentage of carbon 1s atoms at the surface remained consistent at ~56% through the bulk whilst O 1s concentration increased with decreasing Si 2p. Both have contributing concentrations to the surface of ~20% of the total whilst O 1s increases to ~30% as Si 2p decreases to ~10% (**Figure 4.11** (*Top*)). A similar trend is also seen in the high resolution scans for carbon 1s contribution. **Figure 4.11** (*Middle* and *Bottom*) show the specific environments of carbon atoms at the very surface of a coating in standard

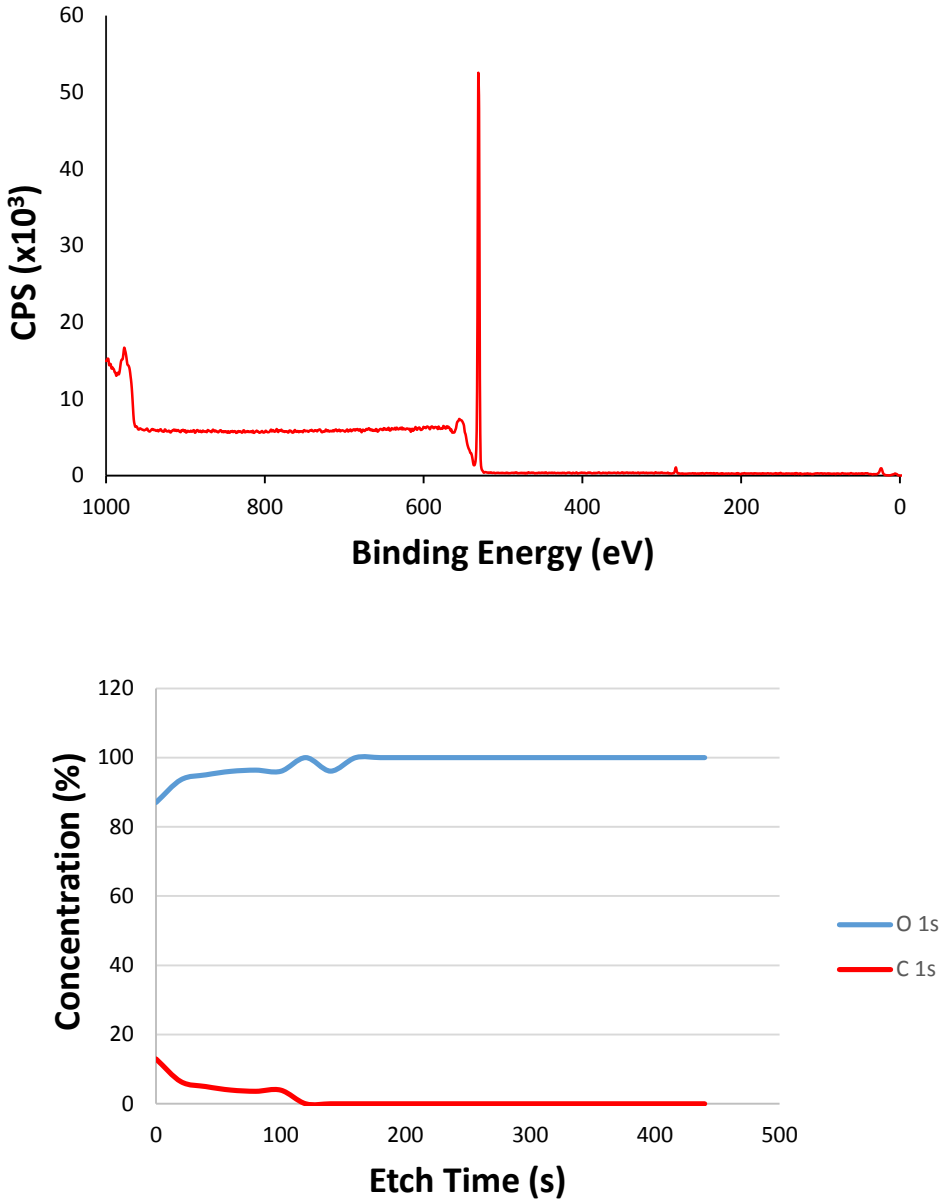

Figure 4.10. (*Top*) XPS wide scan spectra of a coating cross linked using 900c and SiDA after being hydrated in pure water and exposed to liquid nitrogen before analysis at -160^{o}C. Representative of scans seen both at the surface and several hundred nanometres into the bulk. Intense peak at 560eV suggests the majority of the surface is comprised of oxygen which implies the surface analysed is mostly frozen water. (*Bottom*) Depth profile through the surface of the sample. Aside from adventitious carbon common to cryo experiments the predominant element through the bulk is water, demonstrating a high likelihood of the water droplet being too large in order for the analysis beam to penetrate the coating itself.

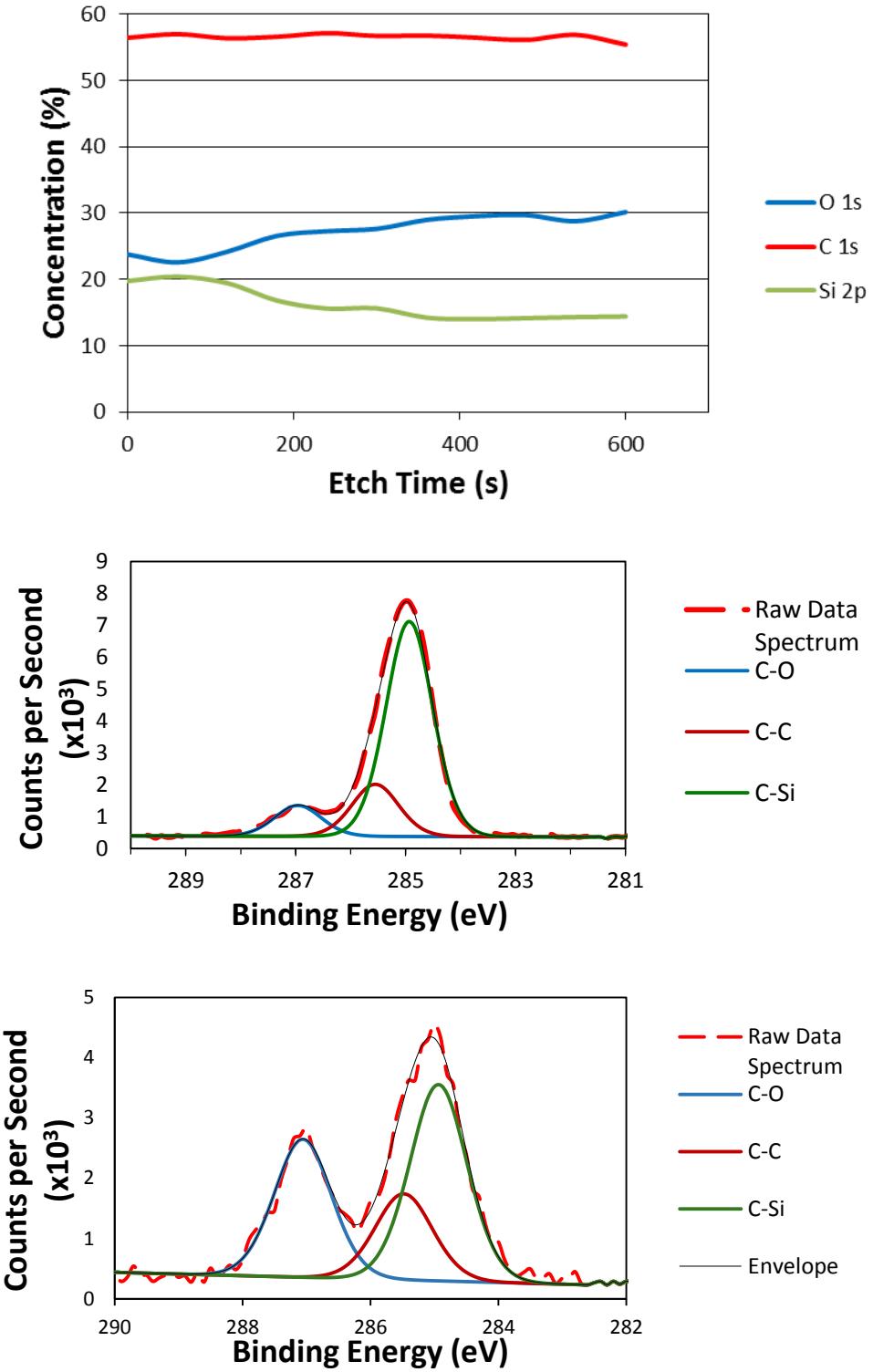

Figure 4.11. (*Top*) Elemental depth profile of 900c & SiDA coating in ambient conditions. Displays the relative concentration of specific elements with etch time. Carbon concentration is consistent through the bulk. Levels of oxygen increase whilst the relative concentration of silicon decreases in comparison with the surface as further etching occurs. (*Middle*) High resolution carbon 1s scan from the uppermost surface region, displays a preponderance for C-Si carbon atoms. (*Bottom*) High resolution carbon 1s scan from the bulk after 500s of etching time. The shoulder region at 287eV indicative of an increased presence of C-O bonded carbon atoms.

conditions and several hundred nanometres into the bulk respectively. As detailed in the previous chapter, after applying synthetic peaks to these carbon scans, the environment most carbon atoms are in is bonded to silicon atoms (the green peak just under 285eV in **Figure 4.11**). There is a contribution from carbon atoms bonded to oxygen atoms as seen by a shoulder at ~287eV. After an etch time of around 200s, two things begin to happen through the bulk. The most obvious change was that in the shoulder at 287eV which increases in size by almost three times, becoming greater in its area than the curve associated with carbon atoms bonded to other carbon atoms. Quantified this shows an increase in atomic concentration from 10% to 33%. This increase in area of this particular synthetic peak coincides with a decrease in area of the other two peaks under the main carbon curve at 285eV. This implies that there is a marked increase in the presence of C-O atoms further through the bulk.

4.3.6. Inductively-Coupled Plasma Mass Spectrometry

ICP-MS was used to determine the extent of catalytic leeching into water after the coating formulations were exposed to pure water over a period of one week. The relative concentrations of the elements phosphorus and titanium were determined as they are the major elements involved in the catalysts used in the cross-linking procedure. **Table 4.1.** shows the concentrations detected in ICP-MS. For each element, the coating which did not contain their catalytic counterpart acted as controls, e.g. for formulation **5** which used TnBT as its cross-linking catalyst (containing titanium). The results for formulation **2** were used for comparison as a phosphorus catalyst was used in its formation.

Titanium levels for all coatings were consistent and were not significantly different from each other, even in the samples where 900c was used as the catalyst. However, for formulations **1** and **2** which used a phosphorus based catalyst, the levels of phosphorus seen in the water were significantly higher than in the control samples.

Table 4.1. Levels of phosphorus and titanium detected in ultrapure water that was used to immerse each coating formulation for one week. Shows no difference in titanium concentration compared to the background but a marked increase in phosphorus when the 900c cross-linked coatings were immersed in water.

	Phosphorus		**Titanium**	
Formulation	mg/L	Standard Deviation Error	µg/L	Standard Deviation Error
1	1.85	0.57	1.69	0.68
2	0.81	0.15	0.92	0.34
3	0.00	0.00	1.20	0.42
4	0.00	0.00	1.37	0.16
5	0.00	0.00	1.64	0.43
6	0.00	0.00	1.18	0.42

4.4. Discussion

4.4.1. Effect of Water on the Physical Properties and Appearance of the Coatings

The change in WCA of the surface of each coating over time is described in **Figure 4.1** (*Top*). The initial contact angle of ~110^{o} for each coating suggests that the surface exists in an expected low-energy hydrophobic state in ambient conditions, given the high content of PDMS groups present in the resin. [246] The wettability of the surface increased on immersion over time as shown by the gradual decrease in contact angle over a period of five minutes before levelling off at ~65^{o}. This reorganisation of the surface is suggested to be related to the reorientation of surface chemistry groups. In comparison to other

reorienting coatings that can take several hours, this process is relatively fast. [247]

The PTFE maintained a strongly hydrophobic contact angle due to its stable chemistry. This implies as discussed that there is potentially a change in chemistry occurring at the surface of the PPR coatings. The water droplet volume did not decrease significantly over the analysis period (**Appendix 3**) so it is unlikely this change in contact angle is due to evaporation of the droplet. Therefore the phenomenon is likely due to the switching of hydrophilic PEG groups towards the surface of the coating, replacing the more hydrophobic PDMS groups. PEG has a recorded contact angle of 20-45 ^{o} which suggests that the change in the surface character of the coating to just a 65^{o} contact angle means the coatings are more hydrophilic in nature after 5 minutes though not to the extent that would be expected for pure PEG.

On removal of the water droplet by shaking, the coating returned to its hydrophobic state within 3 seconds meaning the system is reversible and is almost instantaneous. The contact angle was also tested after three months in artificial sea water but no difference was seen in the initial contact or the rate of reorientation. There has of yet been no definitive link confirmed between the wettability of a surface and its antifouling properties. However, as has been stated an amphiphilic coating provides both antifouling properties as well as increased durability, therefore these results suggest that in a marine environment the surface of this particular coating has a desired characteristics for its purpose.

The effect that temperature has on both the rate of reorientation and also the initial contact angle of the coatings themselves is marked. At temperatures between 0 and 10^{o}C the surface initially had a contact angle of that seen after five minutes at room temperature, one relating to an amphiphilic surface. The lowest temperature where reorientation still occurred was 14 ^{o}C. Therefore this suggests a transition temperature of the polymer at this point where the PEG groups become more motile. At temperatures above room temperature (~50 ^{o}C)

the contact angle did not change but the reorientation process was more rapid. However, the volume of the droplet decreases much faster at higher temperatures and it is difficult in this case to separate the effect of temperature on the rate of switching from evaporation artefacts. Sea temperatures rarely reach such heights however, with the Persian Gulf for example being at around 35 ^{o}C in summer.

The change in morphology of the surfaces on exposure to a simulated marine environment was seen in AFM images. Surface features were compared between dry surfaces and those exposed to ASW for at least 5 minutes to allow for complete reorientation. **Figure 4.1** (*Bottom*) shows AFM height images of the resin both in ambient conditions (*left*) and immersed in ASW (*right*). All the coating's surfaces show a fine, somewhat porous networked structure in air in images between 200 nm and 1 μm, likely resulting from the cross-linking process. The loss of detail in the water-immersed AFM image (**Figure 4.1** (*Bottom Right*)) would suggest a swelling of the surface which corresponds to the hypothesis of a switching effect, seen in the water contact angle measurements, as a morphological consequence of a reorientation of the surface chemistry. The decrease in surface roughness of the surface with contact angle is expected from the extensive work in this area. [230] It has been shown that if a surface is hydrophobic, the rougher it is the more hydrophobic it is likely to be, therefore a decrease in contact angle with surface roughness is expected.

The mechanical properties of the surface attained by AFM were less clear as to the differences that immersion in water makes to the surface over five minutes. Though the Young's moduli were significantly different, the difference was minimal (just 10kPa lower in water) and with AFM being particularly temperamental with regard to minor changes in environment, it is hard to make a conclusion based on the results obtained. Though the error bars are not overlapping, the fact that different tips were used means it cannot be asserted conclusively that these differences are significant, due to the potential spring constant error. **Figure 4.4** (*Bottom*) shows the changes in surface properties over longer time scales. After 2 hours in water, the adhesion decreases and the

stiffness increases. On the macroscale PEG is generally stiffer than PDMS so it may be possible that over an extended period of time the difference in mechanical properties of the coatings become more pronounced. [248] The reduction in adhesion is expected as in ambient conditions there is generally water present in the system (due to environmental humidity) which aids the adhesion forces via capillary action, drawing the AFM tip into the sample. Obviously in an entirely liquid environment this contribution to adhesion is removed therefore leading to a reduction in the adhesive forces present in the system.

4.4.2. Chemical Confirmation of Surface Reorientation

ToF-SIMS was used to combine chemical data with the physical changes described above. The depth profile in **Figure 4.7** (*Bottom*) is of the coating in a fully hydrated state. This was observed by detection of $H(H_2O)_n^+$ secondary ions seen in **Figure 4.6** (*Bottom*), which confirm a frozen hydrated state meaning the chemistry of the surface could also be seen. [245] In the initial surface region, there is a steady decrease in ion intensity of the PEG group $C_2H_5O^+$. There were observable minor increases in the $SiC_3H_9^+$ ion intensity. This suggests that this observation is not a factor of ionisation inhibition, which would result in a decay of all ion species. Therefore it is likely that concentration of the hydrophilic groups is higher at the surface than the bulk, providing credence to the reorientation hypothesis discussed above. **Figure 4.7** (*Top*) shows a depth profile of the coating in an ambient state, which demonstrates steady state concentrations of the PDMS ions and those representative of the hydrophilic groups after a ten second etch time.

No changes were observable between relative intensities of PDMS the hydrophilic groups detected throughout the surface layers demonstrating the difference between the chemistry in a non-hydrated and a hydrated state. Shown in **Figure 4.6** (Top) is the surface ion spectra of the dehydrated coating with prominent PDMS peaks at 73 m/z ratio. Similarly to the XPS data seen in the previous chapter, the surface as well as the bulk is dominated by PDMS. A

3D visualisation of the profiles are included in **Figure 4.8**. The ion associated with the hydrophilic PEG have a uniform intensity throughout the profile in its non-hydrated state but more prominence at the surface in the hydrated state. High concentrations of metal salts are found in ASW which can change the ionisation potential of certain molecular fragments in ToF-SIMS. Certainly this effect is enhanced in the surface transient region (where molecular ion signal increases to a maximum at the beginning of a spectrum and decreases very slightly afterward). Due to this phenomena, deionised water was selected to hydrate the surface to provide the best simulation for a marine environment in which to analyse the surface. It is also necessary to note that hydration can alter ionisation probablility of molecular fragments, hence the differences seen between the intensities between the ions representing hydrophilic groups in **Figure 4.6**. This is a factor of matrix induced ionisation. [249] Therefore, the trend displayed by the profile is the more interesting feature of it, rather than the specific values displayed.

A similar experiment was attempted using XPS in order to quantify these surface changes. One of the major difficulties with this method is ensuring that the water left on the surface after immersion does not obscure the surface. This is particularly difficult given the high hydrophobicity of the sample causing water to often fall off the sample before being frozen. Though this method was successful in ToF-SIMS, it took several attempts and proved difficult to replicate in XPS. **Figure 4.10**demonstrates this issue clearly. The predominance of oxygen at the surface and also through the bulk with little to no contribution from any other elements means it is likely that the entire sample is comprised of the ice layer on top of the coating. It was also difficult to control the temperature to such an extent where the ice could be removed without affecting the frozen surface.

Another issue which may explain the problem of analysing such a surface is the analysis depth of XPS which can be up to 10 nm. Given WCA measurements are able to detect changes at 1 nm, it may be possible that even if the surface was detected in a hydrated state, the subtle surface switching effect may not have been visible. This is because the depth X-ray penetration

may capture bulk properties contributing to the surface spectra. Depth profiling of the coatings in their ambient state was run in order for comparison. **Figure 4.11** shows an increase in the total detected oxygen through the bulk implying an increase in the concentration of PEG further away from the surface. This is further demonstrated by the high resolution carbon scan in **Figure 4.11** (*Bottom*) which shows an increase in the percentage of carbon atoms bonded to oxygen. This is seen with the larger shoulder at 287eV. This is expected when PEG concentration in a silicone based polymer increases at the surface. [247] It should therefore be expected that if the surface were in a hydrated state, the high resolution C 1s peak should be similar to that seen further in the bulk in ambient conditions. It stands to reason then that angle resolved XPS would likely be better for this particular experiment to detect more subtle surface changes but only if the optimum volume of water can be maintained on the sample such that pure ice does not dominate the spectra.

After the immersion of the coatings in sea water for a period of three months, there were residues remaining on the surface even after it had been rinsed in pure water (**Appendix 4**). Further analysis using AFM, ToF-SIMS and SEM showed this very thin scum like residue is comprised of several elements. This change in appearance at the surface was subtle on the macroscale thus making it difficult to record using a standard camera. AFM imaging (**Figure 4.3**) shows this change in the surface clearly. The flat network structure is no longer seen and the surface itself is not formally structured.

Salts such as sodium chloride and magnesium chloride were present on the surface. This was seen in ToF-SIMS spectra in which the immersed samples had more intense metal ion peaks than non-immersed samples **(Figure 4.9)**. The presence of such ions was also consistent across the sample as showed by the distribution of the ions in the images seen in **Figure 4.9**. The extent of the adherence of salts to the surface were compared with that of a standard glass slide in **Appendix 5**. The glass was rinsed but still had swathes of sodium salts across the surface. Though not necessarily a fatal flaw of any coating, these salts could be used by opportunistic organisms as a conditioning film. Corroborating this chemical data, the SEM images in **Figure 4.5** show a

variety of crystalline like structures which grew in size over a period of several weeks. It is important in this case to consider that the PPR coating may need cleaning or reapplication every few weeks in order to prevent further deposition of chemicals which may cause a conditioning film to develop.

It is well established that various length proteins, oleic acids and sugars attach and develop conditioning films on a surface substratum. [18] ToF-SIMS analysis of these immersed surfaces found the presence of amino acid residues through representative peaks such as those of asparagine at 70 m/z and also glutamine at 84 m/z which indicate the presence of proteins. [250] Due to the inherent nature of ToF-SIMS as a fragmentation technique and the complex nature of sea water it would be an immensely complex process to be able to specifically identify what these proteins are. These proteins could either belong to cells (bacterial cell walls) or may be just free floating proteins but this would require polymerase chain reaction or other DNA amplification methods as well as bioinformatic processing to clearly determine the identity of such proteins. It was also not clear in SEM as to what the identity of the contributing elements to these leftover aggregations were. The density and complexity of the features which were formed at the surface made identifying individual elements of them too difficult to ascertain with certainty. However, with previous work done in this area, it is possible to assert that the likeliest identities of the elements which made up this surface film were provided by a mixture of proteins, salts and bacterial species.

Leeching of catalyst can potentially be damaging for ecosystems depending on the material. ICP-MS on water which had been used to immerse all the formulations of the coating showed that there is some leeching of phosphorus as it was detectable and showed significantly higher levels than in the control measurements (**Table 4.1.**). Titanium however did not leech into the water, at least not at sufficient concentrations which could be detected over background levels. Tin cannot readily be detected in ICP-MS so it could not be determined if the SnO drying agent leeched into water on immersion.

4.5. Conclusions

Surface sensitive techniques were used to identify and characterise a reorientation phenomenon of a novel PDMS based polymer coating containing PEG domains. Chemical and physical techniques were combined in order to determine the explanation for a change in wettability at the surface of the different coatings from hydrophobic at ambient conditions to amphiphilic over a period of five minutes immersion. This was confirmed by WCA. The coating returned to its standard orientation within three seconds of water being removed from the surface, making the process quickly reversible. Contact angle measurements using variations in temperature showed there is a transition temperature of 14^{o}C for the PPR polymer where PEG groups become more mobile. AFM images showed a change in the surface topography as a form of swelling when the surface was hydrated in ASW, with a detailed network becoming less distinct. XPS and ToF-SIMS confirmed a predominantly PDMS based surface in its non-hydrated state. Confirmation of swelling in a hydrated state was seen by the presence of water throughout the depth profile of the coating. The profile also showed that the PEG groups are more prevalent at the surface of the coating than in the bulk when water immersed as opposed to the uniformity observed in the coating's state in ambient conditions. Coatings cross-linked using 900C had phosphorus leech out of the coating when immersed in water. This was not true for the titanium in the coatings catalysed using TnBT.

The next stage will be to determine the ability of these coatings to prevent bacterial adherence and ascertain what effect this ability of the coating to chemically switch has on its desired function.

Chapter 5

Assessing the Ability of PDMS Based Polymer Films at Preventing Adhesion of *Pseudomonas aeruginosa*

5.1. Introduction

In order to understand the potential of the studied novel polymers to prevent biofouling in a marine environment, it is important to test this in a controlled setting using model organisms. The experimentation was designed to provide the following information: (i) the difference between the coatings at preventing adherence of certain bacteria species, (ii) the mechanistic details of attachment of such bacteria and (iii) whether this mechanism is destructive to the bacteria rather than anti-stick.

Pseudomonas aeruginosa (PA01) is often used as a model bacteria as it is a common gram negative species which is ubiquitous and easy to grow in a laboratory. It has been used to demonstrate the potential of coatings to prevent biofilm formation on medical catheters by determining the reduction in the coverage between samples or the reduction in optical density of bacterial solutions. [251, 252]

With ecology and conservation being of primary importance in the current era, it is important to ensure that current coating technologies are not harmful to the environment. To this end, Live-Dead staining is often used to determine the percentages of those bacteria that are still alive on analysis. [253] This is often used to determine bacterial heterogeneity of a biofilm. [254, 255]

By capturing real-time videos of bacteria, it is possible to study the ways in which they move across a surface, therefore giving an insight as to why they do or do not adhere to a surface. These data can specifically consider how or why specific bacteria such as PA01 form biofilms. These methods can be applied to identifying appendage-specific mechanics when such bacteria are on a surface. [256, 257] This has also been applied to tracking the 3D swimming of bacteria

(PA01) and also marine biofouling organisms such as barnacle cyprid larvae. [258, 259] This information has been combined with microfluidic data to determine attachment strength of bacterial coatings and at what levels of shear bacteria are removed from surfaces. Again this has been done using both models such as PA01 and also bacteria associated with marine environments such as *Cobetia Marina* and other marine organisms. [260-262]

5.1.1. Aims

The intention of this work was to compare the ability of each of the amphiphilic coating formulations described above to prevent the biofilm formation of PA01 compared to a PDMS standard. PDMS does not reorient in solution as has been proposed for the novel polymer films studied here. This insight could then be used to consider if aspects of the polymer surface chemistry altered their anti-bacterial properties. The next stage was to determine whether the chemistry of the coating was harmful to the bacteria using live-dead staining in order to indicate that the mechanism of action of the coating is not detrimental to the environment. This was particularly important as the 900c coating was demonstrated in the previous chapter to leech into the water surrounding it. The movement of bacteria towards and on the surface of the coatings was tested to see how the amphiphilic coating specifically affects their behaviour. Finally, flow experiments were undertaken to determine the strength at which PA01 attaches to the surface of the coatings.

5.2. Methods

5.2.1. Coating Development

The six coating formulations described in **Methods 2.2.** were applied to glass slides using a draw-down paint applicator depositing uniform 100µm thick coatings. Cured, pure PDMS sheet, Bard silicone Foley catheters and glass slides were used as controls. Before incubation with bacteria the samples were all UV sterilised. Coatings were also left in artificial sea water for 6 months to study the effect this had on their ability to prevent bacterial adherence. For movement and adhesion experiments the coatings applied to glass cover slips using a spray gun were used.

5.2.2. Bacterial Screening

Pseudomonas aeruginosa (PA01) pathogens were transformed with pME6032ΔlaclQ::MCherry Tc resistant plasmids which express the protein mCherry to allow for analysis of coverage of these bacteria on the surface via fluorescence. These strains were grown routinely on Luria Bertani agar plates at 37^{o}C. A single colony was placed in 10mL of LB broth overnight at 200RPM and 37^{o}C. This protocol was selected due to its use as a simulation of conditions inside catheters though the attributes of a successful coating are similar regardless of conditions. [249] For standardisation of the experimental conditions, chemically defined RPMI-1640 (Sigma, UK) medium was used. UV-sterilised slides coated in PPR were incubated in 15ml of RPMI medium. These slides were inoculated with diluted mCherry containing bacteria from cultures grown at 37^{o}C overnight and shaken at 60RPM for 72 hours (OD_{600} = 0.01). At this point the slides were washed three times with 15ml PBS for 10 minutes at room temperature. Salts were removed by rinsing the samples with millipure water. These samples were analysed immediately in order to prevent the formation of dried patches across the surface of the slide. They were assessed using a Carl Zeiss LSM 700 laser scanning microscope with ZEN 2009 imagine software (Oberkochen, Germany). Coverage of bacteria across

the samples was analysed using open source ImageJ 1.48 software (National Institutes of Health, US).

For LIVE-DEAD staining of the viability of bacteria, non-transformed PA01 bacteria were used. After washing, bacteria were stained at room temperature for 30 minutes using a *Molecular Probes* L-7007 LIVE/DEAD® *Bac*Light™ (LD) Bacterial Viability Kit (Thermo Fisher Scientific, USA). 2.06µL of Syto9 (green fluorescent for live bacteria) and 2.08µL of propidium iodide (red fluorescent for compromised membranes) dyes were mixed in 5mL of water. 200µL of the stain was applied to each PA01 exposed sample and these were covered to avoid direct sunlight and incubated for 30 minutes. These samples were then rinsed with water before observation using laser scanning confocal microscopy.

5.2.3. Growth Curves

mCherry transformed strains of PA01 bacteria were streaked on LB agar plates and grown overnight in a 37^{o}C oven. Sterile plastic loops were then used to remove a single colony of bacteria. This was placed in 10mL of LB broth overnight at 200RPM and 37^{o}C. Bacterial solutions of absorbance OD_{600} = 0.01 were added to 13.5ml of RPMI and 1.5mL of differing concentrations of either 900c or TnBT dissolved in water. Another experiment was run using LB media in place of the RPMI media. A wild-type with no catalyst was used as a control. The absorbance of the solution at OD_{600} was recorded in an Evolution 60S UV spectrophotometer by Thermo Fischer at different time points throughout a 48 hour period. The solutions were maintained at 37^{o}C and 200RPM for the entire run.

5.2.4. Tracking of Bacterial Surface Movement

PA01 on the surface of the coatings were videoed using a Nikon Eclipse Ti 2000 inverted DIC at 40x magnification in bright field mode at 50Hz for 10 seconds each minute after immersion in media. 150 x 150 µm areas were taken.

Pseudomonas bacteria in Midlog-phase for 2 hours were analysed after inoculation in RPMI-1640 medium at 37 °C and OD_{600} = 0.03.

To track bacteria in time series stacks every frame were preprocessed in Matlab (Mathworks) by subtracting an image captured behind the focal plane. A threshold was then set in ImageJ 1.44 software to identify which pixels did or did not contain a bacteria. Object analysis was obtained in ImageJ with ellipse fitting, acquiring the centre of mass and the perimeter around the bacteria.
Bacteria positions were joined into tracks with the use of a custom designed script in Matlab (Carabelli & Hook).

The instantaneous speed was calculated using **Eq 6**.

$$\vec{v}_i = {|\vec{x}(t_{i+1}) - \vec{x}(t_i)|}/{\Delta t} \qquad \text{(Equation 6)}$$

where $\Delta t = t_{i+1} - t_i$ while the average speed was calculated via **Eq.7**.

$$\vec{v}_{average} = \frac{1}{n}\sum_{i=1}^{n}(\vec{v}_i) \qquad \text{(Equation 7)}$$

where n is number of points in the track. The sum of distances $\overrightarrow{SD_{cm}}$ from the centre of mass is calculated as **Eq.8**.

$$\overrightarrow{SD_{cm}} = \frac{1}{n}\sum_{i=1}^{n}\left(\left(\vec{R}_i\right) - \left(\vec{R}_{cm}\right)\right) \qquad \text{(Equation 8)}$$

where $\vec{R}_i$ is the position vector of the ith point on the trajectory, and $\vec{R}_{cm}$ is the centre-of-mass of all points. This parameter gives information about the average displacement between points in the trajectory.

The standard deviation travel angle was defined as the standard deviation considering all angles obtained between a bacterium's instantaneous velocity vector and the *x* axis. This parameter gives information about directionality.

Bacteria were classified as stationary or swimming bacteria using a speed cut-off set at 20 μm sec^{-1}.

5.2.5. Microfluidic Strength Detachment Assay

The strength of adhesion of *P. aeruginosa* on surfaces was assessed against a glass borosilicate positive control using a microfluidic assay developed by Christophis *et al*. [261] Microchannels (14 mm × 1 mm × 50 μm) were used, comprised of PDMS through Xurography (a cost effective alternative obtained with ultra-rapid prototyping). Double-sided tape with known thickness, cut by a knife plotter was embedded between the PDMS membrane and a surface. The channel was the result of the removal of the regions that had been cut. PDMS was squeezed on a coverslip with the surface of interest through a clumping system. A neMESYS low pressure precision syringe pump (Cetoni GmbH, Germany) was controlled by the neMESYS User Interface inbuilt computer and was used to aspire medium and generate flow inside the channel. The shear stress (τ) was described through Poiseuille's model as the force exerted onto channel walls which can be calculated using Equation 9. [262]

$$\tau = \frac{6\,Q\,\mu}{h^2 w} \qquad \text{(Equation 9)}$$

Q is the flow rate, μ is the liquid viscosity and *h* and *w* are the height and the width of the channel respectively.

The system was mounted onto an inverted microscope. Bacteria were first inoculated with RPMI-1640 medium at 37 °C and $O.D_{600nm}$ = 0.03 in midlog-phase for 2 hours.

The removal process was obtained by applying a weak flow (0.0276 ml min^{-1}) with a shear stress of ≈ 0.01 dyn cm^{-2}, which was subsequently increased stepwise with an increase of 26% every step until a maximum shear stress of ≈ 5,000 dyn cm^{-2} was reached.

5.3. Results

5.3.1. Bacterial Coverage

After 3 days of incubation in RPMI media containing PA01 bacteria, confocal microscopy was used to determine biofilm coverage across the surface of the coatings plus a non-reorienting PDMS standard. **Figure 5.1** (*Upper*) displays a sample of these microscopy images. The PDMS standard qualitatively had a greater coverage of bacteria across its surface. This is opposed to the image for coating formulation **2** which appeared to have the lowest biofilm formation. This particular sample demonstrated large areas with no visible bacteria, different from other samples where the coverage was consistent over the whole surface. Clean glass had comparatively lower bacterial coverage than PDMS, more similar to the amphiphilic coatings but not quite as low coverage on average. None of the samples appeared to promote a complete biofilm, with gaps appearing between small areas of bacteria aggregation. Formulation **5** demonstrated an almost defined circle or rod shape of bacterial grouping together as opposed to the more random distribution seen in the other samples. The coatings displayed were representative of the formulations which used the same cross-linking catalyst, e.g. **2** is similar to **1** and **5** is similar to #s **3**, **4** and **6**.

Phase microscopy images of the same surface are shown in **Figure 5.1** (*Lower*). The patterns of bacteria accumulation across the surface were similar in comparison to the confocal microscopy images. The glass slide had no distinct film formation with limited clumping together but with a greater total surface coverage. On the amphiphilic coating the circular shapes were again prominent.

Comparison samples of all the coating formulations were exposed to bacteria after being immersed for six months in artificial sea water. This was in order to determine whether their surface anti-bacterial properties would be affected by the physical and chemical environment they would be exposed to in a marine

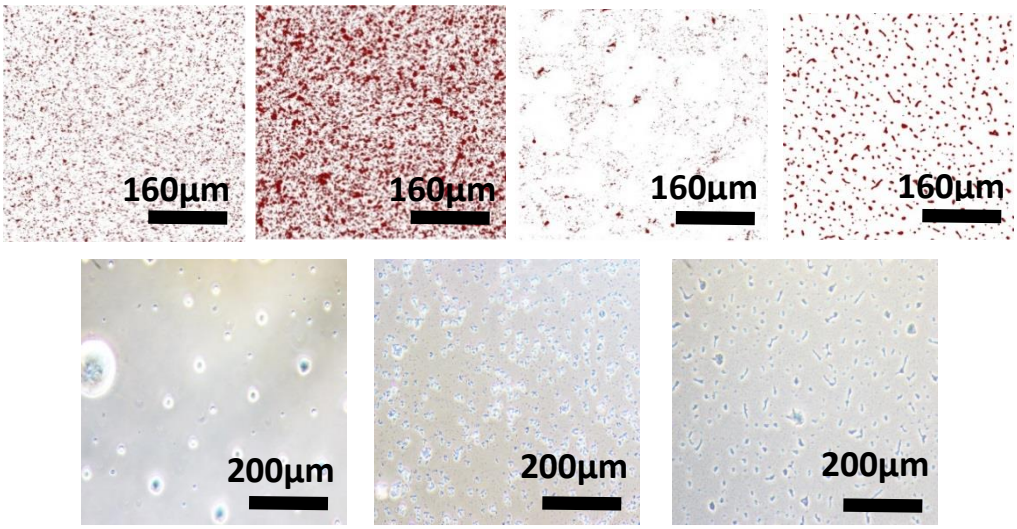

Figure 5.1. (*Top Left to Right*) Confocal microscopy images displaying *Pseudomonas aeruginosa* coverage on glass, a cured PDMS sheet and coating formulations **2** and **5**. Coatings cross-linked using phosphorus catalyst displays the least coverage. (*Bottom Left to Right*) Phase microscopy image of coating formulation **5** without bacterial coverage, glass and formulation **5** with bacteria adhered to the surface.

environment. The numerical values of the bacterial coverage of both fresh and immersed samples alongside positive controls are compared in **Figure 5.2** (*Top*). Coating formulation **2** had the lowest average coverage in both fresh and water exposed conditions. Formulations **1**, **4** and **6** displayed similar coverage, no matter whether they had been exposed to marine conditions or not. Formulations **3** and **5** showed a slight reduction in percentage coverage. All of the formulations had markedly lower bacteria coverage than the PDMS standard. The two experiments were compared graphically in **Figure 5.2** (*Bottom*). The R^2 value for the fit of the points was 0.5, suggesting the model sample environments partly explains the variation between the samples though not fully. Almost all of the coatings on average had less bacterial coverage after immersion than when a fresh sample was used. Only formulations **3** and **5** were significantly different before and after immersion.

5.3.2. Live/Dead Staining

Stains used to analyse compromised bacterial membranes were used to assess the mechanism by which the coatings might prevent bacterial adherence. These stains can also analyse whether the surface chemistry is potentially harmful to

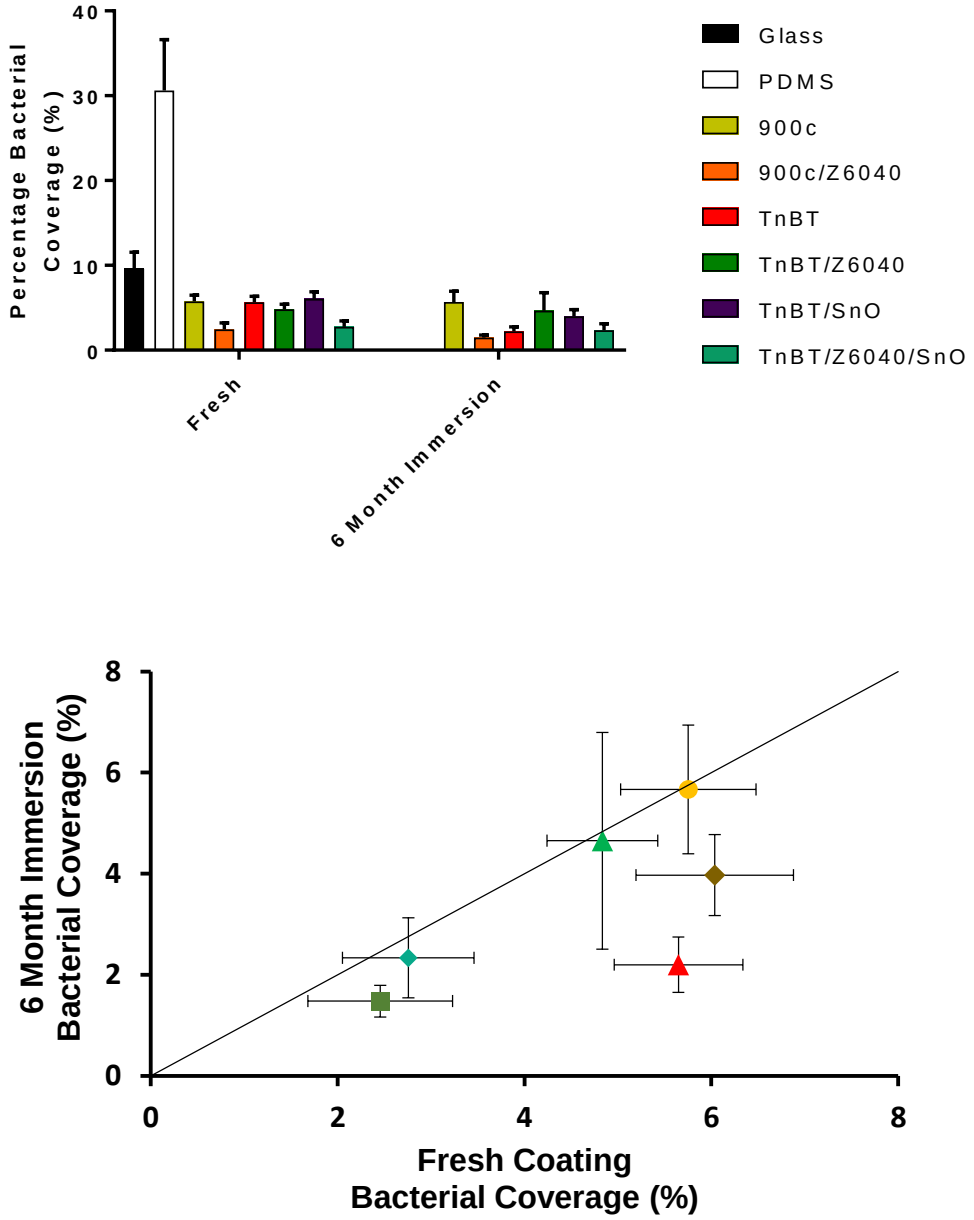

Figure 5.2 (*Top*) Bar chart displaying the individual means of *Pseudomonas* aeruginosa coverage of each coating formulation along with glass and PDMS controls. Anti-bacterial performance is consistent regardless if left in water for 6 months or not. (*Bottom*) Graph comparing bacterial coverage of fresh coatings to those immersed in artificial sea water for 6 months. Line of X=Y fitted through the centre of the graph. $R^2 = 0.5$. Anti-bacterial properties are maintained over the period of immersion.

biological systems in a marine environment. Confocal microscopy images of surfaces stained using Syto9 and propidium iodide are displayed in **Figure 5.3** (*Top*). All the images show different levels of bacterial coverage but all are dominated by a strong green colouring, implying that the bacteria across the surface are alive. There were minor areas of red seen in the upper right hand

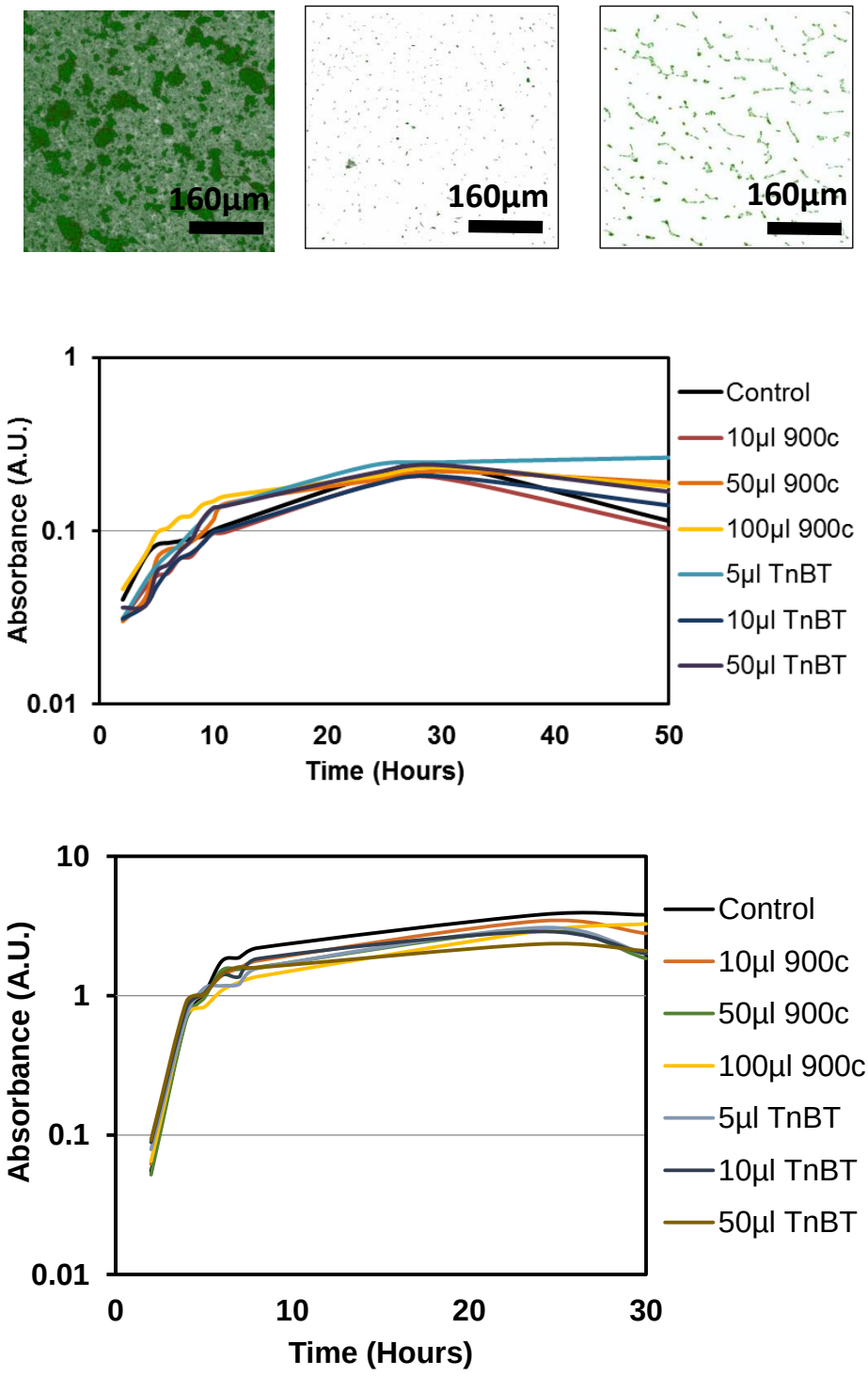

Figure 5.3. (*Top Left to Right*) Confocal microscope images of Live/Dead stained PA01 on PDMS, formulation 1 and formulation 5 respectively. All display adhered bacteria are generally alive, displaying the coating likely does not have any harmful effect on bacteria. (*Middle*) PA01 growth curve of bacteria in RPMI media and 900c or TnBT catalyst. Generally slow growth seen but not as an affect of catalyst as all samples demonstrate similar rates of change in absorbance. (*Bottom*) PA01 growth curve of bacteria in LB media and 900c or TnBT catalyst. Rates of change of absorbance are faster than in RPMI and are similar in all samples implying the catalysts do not have a negative effect on bacteria or their growth rates.

corner of the PDMS control but almost no red regions were seen in any of the amphiphilic coating formulations. As before the images displayed were symptomatic of those seen for other formulations cross-linked using the same catalyst. The patterns of biofilm formation on the coating were also similar to those seen in the mCherry bacteria.

5.3.3. Growth Curves

Live/Dead staining can not conclusively determine whether the surface chemistry is adversely affecting model marine organisms as it only considers bacteria at the surface. In this case, pure catalyst was used to determine how it affects the growth rate of bacteria. **Figure 5.3** (*Middle* and *Bottom*) show how the optical density of bacterial culture changed over time when the incubation medium was RPMI or LB respectively. In both samples the exponential growth phase began almost instantaneously and the rate of bacterial growth in the log phase appeared to be entirely unaffected when either of the 900c or TnBT catalysts were present, regardless of the concentration. Higher concentrations could not be used as they made the solutions too cloudy, which would have affected the measurements. The stationary phase was reached more rapidly in the LB run at just under 10 hours. It took the RPMI sample nearly 30 hours to reach the same stage and almost instantaneously reverted to the death phase. All the samples retained similar absorbance values to each other through the whole cycle.

5.3.4. Bacterial Movement

To further ascertain the mechanism and therefore the reason why bacteria do or do not adhere to the surface of the coatings was assessed by tracking the movements of PA01 in log phase using DIC microscopy. Videos over a period of 10 seconds were analysed using a bespoke Matlab script. A representative track of bacterial movement across the surface on glass and on coating formulation **3** are displayed in **Figure 5.4**. More tracks were seen on the samples using glass as a control surface. They appeared to move in less defined ways, moving in circles and more curved trajectories than on the polymer

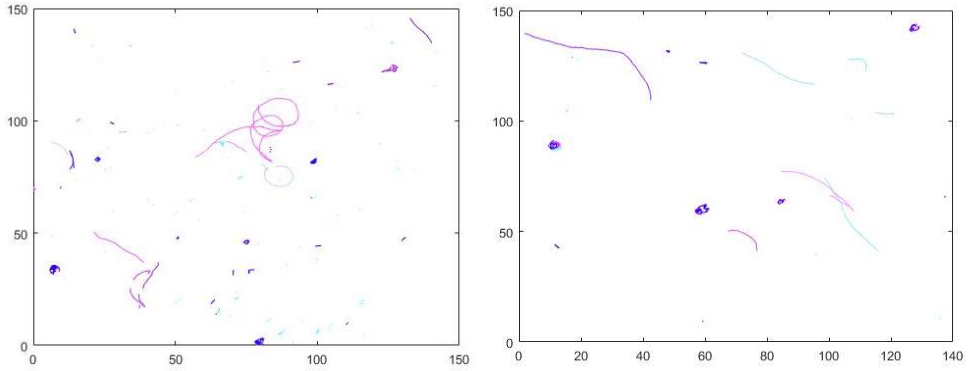

Figure 5.4. (*Left*) 150 x 150µm movement tracking diagram of PA01 on glass. Limited movement seen across the surface, majority of bacteria are stationary so do not appear on the track. (*Right*) 150 x 140µm movement tracking diagram of PA01 on sample formulation 3. Less bacteria at the surface hence the lower number of tracks compared to glass. The chemistry of the surface likely does not affect how bacteria move at the surface.

surface. The presence of less bacteria (demonstrated in section **5.3.1.**) means that there were less visible tracks on the surface of the amphiphilic coating. Of the few tracks recorded the movements are more predictable, with the bacteria moving in somewhat curved lines but not to the extent seen on glass. On the glass cover slip there are a number of dots on the figure meaning the bacteria are just twitching or remaining reasonably still for the duration of the video. The same is true for the surface of formulation **3** but they are 10% fewer in number. To assess more subtle details of bacterial movement, the average speed of the bacteria on the surface and sum of mean distances (or the average displacement of points along the track) was examined (**Figure 5.5** (*Top Left and Right*)). The averages ranged from 30 to 40µm/second on glass and 23 to 30 µm/second on coating formulation **3**. The mean values were more consistent on the polymer over time than on the glass control which saw a trend of an increase in the average speed of PA01. The range of the data was relatively uniform regardless of the sample or the timings. However, for the sum of the mean distances, the points of displacement on the track were clearly lower (the difference in significance could not be determined due to the difficulty in repeating the experiment). The length of time of immersion of the coating did not present a trend in terms of the sum of mean differences, with the values fluctuating between set levels (for glass 300 to 500µm and for coating formulation **3** from 75 to 180µm).

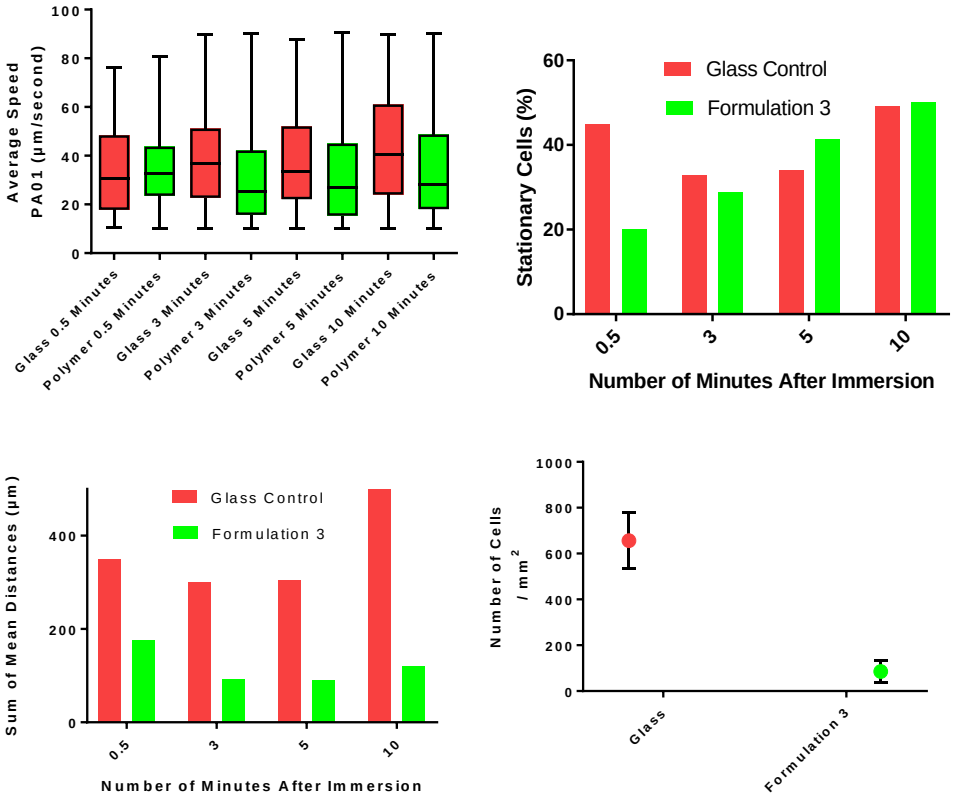

Figure 5.5. (*Top Left*) Graph of the range of the average speeds of PA01 movement on the surface over 10 seconds on glass and formulation 3. Little differences discernible between any of the measurments. (*Top Right*) Graph of the percentage of stationary cells on the surface of the sample. Aside from at 0.5 minutes there is no significant difference between samples and timings. (*Bottom Left*) Graph of the sum of mean distances from the centre of mass. Lower mean distances seen for the polymer compared to the glass. (*Bottom Right*) Number of cells seen on the surface at the beginning of the run. As expected there were much less bacteria on the surface of the amphiphilic polymer than the glass control.

The number of stationary cells was analysed by subtracting the total of cells moving on the surface moving (calculated in the script) from the total number of bacterial cells. Aside from the initial time point of 0.5 minutes where there are vastly more stationary cells on the glass surface than the polymer, there were no clear differences between the two samples. However, the polymer coating did display an increase in the number of stationary cells over time, increasing from 20% to nealy 50%. The percentages on the glass control showed no trend over time. To corroborate the coverage data obtained using confocal microscopy, the number of bacterial cells adhered to the coating were

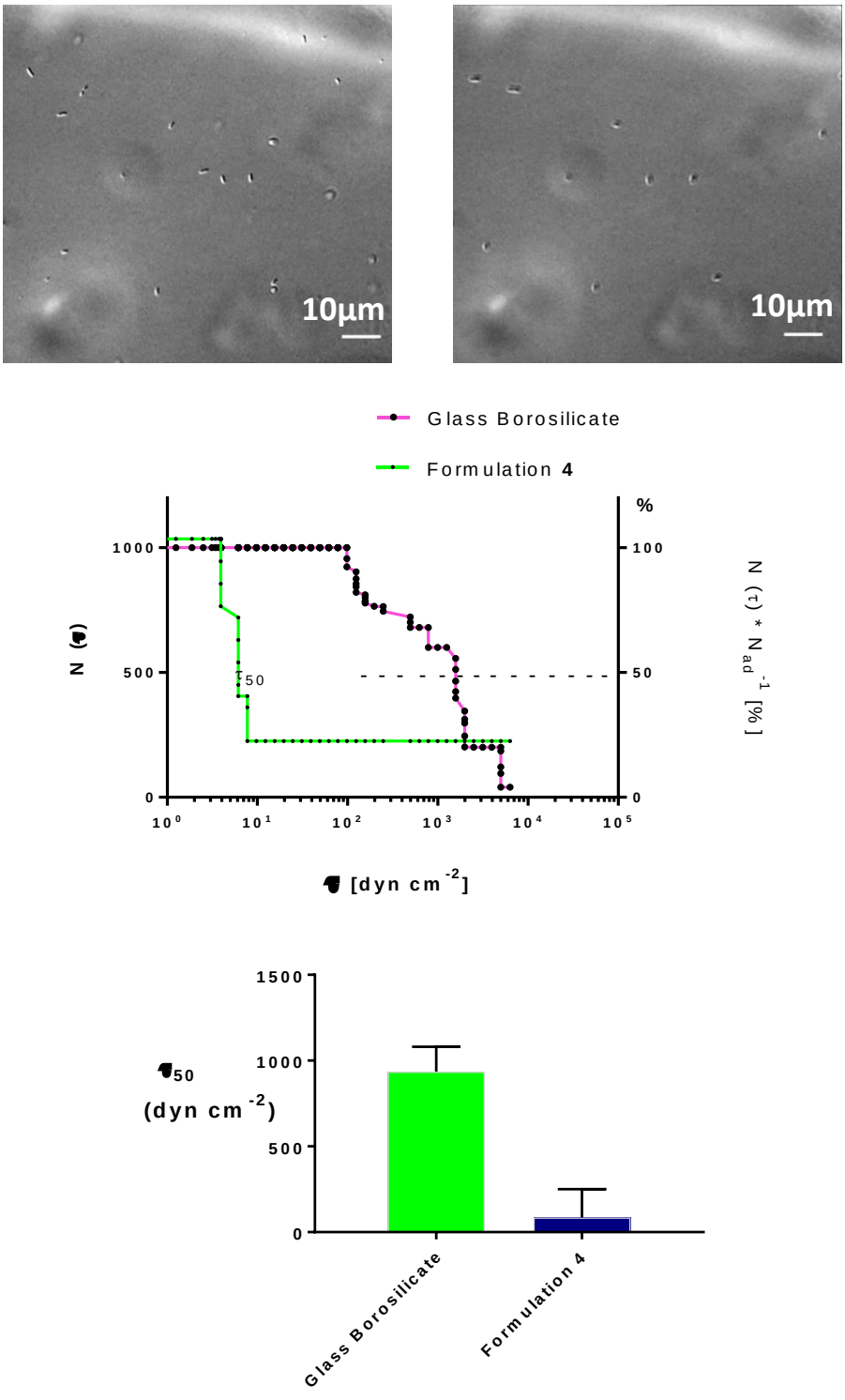

Figure 5.6. (*Top Left*) Still taken from the zero time point of a DIC video of PA01 on the surface of formulation 4. (*Top Right*) Still taken from a DIC video after PA01 subjected to greater flow conditions. Less bacteria are seen after exposure to flow. (*Middle*) Graph displaying the removal of bacteria from positive control glass borosilicate and coating formulation 4 as a function of an applied shear stress. In this case, 10 dyn/cm^2 corresponds to 1 Pa. (*Bottom*) Average critical shear stress needed to detach 50 % of the adherent PA01 from the surface of the samples. Amphiphilic coating demonstrably decreases the strength that bacteria attach to the surface.

counted. Whereas glass had around 700 cells/mm^2 coating formulation **2** had under 100 (**Figure 5.5** (*Bottom Right*)).

5.3.5. Adhesion Assays

Foul release coatings are designed to reduce the strength that bacteria adhere to their surface. To quantify the effectiveness of the amphiphilic coatings at reducing bacterial adherence, sheer stress adhesion assays were run using DIC microscopy. **Figure 5.6** (*Top Left and Right*) displays still images of coating formulation **4** with bacteria on their surface before and after flow was applied. In the right hand image only half of the bacteria remain compared with the image on the left. The flow rate at which 50% of the bacteria are removed is used to determine the τ50 or strength of adhesion for a particular bacterial species to that surface. The graph used to determine this value is shown in **Figure 5.6** (*Middle*) comparing bacterial % coverage against sheer stress. For the coating this value was two orders of magnitude lower than for the amphiphilic coating, being ~1000 and 10dyn cm^{-2} respectively.

5.4. Discussion

After exposure of each coating formulation to PA01 over 72 hours, each of the formulations were qualitatively (by image inspection) and quantitatively (using the total biofilm coverage) better at preventing biofilm formation than the non foul-release PDMS control. The average coating was around eight times more effective at preventing the adhesion of PA01 as compared to PDMS. Formulation **2** cross-linked using the phosphorus catalyst was the most effective at preventing bacterial adherence but it was not this particular attribute that made it adept at doing so as Formulation **1** with the same catalyst performed the least well over the six month period. The coatings which contained a silicon based drying agent performed better. The relatively minor differences observed between the samples need to be considered in the context the error bars that indicate that none of the coatings (aside from formulation **2** after six months) performed significantly better than the others. Given the

limited differences between the samples it may be that choosing the best coating arises from minor disparities in performance alongside other issues such as cost and ease of application. The experiment itself was complicated by the fact that when using glass slides, floating bacteria accumulated at the meniscus point where the top of the bacterial solution met the slide, saturating the confocal microscope images (**Appendix 6**). This biofilm extended into solution meaning that for an accurate reading, a greater volume of solution needed to be used, to provide adequate space below this accumulation for an image to be recorded. This is an important consideration for potential improvements to the coatings, as potentially strong accumulation at the point of contact with water on a seafaring vessel could have negative consequences such as increased biofouling. This is particularly true at this interface, where the aggregation of foulants could occur too high up the side of the ship to use the ocean flow to brush off these foulants, but be low enough to still cause some frictional drag.

The morphology of the biofilm on the controls and the coatings differed from each other. On the coatings with titanium as its cross-linker, distinct dots were visible with little joining up of these areas as compared to the PDMS control. This was similar to the glass control though the dots were generally smaller on glass, though more numerous, giving a higher total coverage of PA01. This suggests that the differences in surface chemistry (even minor ones between the coatings) do affect how bacteria interact with the surface. For coating formulation **2** the areas of coverage are separate from each other which may suggest that the coating's mechanism of action makes it more difficult for bacteria to adhere strongly enough to the surface in order that it can move across the surface and join with other bacteria to form a biofilm. The fact that this consistent appearance of PA01 on the different surfaces is also seen in phase microscopy suggests that this biofilm pattern is not likely to be random.

The length of time the samples were left in sea water also made no difference to their foul prevention properties. Each sample was essentially equally as effective (with minor exceptions) after six months immersion than before. The coatings were exposed to laboratory conditions with no physical forces being

applied to the coatings such as scratching or bumping, and the sample of sea water was likely not fully representative of the range of conditions the coatings would have to withstand. Therefore it cannot be concluded with certainty that the coatings will be as effective in a marine environment. However, with little to no delamination of the coating observed, it is clear that the water itself will not cause detachment of the coating to a particular substrata.

Though this particular experiment did provide a strong indication that the coatings are effective at preventing bacterial attaching to the surface, it is less useful at determining whether they act as good foul-release coatings. Foul-release implies that the coatings are good at reducing the strength that bacteria attach to them. In real world applications, foul-release technology uses the flow of water to remove foulants from the hull of ships. Foul-release potential is not easy to determine over a long period of time in low flow conditions. It was attempted to test coatings that were shaken at 60RPM against a set that wasn't shaken. This was to see if the shear forces in the shaker made the foul-release properties of the coating more pronounced. No significant differences between the samples or experiments that are not already described were seen. It could have been concluded at this point that the coatings were therefore no more effective at foul-release than other polymers, however the shear forces were likely not high enough to conclude this, therefore an adhesion assay was run on the samples. A lower flow rate by two orders of magnitude was required to remove 50% of the bacteria from the surface of the polymer films than on a glass control. This confirms that the coatings have improved foul-release properties to other surfaces that don't have low energy or foul-release properties. The low surface energy of the coatings is therefore able to reduce the ability of bacteria to adhere to the surface.

Tracking the movement of bacteria did not provide a clear distinction between the behaviour of PA01 glass and the PPR coatings, nor did it provide clarity as to how these coatings better prevent bacterial attachment. Though the number of bacteria present on the surface of formulation **2** was lower on the coatings than on glass, the tracks themselves were not markedly different. Different kinds of tracks are visible in **Figure 5.4** but there was no clear pattern in repeat

experiments as to the specific kinds of behaviour the bacteria undertake when on the coatings as opposed to glass. The fact that small dots are visible in the tracks show that there is likely to be a certain amount of twitching by bacteria on the surface of both the glass and the coating. Often differences can be observed by minor movements of the bacteria, such as twitching or slingshotting and need to be observed over a much longer time period, as opposed to the 10 second snapshots described herein. [263, 264] Despite the morphological differences seen above in the formation of biofilms across the samples, there are no clear indicators in the behaviour of individual bacteria that suggest why this may be the case.

The average speed of the PA01 cells was also very similar between glass and the coatings. This suggests that these particular measurements are not the optimal way of measuring the mechanistic action of these particular foul release coatings. Though the displacement points on the paths differ between the two samples, there is no other data that agrees with or provides an indication of a trend, so the explanation for this difference is not possible to assign conclusively. Therefore, the adhesion data is more differentiating as to the process that is occurring. The coating does not alter bacterial response but merely makes it more difficult for the bacteria to adhere to this particular surface as strongly as would be required to form biofilms.

Live/Dead staining of the coatings showed that the coatings are unlikely to be toxic to a marine ecosystem. There was a clear prevalence for green (alive) bacteria attached to the surface of the coatings. This implied that the bacteria were generally alive on attachment and very little non-specific binding of dead bacteria was occurring. The results (in terms of the bacteria colour) were similar in comparison to pure PDMS and glass, which are known non-toxic materials. [265] Therefore, the mechanism of action that prevents bacterial attachment to the coatings is predominantly foul-release and non-fouling rather than destructive and specifically anti-fouling, at least against the model bacteria PA01. This was further confirmed by the fact that even after adhering to the surface after ten minutes, bacteria were still moving around the surface as seen in the movement trackers. More specific marine foulants such as

Cobetia marina or the barnacle species *Balanus Amphitrite* would have to be tested to definitively conclude the non-toxic nature of these coatings but the results above are clearly promising.

The non-destructive mechanism of action at the surface of the coatings does not necessarily demonstrate that the catalyst that leeches out of them is not toxic in the marine environment. In chapter 4, the phosphorus based catalyst 900c was shown to leech from the coatings into water. Bacterial growth curves were able to confirm that regardless of the bacterial growth medium, 900c and TnBT catalysts did not adversely affect the growth of bacteria in solution. The rate of growth in log phase and the similarity in the growth curves as a whole were very similar regardless if the catalytic solution was present in the growth medium or not. Therefore, the leeching of elements of the coating matrix into a marine environment would be unlikely to negatively impact the ecosystem.

5.5. Conclusions

The PPR coatings are very adept at foul-release, decreasing the strength of the rate of flow required to remove *Pseudomonas aeruginosa* from their surface by a nearly two orders of magnitude. Though this was only tested on coating formulation **4**, given the similarity of all the coating formulations in both their chemistry and ability to prevent bacterial attachment, it is likely the other coating formulations are equally effective at this task. The low surface energy of these coatings also means that bacteria struggle to stick to them in the first instance, as seen by a decrease in coverage of around 8 times between formulation **2** and a PDMS standard. Therefore the amphiphilic nature of this coating has an important effect in preventing bacterial attachment, as it performed better in solution than a control which was known not to reorient.

Observing the movement of bacterial cells on the surface was less effective at providing mechanistic detail, requiring further analysis. However, it did corroborate data from confocal microscopy in that the numbers of PA01 cells at the surface were lower than on a glass control.

The non-fouling mechanism of the coating can also be assumed to be non-toxic given the lack of non-specific adherence of dead bacteria to the coatings.

The work of this chapter, whilst providing a good base for understanding the potential for these coatings to prevent fouling formation, has only studied one species of bacteria. Field tests will be required to conclude whether the coatings are an effective material for their function.

Chapter 6

Field Trials to Determine the Effectiveness of Amphiphilic Polymers at Preventing Biofouling in a Marine Environment

6.1. Introduction

Characterising potential foul-release coatings in a lab-based setting can answer very specific questions about how surface properties are able to hinder specific bacterial species from adhering to their surface. However, it does not necessarily give clear insight as to how successful the coatings are at preventing more complex marine biofouling. The biofouling process requires a number of different components, from oleic acids and long chain sugars to macrofoulers such as barnacles. The simulation of this process of the formation of biofilms is difficult to replicate in the laboratory. Therefore, exposing novel coating candidates to a true marine environment such as on a buoy or on a plate in a harbour for a defined period of time is a needed and effective method to assess how successful coatings are at reducing biofouling. Inspection of the coatings after immersion can give a qualitative perception of how much coatings can prevent fouling. For quantitative data however or when analysing more subtle changes, alternative approaches are required that are often dependent on the kind of species being analysed. For example, the effect of the roughness of coatings on the recruitment of *Balanus improvises* barnacles was analysed by Berntsson *et al*. [268] Over a period of five months and at four different depths the total number of barnacles counted was reported to define settlement intensity. Alternatively, Palletier *et al*. compared several different techniques used to assess field trials. [269] Firstly, using a method devised by Trees *et al.* they were able to analyse the growth of algal biomass over time. [270] Epiflourescence microscopy was used to determine the variation in the number of microalgae species that comprised the developed biofilms. In another study dry weighing of the residual biomass was used by Artham and Doble to quantify the levels of biofouling that remained on the surface after three months in a marine environment. [271] This was compared to lab based tests which confirmed differences in polymer surface degradation.

Alternatively, in researching other forms of biofouling such as those that occur on medical devices such as implants, these techniques could potentially be applied to the marine fouling field. The vast number of catheters used per year and the problems patients experience with biofouling and subsequent infection make them one of the most studied medical devices. Brydon *et al*. isolated protein from biofilms that had been formed on the surface of silicone rubber catheters. [272] Western blotting and gel electrophoresis was used to identify the adhered proteins. QCM-D, AFM and ToF-SIMS have also been used to study the competitive exchange of blood serum proteins by other proteins with stronger binding affinities, known as the 'Vroman Effect'. [273]

Due to the complexity of marine fouling, its variation with on temperature, environment and location around the world, the chosen analysis method is of particular importance. Fortunately, the experiments commonly used to analyse marine fouling are often simple and ubiquitous so can generally be applied to the majority of novel samples to get a perception of the ability of a coating to prevent biofouling.

6.1.1. Aims

To elucidate the foul-release properties of the amphiphilic coating described thus far, field tests were carried out in a European location. Protein and carbohydrate assays were selected in order to look at subtle changes between samples and to complement work conducted previously in another European site. Microscopy was also used to provide more crude analysis of the percentage coverage of biofouling on four of the different coating formulations.

6.2. Methods

6.2.1. Deployment at Marine Site

Six replicate slides for sample formulations **1**, **2**, **3** and **5** were deployed in an engineered test rack (**Figure 6.1**) designed for marine deployment. [274] This was to ensure each chemical used in cross-linking was examined at least once. The samples were submerged for seven days on a buoy at Port de Brest, France (**Figure 6.2**). This was performed in the first week of June 2015. The average sea water temperature was 13.9-14.5^{o}C over the period from the 8th to the 15th of June.

6.2.2. Protein Adsorption Assay

To determine the protein adherence to the surface a modified Lowry assay was used by Kim Nolte *et al*. at Ruhr Universität. [275] A 40mL modified Lowry reagent was devised using Milli-Q water. Folin Ciocalteu's phenol solution was diluted in this water at a 1:5 (v/v) ratio and was stored at room temperature. All samples were rinsed with Mill-Q water before analysis and where then placed in a 50mL sample tube. These tubes were filled with ultra-pure water and sonicated for five minutes. 3000RPM centrifugation was applied for five minutes at room temperature in order to remove particulates that may have been suspended in the solution after sonication. A 0.5mL aliquot of the sample was added to a 7mL sample tube containing 0.5mL of Lowry reagent solution. This was incubated and mixed for 20 minutes at room temperature. Then 0.25mL of Folin-Ciocalteu's phenol solution was added to the sample tube and shaken and incubated at room temperature for 30 minutes. Absorbance of the solutions was measured using UV-Vis spectroscopy at 750 nm (n = 3). These were compared with values from calibration curves produced before analysis (**Appendix 6**).

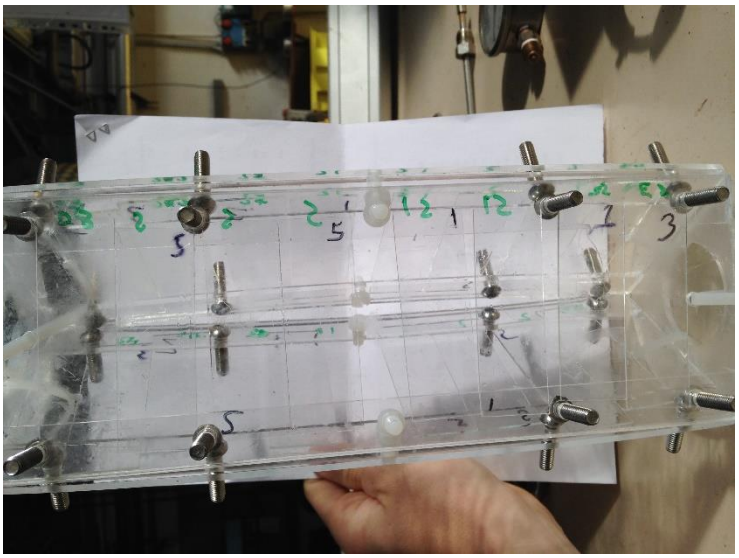

Figure 6.1. Deployment structure for field testing containing slides coated with amphiphilic PDMS based polymers.

6.2.3. Carbohydrate Adsorption Assay

The total carbohydrate content on the surface of the samples was analysed using a modified Dubois method. [276] This was also carried out by Kim *et al*. A phenol solution 5% (w/v) was made up with Milli-Q water and 95-97% sulfuric acid. The retrieved field samples were rinsed using Milli-Q water before analysis and added to a 50mL sample tube. These tubes contained ultra-pure water and were sonicated for five minutes. This was followed by centrifugation at 3000 RPM for five minutes at room temperature to remove particulates. 0.5mL of the sample was taken and added to a 7mL sample tube containing 0.5mL phenol solution and 2.5mL sulphuric acid. This was mixed immediately. The samples tubes were then incubated for 10 minutes at room temperature then for 15 minutes at 30 ^{o}C. After five minutes at room temperature to rest, the absorbance was measured at 480 nm in UV-vis to determine acidic carbohydrate followed by 490 nm for the determination of neutral carbohydrates (n = 3).

6.2.4. Microscopy

The coated glass slides for Microscopy were fixed in glutaraldehyde, rinsed and air dried. A Nikon ti eclipse phase contrast microscope with a Texas red

Figure 6.2 Geographical location of Port de Brest, where the samples were subjected to a marine environment.

filter setting in destructive phase contrast mode was used. Auto fluorescence of chlorophyll at 465 nm were used for imaging and determination of area of coverage due to fouling. Four images were taken from different points of the slide and coverage was determined using the inbuilt Nikon NIS elements software.

6.3. Results

6.3.1. Protein Adsorption Assay

In protein assays, usually the concentration of protein would be recorded. However, as seen in **Figure 6.3** (*Top)* the absorbance values were low and in some cases negative thereby implying measurements were below the level of detection and noise was significant in relation to signal **Appendix 7**. This also included the negative glass control. Glass has no known anti-fouling or foul-release properties. There were consistently low values seen in all of the batches analysed. Large error bars were also seen implying there is no significant differences between the samples, often being larger than the absorbance value themselves.

6.3.2. Carbohydrate Adsorption Assay

The carbohydrate assay saw similar issues, with values too low to determine carbohydrate biofouling concentration at the surface, regardless of which sample was analysed (**Figure 6.3** (*Bottom*)). The large error bars make it impossible to distinguish between samples, even between the control and the coatings themselves.

6.3.3. Microscopy

The autoflourescence of chlorophyll was detected and analysed using fluorescence microscopy and was a marker to evaluate the percentage area of coverage of each sample. Representative images of the control and formulation **2** can be seen in **Figure 6.4** (*Top*). The percentage coverage of each sample was determined using this marker and the relative differences are displayed graphically in **Figure 6.4** (*Bottom*). The results were more stable than in the protein assays with quantification being possible. The percentage coverage on each sample was similar, with formulation **5** being the most heavily fouled and formulation **1** least. The coatings were not fouled any less than the negative

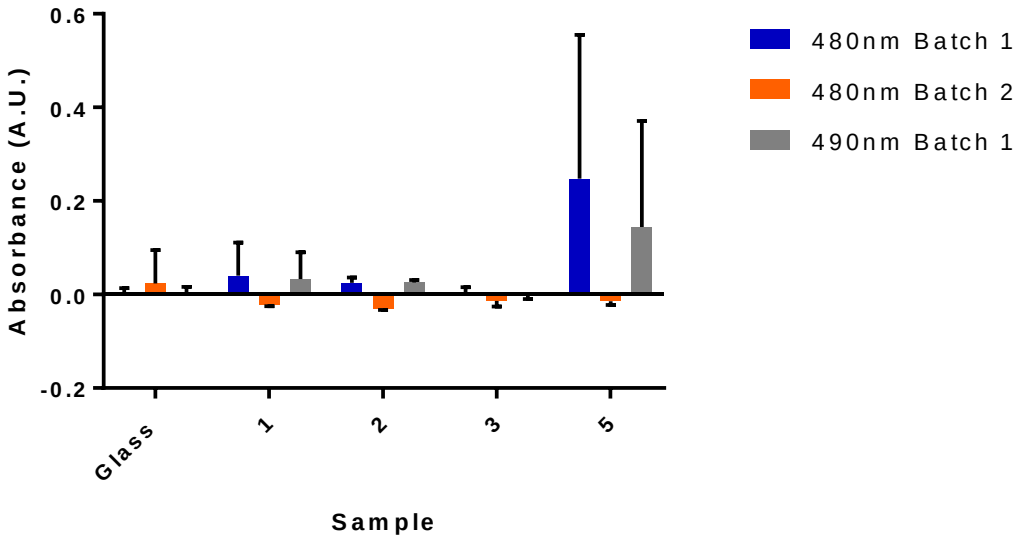

Figure 6.3. (*Top*) Absorbance of four coating formulations and glass at 780 nm after processing using a standard protein assay. The samples are all inconsistent with large error bars making it difficult to distinguish between samples or draw conclusions from the data. (*Bottom*) Absorbance of four coating formulations and glass at 480/490 nm after processing using a standard carbohydrate assay. Similar to the protein experiment the samples are not significantly different from each other, making it difficult to distinguish between them or draw conclusions from the data.

control. Given the size of the error bars it could be observed that there were no significant differences between any of the samples.

6.4. Discussion

During testing for biological matter on the surface of the polymer films, it became apparent that the coatings were not stable enough to mechanically scrape off the biofilms. Sample formulations **1** and **5** were the most fragile coatings, followed by **2** with **3** having the best stability for this particular test. This may explain the inconsistent and hard to analyse results seen in both the assays attempted. This partial detachment of the coating on scraping it likely had an effect on the solutions devised and therefore the final absorbance value. However, the negative control did not show notably higher fouling (by determination of protein or carbohydrate concentration) than the other coatings nor was the spread in the data any more consistent between different runs. In the protein assay it is possible that for the first run the Folin-Ciocalteu's reagent had

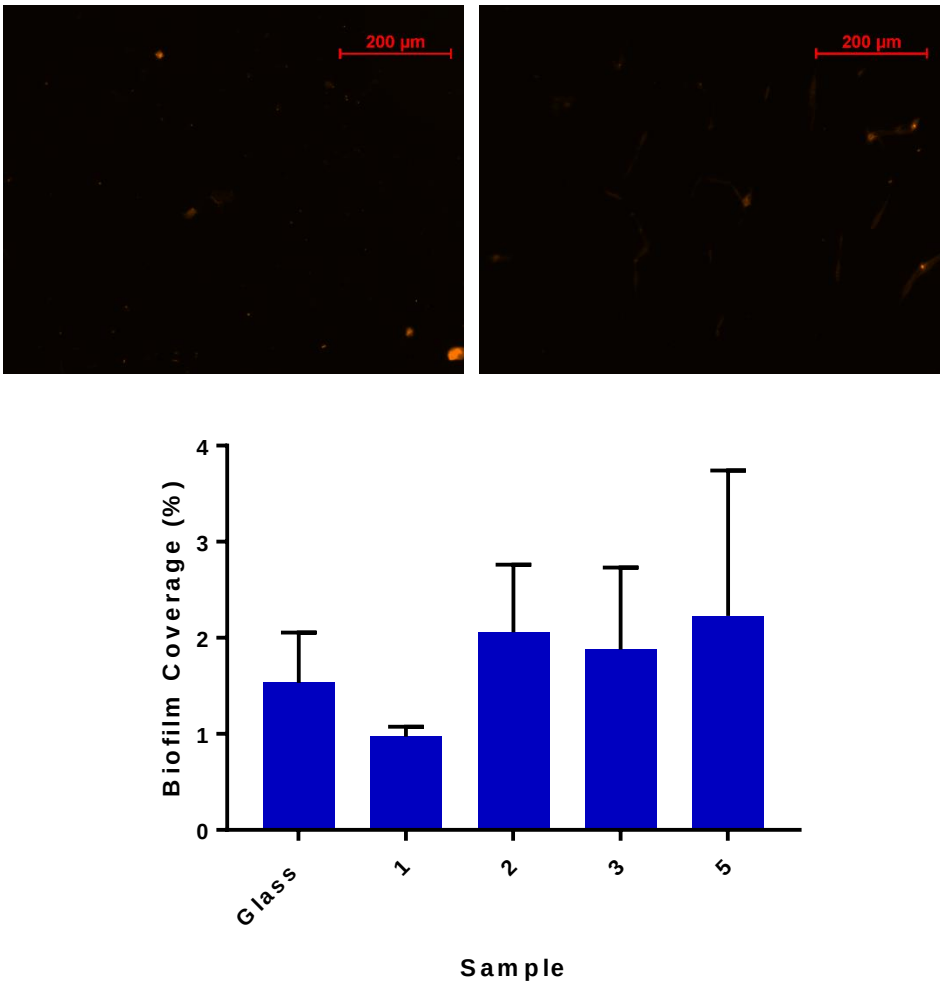

Figure 6.4. (*Top*) ~1 x 0.8 µm fluorescence microscopy images of glass and formulation 2 respectively. Area coverage of the samples with biofouling determined using chlorophyll autofluorescence (seen in orange). (*Bottom*) Bar chart displaying the average coverage over three areas on the sample. No significant differences were seen between the samples. This low level of fouling even on the negative control could be due to low fouling pressure.

been exposed to light for an overly long period of time before running the assay so a fresh batch was used for the second. As seen from the results however, there was no clear trend between the two runs to assert that using a new reagent produced significantly different results. The large negative value on the glass control in the second run corroborates this asertion.

Microscopic methods avoid the potential problems associated with mechanical strength of the coating, but did not provide a clearer indication as to the whether the coatings were more effective than the glass negative control. The error bars were smaller meaning the data itself was more stable and reliable.

However, due to the low fouling these error bars were rendered larger in comparison between samples. There is clearly no significant difference between the samples in this analysis.

There are potentially several reasons for the inconclusive results. Despite studies by Chapman *et al.* demonstrating that one week exposure in Poolbeg Marina in Dublin was sufficient for particular studies, in the case of this work in Brest it was likely too short. [277] However in a 2012 study also by Chapman the protein and carbohydrate presence on the surface of coatings over six weeks and found larger changes after week four. [274] Though the differences between the synthetic macroalgae polymers and the controls were significant, it does not show sufficiently whether this trend would be sustained over a longer period. Other studies have also erred towards using longer immersion periods of at least 12 months. [167, 278, 279] For example, Bressy *et al.* aimed to determine the efficacy of biocidal coatings in Brest and other locations in Toulon and Lorient. [280] These took place over a period of 12 months. Not only were there differences in the amount of fouling in the different cities, but also between sites located in the same city. The macrofouling communities present over this period of time were notably different. There are currently a number of international standards for testing such antifouling coatings in shallow submergence (such as that of a buoy). [281, 282] It is recommended that the coating panels are exposed for a *minimum* of one year, combined with a monthly fouling census.

For industrial relevance, trials usually last for several months over the April-October period, when microorganisms are more active. As the study was carried out in June this should not have been an issue though the length of the trials were potentially insufficient. The fouling pressure may have coincidentally been lower due to general unpredictability of the natural environment. Given the often differeing fouling pressures in sites that are close together this is highly probable. The sea temperature in Brest during the first week of June 2015 was not notably different from those of the same week in 2014 or 2016, so there was unlikely to be a significant change in the fouling species present.

6.5. Conclusions

The marine trials carried out were not sufficient to determine the ability of the amphiphilic coatings to prevent or release fouling. The major problem was that the methodology was flawed. This was for the following reasons, firstly the trials were not sufficiently long enough with most studies in the literature testing over a period of many weeks at minimum but ideally for around one year. Given the environmental conditions were not significantly different from previous years and studies, this can be quite strongly asserted. It may have been possible though that the fouling pressure was particularly low for the week in question. Secondly the coatings were not mechanically durable enough to withstand scraping of biofilm from their surface. The results of these tests could not be used to ascertain with any certainty as to the best coating formulation. For future work it would expected to be able to discriminate between candidate coatings and the negative control when the immersion parameters are optimised.

Chapter 7

Conclusions and Future Work

7.1. Conclusions

The aim of this work was to analyse the physical and chemical surface properties of a low surface-energy novel silicone-based foul-release coating and to determine the ability of the coatings to prevent bacterial attachment and to limit the adhesion forces of foulers. The coating devised by *Dow Corning* contained PEG groups which affected the surface character on exposure to water with a switching effect observed. Surface analysis was necessary due to the differences between the bulk and surface chemistry. The ability to use a variety of techniques on all formulations to compare them shows this methodology is effective for researching coatings for marine applications.

In Chapter 3 two methods of application of coatings were compared that simulated those that would be used in industry. Due to the high speed of drying of the coatings it is best that such coatings would be applied to ships using an airbrush that was cleaned often. Brushes would be quickly ruined and would be a waste of resources.

The surface was shown to be very flat, consisting of a fine network nanoscale structure which was dominated by PDMS, making it strongly hydrophobic. Despite two different catalysts being used and several different drying agents, there appeared to be little effect on the overall surface character of the different formulations aside from the detection of atoms, which comprise these catalysts in ToF-SIMS. PEG was also detected but not as strongly as PDMS which is more numerous in the number of groups in the total polymer chain.

In Chapter 4 similar surface properties were analysed though in a hydrated environment to better determine the character of the surface when it is in a marine context. A switching effect was shown to occur with a large decrease in contact angle that took five minutes to complete and was reversible within

seconds. ToF-SIMS confirmed this change in surface chemistry with an increase of PEG at the surface compared to the bulk after immersion in water. This change was very subtle which may explain the difficulty XPS had in confirming this observation due to its lower surface sensitivity.

The switching of surface chemistry was also seen topographically when AFM was used as the fine, detailed network structure was replaced with a less intricate appearance likely due to swelling of the surface. 900c the phosphorus based catalyst was demonstrated to leech from the coating matrix but the bacterial data in Chapter 5 showed that *Pseudomonas* was not harmed by the catalyst in water so this is unlikely to have an adverse effect on the marine ecosystem.

In Chapter 5 it was shown that this switching polymer is significantly better at preventing attachment of *Pseudomonas aeruginosa* than a PDMS standard. The coatings generally showed 10 times less bacterial coverage after three days than the standard. Through live/dead staining it was determined that the coatings are non-toxic to adhering foulers and not harmful to the marine environment. The fact that the mechanism of action of the coating is non-destructive therefore shows that bacteria will not undergo evolutionary pressure to survive, meaning they will be less likely to adapt adhesion proteins to the coating.

The coating was shown to not affect how bacteria move across the surface from a glass standard but did lower the overall energy that bacteria were able to adhere to the surface by several orders of magnitude. This makes it possible for water flow to remove bacteria from this coating if it were to be applied to the hull of a ship. Such assays could be applied to other applications such as adherence of bacteria to medical devices.

Chapter 6 demonstrated the attempt at applying the coatings to a true marine environment and whilst unsuccessful in determining the ability of the coating formulations at preventing fouling, it did show the importance of using a sufficient length of time of immersion in testing such coatings. Perhaps also

using a variety of different locations would have provided greater clarity as to why the tests were not successful, whether due to low fouling pressure or otherwise. Also, the fact that the coating was not mechanically strong enough to have the fouling scraped from its surface suggests that it may need frequent reapplication when used on boats to ensure consistent performance.

7.2. Future Work

The most important next stage in this work would be to repeat the sea trials over a period of twelve months with testing each month to note changes in coverage of specific foulers such as molluscs and also in differences in the concentration of surface chemicals such as proteins and carbohydrates. Ideally this would involve taking readings from different places in the same region as well as in different environments around the world, due to changes in temperature and the varied composition of marine life. Due to the variability in biological measurements it may also be fruitful to compare other coatings in the literature simultaneously. It can be difficult to compare results from the literature to each other making it essential to compare different coatings at the same time. In this case it would also be beneficial for the already produced standards to be adhered to by all groups undertaking coverage studies in a marine environment.

With regards to lab based bacterial testing, as only *Pseudomonas* was used as a model to determine coverage across the surface and anti-adherence properties, it would be important to test other more specific marine bacterial species such as *Cobetia marina* or *Marinobacter hydrocarbonoclasticus*. Such species could also be incubated simultaneously to investigate how competition may affect biofilm formation on these coatings. Protein and carbohydrate assays would also help understand the ability of the coatings to prevent conditioning film formation. The adhesion assays could potentially be applied to other marine organisms such as *Hydroides Elegans* or *Ulva* algae to obtain a more all-encompassing idea of the ability of the coating to limit the wide variety of species that attach to its surface. Modelling of PDMS coatings containing various concentrations of PEG could also provide a useful predictive

description of the ability of such coatings to prevent fouling by either individual bacteria or general fouling in a marine environment.

2D tracking of the bacteria above the surface was not able to detect differences in how *Pseudomonas* 'felt' its way towards the surface of the coating compared with pure glass. However, there is current research suggesting that 3D tracking can be used to analyse exploratory behaviour of *Ulva linza* (green algae) as they approach the surface. [283] This could be used to analyse more subtle movements such species make towards these switching coatings. This technique has been applied to *Pseudomonas* as well so would fit with the presented body of work. [258]

Angle-resolved XPS could be used to corroborate the data that was found in ToF-SIMS. Due to the lower surface sensitivity of XPS this would give a more surface sensitive description of the surface chemistry. This has been used to look at surface reorganising coatings by Chen *et al.* [284] The rate of reorganisation of a coating back to its native state after hydration is often not reported sufficiently, which will need to be better understood when developing coatings as the higher sections of boats that are not always in contact with water may experience greater fouling. To conclusively define this switching effect it would be ideal to take ToF-SIMS or XPS spectra at different time points of hydration between one and five minutes to (semi) quantitatively assign the change in surface chemistry.

Chapter 8

Bibliography

1. Plutarch. (2009) Essays and Miscellanies, the Complete Works Volume 3. *The Project Gutenberg EBook of Essays and Miscellanies*.

2. Loeb, G., Laster, D., & Gracik, T. (1984) The Influence of Microbial Fouling Films on Hydrodynamic Drag of Rotating Discs. Costlow JD, Tipper RC (eds) Marine Biodeterioration: an interdisciplinary study. *US Naval lnstitute Press*, Annapolis, 88-100.

3. Cubasch, U. *et al.* (2013) Introduction. In: Climate Change 2013: The Physical Science Basis. Contribution of Working Group I to the Fifth Assessment Report of the Intergovernmental Panel on Climate Change [Stocker, T.F., D. Qin, G.-K. Plattner, M. Tignor, S.K. Allen, J. Boschung, A. Nauels, Y. Xia, V. Bex and P.M. Midgley (eds.)]. *Cambridge University Press*, Cambridge, United Kingdom and New York, NY, USA.

4. Lindholt, K. *et al.* (2015) Effects of Biofouling Development on Drag Forces of Hull Coatings for Ocean-Going Ships: A Review. *Journal of Coatings Technology and Research*, 12(3), 415-444.

5. Bohlander, G. S. (1991) Biofilm effects on drag: measurements on ships. Bufton, R., Yakimiuk, P., Williams, K., (eds) Polymers in the marine environment. *Transactions of the Institute of Marine Engineers*, 103, conference 3, p 135-138.

6. Callow, M. E., & Callow, J. A. (2002) Marine biofouling: a sticky problem. *Biologist*, 49(1), 1-5.

7. Bott, T. R. (2011) Industrial Biofouling, Oxford: *Elvesier*.

8. Donlan, R. (2002) Biofilms: Microbial Life on Surfaces. *Emerging Infectious Diseases*, 8(9), 881-890.

9. Callow, M. E. & Fletcher, R. L. (1994) The Influence of Low Surface Energy Materials on Bioadhesion – a Review. *Special Issue of Marine Biofouling and Corrosion*, 34(3-4), 333-348.

10. Maki, J. C. & Mitchell, R. (2002) Biofouling in the marine environment. Encyclopedia of environmental microbiology, Edited by: Bitton, G. 610–619. New York, NY. *John Wiley and Sons*.

11. Shan, C. *et al.* (2011) Progress of Marine Biofouling and Antifouling Technologies. *Chinese Science Bulletin*, 56(7), 598-612.

12. Hellio, C. *et al.* (2009) Algae as marine fouling organisms: adhesion damage and prevention. In: Hellio, Claire and Yebra, D., eds. Advances in Marine Antifouling Coatings and Technologies. *Woodhead Publishing*, Cambridge, pp. 80-112.

13. Høiby, N. *et al.* (2009) Antibiotic Resistance of Bacterial Biofilms. *International Journal of Antimicrobial Agents*, 35(4), 322-332.

14. Luciana V. T. M. *et al.* (2009) The Effect of Biofouling on Localized Corrosion of the Stainless Steels N08904 and UNS S32760. *International Biodeterioration & Biodegradation*, 63(5), 607-614.

15. Chambers, L. D. *et al.* (2006) Modern Approaches to Marine Antifouling Coatings. *Surface and Coatings Technology*, 201(6), 3642-3652.

16. Meseguer, D., Kiil, S. K., & Dam-Johansen, K. (2004) Antifouling Technology – Past, Present and Future Steps Towards Efficient and Environmentally Friendly Antifouling Coatings. *Progress in Organic Coatings*, 50(2), 75-104.

17. Lau, S. C., Harder, T., & Qian, P. Y. (2003) Induction of Larval Settlement in the Serpulid Polychaete Hydroides Elegans (Haswell): Role of Bacterial Extracellular Polymers. *Biofouling*, 19(3), 197-204.

18. Siboni, N. *et al.* (2007) Conditioning Film and Initial Biofilm Formation on Ceramic Tiles in the Marine Environment. *FEMS Microbiology Letters*, 274(1), 24-29.

19. Garg, A., Jain, A., & Bhosle, N. B. (2009) Chemical characterization of a marine conditioning film. *International Journal of Biodeterioration & Biodegradation*, 63(1), 7-11.

20. Lorite, G. S. *et al.* (2011) The Role of Conditioning Film Formation and Surface Chemical Changes on *Xyelella fastiodiosa* Adhesion and Biofilm Evolution. *Journal of Colloid and Interface Science*, 359(1), 289-295.

21. Poleunis, C., Rubio, C., Compère. C., & Bertrand, P. (2003) ToF-SIMS Chemical Mapping Study of Protein Adsorption onto Stainless Steel Surfaaces Immersed in Saline Aqueous Solution. *Applied Surface Science*, 203-204, 693-697.

22. Compère. C. *et al.* (2001) Kinetics of Conditioning Layer Formation on Stainless Steel Immersed in Seawater. *Biofouling*, 17(2), 129-145.

23. Cooksey, K. E. (1995) Adhesion of Bacteria and Diatoms to Surfaces in the Sea: a review. *Aquatic Microbial Ecology*, 9, 87-96.

24. Dexter, S. C. (1979) Influence of Substratum Critical Surface Tension on Bacterial Adhesion. Interface, 70(2), 346-354.

25. Donlan, R. M. (2002) Biofilms: Microbial Life on Surfaces. *Emerging Infectious Diseases*, 8(9), 881-890.

26. Garrett, T. R., Bhakoo, M., & Zhang, Z. (2008) Bacterial Adhesion and Biofilms on Surfaces. *Progress in Natural Science*, 18(9), 1049-1056.

27. Kanematsu, H. & Barry, D. M. (2015) Conditioning Films. Biofilm and Materials Science, *Springer International Publishing, Switzerland*.

28. Bott, T. R., & Miller, P. C. (1983) Mechanisms of Biofilm Formation on Aluminium Tubes. *Journal of Chemical Technology and Biotechnology*, 33B, 177-184.

29. Zisman, W. A. (1964). Relation of the Equilibrium Contact Angle to Liquid and Solid Constitution. *Advances in Chemistry Series*, 43(1), 1-51.

30. Bar-zeev, E. *et al.* (2012) Revised Paradigm of Aquatic Biofilm Formation Facilitated by Microgel Transparent Exopolymer Particles. *Proceedings of the National Academy of Sciences*, 109(23), 9119-9124.

31. Schultz, M. P., Bendick, J. A., Holm, E. R., & Hertel, W.M. (2011) Economic Impact of Biofouling on a Naval Surface Ship. *Biofouling*, 27(1), 87-98.

32. Camps, M. *et al.* (2014) Antifouling Coatings Influence both Abundance and Community Structure of Colonizing Biofilms: a Case Study in the Northwestern Mediterranean Sea. *Applied and Environmental Microbiology*, 80(16), 4821-4831.

33. Ritter, A. *et al.* (2012) Proteomic Studies Highlight Outer-Membrane Proteins Related to Biofouling Development in the Marine Bacterium Pseudoalteromonas sp. D41. *Proteomics*, 12(21), 3180-3192.

34. Zodrow, K. R., Bar-Zeev, E., Giannetto, M. J., & Elimelech, M. (2014) Biofouling and Microbial Communities in Membrane Distillation and Reverse Osmosis. *Environmental Science & Technology*, 48(22), 13155-13164.

35. Goulitquer, S., Potin, P., & Tonon, T. (2012) Mass Spectrometry-Based Metabolomics to Elucidate Functions in Marine Organisms and Ecosystems. *Marine Drugs*, 10(4), 849-880.

36. Silva, O. N. *et al.* (2016) Structural Studies of a Lipid-Binding Peptide from Tunicate Hemocytes with Anti-Biofilm Activity. *Scientific Reports*, 6, 27128.

37. Xu, W., & Faisal, M. (2010) Factorial Microarray Analysis of Zebra Mussel (*Dreissena polymorpha*: Dreissenidae, Bivalvia) Adhesion. *BMC Genomics*, 11, 341.

38. Zhang, K. *et al.* (2006) Identifying Pioneer Bacterial Species Responsible for Biofouling Membrane Bioreactors. *Environmental Microbiology*, 8(3), 433-440.

39. Chapman, J. *et al.* (2013) Antifouling Performances of Macro- to Micro- to Nano-Copper Materials for the Inhibition of Biofouling in its Early Stages. *Journal of Materials Chemistry B*, 46(1), 6194-6200.

40. Pugh, S. J., Hewitt, G. F., & Muller-Steinhagen, H. (2003) Fouling During the Use of Seawater as Coolant – The Development of a 'User Guide'. *Engineering Conferences International*.

41. Doghri, I. *et al.* (2015) Marine Bacteria from the French Atlantic Coast Displaying High Forming-Biofilm Abilities and Different Biofilm 3D Architectures. *BMC Microbiology*, 15, 231.

42. Dang, H., & Lovell, C. R. (2000) Bacterial Primary Colonization and Early Succession on Surfaces in Marine Waters as Determined by Amplified rRNA Gene Restriction Analysis and Sequence Analysis of 16s Rrna Genes. *Applied and Environmental Microbiology*, 66(2), 467-475.

43. Stoodley, P., deBeer, D., & Lewandowski, Z. (1994) Liquid Flow in Biofilm Systems. *Applied and Environmental Microbiology*, 60(8), 2711-2716.

44. Wood, S. R. *et al.* (2000) Architecture of Intact Natural Human Plaque Biofilms Studied by Confocal Laser Scanning Microscopy. *Research Reports: Biomaterials & Bioengineering*, 79(1), 21-27.

45. Wilking, J. N. *et al.*(2012) Liquid Transport Facilitated by Channels in *Bacillus subtilis* Biofilms. *Proceedings of the National Academy of Sciences of the United States of America*, 110(3), 848-852.

46. Hermanowicz, S. W. (1999) Two-Dimensional Simulation of Biofilm Development: Effects of External Environmental Conditions. *Water Science and Technology*, 39(7), 107-114.

47. Noguera, D. R., Pizarro, G., Stahl, D. A., & Rittmann, B. E. (1999) Simulation of Multispecies Biofilm Development in Three Dimensions. *Water Science and Technology*, 29(7), 123-130.

48. Eberl, H. J., Picioreanu, C., Heijnen, J. J., & van Loosdrecht, M. C. M. (2000) A Three-Dimensional Numerical Study on the Correlation of Spatial Structure, Hydrodynamic Conditions and Mass Transfer and Conversion in Biofilms. *Chemical Engineering Science*, 55, 6209-6222.

49. Characklis, W. G., & Wilderer, P. A. (1989) Structure and Function of Biofilms. *John Wiley & Sons, Chichester, UK*)

50. Gieseke, A. *et al*. (2001) Community Structure and Activity Dynamics of Nitrifying Bacteria in a Phosphate-Removing Biofilm. *Applied and Environmental Microbiology*, 67(3), 1351-1362.

51. Cobb, G. D., & Bouwer, E. J. (1991) Effects of Electron Acceptors on Halogenated Organic Compound Biotransformation in a Biofilm Column. *Environmental Science and Technology*, 25(6), 1068-1074.

52. Da Fonsêca-Genevois, V. *et al.* (2006) Colonization and Early Succession on Artificial Hard Substrata by Meiofauna. *Marine Biology*, 148(5), 1039-1050.

53. Winfield, I., Abarca-Arena, L. G., & Cházaro-Olvera, S. (2007) Crustacean Macrofoulers in the Veracruz Coral Reef System, SW Gulf of Mexico: Checklist, Spatial Distribution and Diversity. *Cahiers de Biologie Marine*, 48, 287-295.

54. Busscher, H. J., & van der Mei, H. C. (2012) How Do Bacteria Know They Are on a Surface and Regulate Their Response to an Adhering State? *Public LibraryOS Pathogens*, 8(1), e1002440.

55. Morisaki, H., Nagai, S., Ohshima, H., & Ikemoto, E. (1999) The Effect of Motility and Cell-Surface Polymers on Bacterial Attachment. *Microbiology*, 145(10), 2797-2802.

56. Klapper, I. *et al.* (2002). Viscoelastic Fluid Description of Bacterial Biofilm Material Properties. *Biotechnology*, 80(3), 289-296.

57. Watnick, P., & Kolter, R. (2000) Biofilm, City of Microbes. *Journal of Bacteriology*, 182(10), 2675-2679.

58. Kogure, K., & Ikemoto, E. (1998) Attachment of Vibrio alginolyticus to Glass Surfaces Is Dependent on Swimming Speed. *Microbiology*, 180(4), 932-937.

59. Allison, D. G. *et al.* (1998) Extracellular Products as Mediators of the formation and detachment of *Pseudomonas fluorescens* biofilms. *FEMS Microbiology Letters*, 167(2), 179-184.

60. Dobretsov, S. *et al.* (2011) Inhibition of Marin Biofouling by Bacterial Quorum Sensing Inhibitors. *Biofouling*, 27(8), 893-905.

61. Davies, D. G. *et al.* (1998) The Involvement of Cell-to-Cell Signals in the Development of a Bacterial Biofilm. *Science*, 280(5361) 295-298.

62. Solano, C., Echeverz, M., & Lasa, I. (2014) Biofilm Dispersion and Quorum Sensing. *Current Opinion in Microbiology*, 18, 96-104.

63. Hassett, D. J. *et al.* (1999) Quorum Sensing in *Pseudomonas aeruginosa* Controls Expression of Catalase and Superoxide Dismutase Genes and Mediates Biofilm Susceptibility to Hydrogen Peroxide. *Molecular Microbiology*, 34(5), 1082-1093.

64. Xavier, K. B., & Bassler, B. L. (2003) LuxS Quorum Sensing: More Than Just a Numbers Game. *Current Opinion in Microbiology*, 6(2), 191-197.

65. Miller, M. B., & Bassler, B. L. (2001) Quorum Sensing in Bacteria. *Microbiology*, 55, 165-199.

66. Christensen, B. E., Kjosbakken, J., & Smidsrød, O. (1985) Partial Chemical and Physical Characterization of Two Extracellular Polysaccharides Produced by Marine, Periphytic Pseudomonas Strain NCMB 2021. *Applied and Environmental Microbiology*, 50(4), 837–845.

67. Paul, J. H., & Jeffrey, W. H. (1985) Evidence for Separate Adhesion Mechanisms for Hydrophilic and Hydrophobic Surfaces in *Vibrio proteolytica*. *Applied and Environmental Microbiology*, 50(2) 431-437.

68. Shea, C., Nunley, J. W., Williamson, J. C., & Smith-Somerville, H. E. (1991) Comparison of the Adhesion Properties of *Deleya marina* and the Exopolysaccharide-defective Mutant Strain DMR. *Applied and Environmental Microbiology*, 57(11), 3107–3113.

69. Burchard, R. P., Rittschof, D., & Bonaventura, J. (1990) Adhesion and Motility of Gliding Bacteria on Substrata with Different Surface Free Energies. *Applied and Environmental Microbiology*, 56(8), 2529–34.

70. Zhao, C., *et al.* (2009) Surface Selection, Adhesion and Retention Behavior of Marine Bacteria on Synthetic Organic Surfaces Using Self-assembled Monolayers and Atomic Force Microscopy. *Ocean Dynamics*, 59(2), 305-315.

71. Fang, H. H. P., Chan, K-Y., & Xu, L-C. (2000) Quantification of Bacterial Adhesion Forces Using Atomic Force Microscopy (AFM). *Journal of Microbiological Methods*, 40(1), 89-97.

72. Díaz, C. *et al.* (2007) Influence of the Nano-micro Structure of the Surface on Bacterial Adhesion. *Structure*, 10(1), 11-14.

73. McEldowney, S., Fletcher, M. (1986) Effect of Growth Conditions and Surface Characteristics of Aquatic Bacteria on Their Attachment to Solid Surfaces. *Journal of General Microbiology*, 132(2), 513-523.

74. Pedersen, K., Olsson, A., & Pedersen, A. (1986) Statistic Evaluation of the Influence of Species Variation, Culture Conditions, Surface Wettability and Fluid Shear on Attachment and Biofilm Development of Marine Bacteria. *Archive of Microbiology*, 145(1), 1-8.

75. Tribou, M., & Swain, G. (2010) The Use of Proactive in-water Grooming to Improve the Performance of Ship Hull Antifouling Coatings. *Biofouling*, 26(1), 47-56.

76. Hearin, J. *et al.* (2015) Analysis of Long-Term Mechanical Grooming on Large-Scale Test Panels Coated with an Antifouling and a Fouling-Release Coating. *Biofouling*, 31(8), 625-638.

77. Fiorini, P., Oehlmann, J., & Stroben E. (1991) The Pseudohermaphroditism of Prosobranchs: Morphological Aspects. *Zoologicher Anzeiger*, 226(1-2), 1

78. Murugan, A., & Ramasamy, M. S. (2008) Biofouling Deterrent Activity of the Natural Product from Ascidian, *Distaplia nathensis* [Chordata]. *Indian Journal of Marine Science*, 32(June 2003), 162–164.

79. Ingle, M. (2007) Naval Sea Systems Command Antifouling Program. International Marine and Offshore Coatings Conference Presentations National Paint and Coatings Association.

80. Patil, J. S., & Jagadeesan, V. (2011) Effect of Chlorination on the Development of Marine Biofilms Dominated by Diatoms. *Biofouling*, 27(3), 241-254.

81. Gipperth, L. (2009) The Legal Design of the International and European Union Ban on Tributyltin Antifouling Paint: Direct and Indirect Effects. *Journal of Environmental Management*, 90(1), S86-S95.

82. Feng, S. J., Wang, Q., Gao, Y., & Huang, G. (2009) Anti-Biofouling Property of a Novel Cross-Linkable Copolymer Grafted onto a Short Semifluorinated Aromatic Side Chain. *Advanced Materials Research*, 79-82, 973-976.

83. Strand, J., Larsen, M. M., & Lockyer, C. (2005) Accumulation of Organotin Compounds and Mercury in Harbour Porpoises (*Phocoena phocoena*) from Danish Waters and West Greenland. *Science of the Total Environment*, 350, 59-71.

84. Tiller, J. C., Sprich, C., & Hartmann, L. (2005) Amphiphilic Conetworks as Regenerative Controlled Releasing Antimicrobial Coating. *Journal of Controlled Release*, 103(2), 355-367.

85. Burmølle, M. *et al.* (2006) Enhanced Biofilm Formation and Increased Resistance to Antimicrobial Agents and Bacterial Invasion are Cuased by Synergistic Interactions in Multispecies Biofilms. *Applied and Environmental Microbiology*, 72(6), 3916-3923.

86. Stoodley, P., Sauer, K., Davies, D. G., & Costerton, J. W. (2002) Biofilms as Complex Differentiated Communities. *Annual Review of Microbiology*, 56, 187-209.

87. Hengge-Aronis, R. (1993) Survival of Hunger and Stress: The Role of *rpoS* in Early Stationary Phase Gene Regulation in E. Coli. *Cell*, 72(2), 165-168.

88. Pradeep, K. S. S., Easwer, H. V., & Maya Nandkumar, A. (2013) Multiple Drug Resistant Bacterial Biofilms on Implanted Catheters – A Reservoir of Infection. *The Journal of the Association of Physicians of India*, 61(10), 702-707.

89. Marconnet, C. *et al.* (2011) Membrane Biofouling Control by UV Irradiation. *Desalination*, 276(1-3), 75-81.

90. Patil, J. S., Kimoto, H., Kimoto, T., & Saino, T. (2007) Ultraviolet Radiation (UV-C): a Potential Tool for the Control of Biofouling on Marine Optical Instruments. *Biofouling*, 23(4), 215-230.
91. Salta, M. (2016) Bubbles versus Biofilms: a Novel Method for the Removal of Marine Biofilms Attached on Antifouling Coatings Using and Ultrasonically Activated Water Stream. *Surface Topography: Metrology and Properties*, 4, 034009.
92. Masseille, H. (1933) Notes sur la sallsure et les procédés d'entretien des carènes Immergées. *Peintures Pigments Vernis*, 10, 232-234.
93. Torr, C. (1895) Ancient Ships. *Cambridge University Press, Cambridge.* 170pp.
94. Neuberger, A (1930) The Technical Arts and Sciences of the Ancients. *The Macmillan Co., New York City*. 518pp.
95. Hagan, P., Price, E., & King D. (2015) Status of Vessel Biofouling Regulations and Compliance Technologies. *Economic Discussion Paper, Marine Environmental Resource Paper*.
96. Scianni, C., Brown, C., Nedelcheva, R., & Dobroski, N. (2013) Hull Husbandry Practices and Biofouling Management of Vessels Operating in California. *Oceans Conference*.
97. Ship Repair and Conversion Technology. (2015) First Quarter.
98. Leighton, T. G., Birkin, P., & Offin, D. (2013) A New Approach to Ultrasonic Cleaning. *Proceedings of Meetings on Acoustics*, 133(5), 075029.
99. Stupak, M. E., García, M. T., & Pérez, M. C. (2003) Non-toxic Alternative Compounds for Marine Antifouling paints. *International Biodeterioration & Biodegradation,* 52(1), 49–52.
100. Hellio, C., *et al.* (2001) Inhibition of marine bacteria by extracts of macroalgae: potential use for environmentally friendly antifouling paints. Korkut, E., & Atlar, M. (2012) An Experimental Investigation of the Effect of Foul Release Coating Application on Performance, Noise and Cavitation Characteristics of Marine Propellers. *Ocean Engineering*, 41, 1-12.
101. Rittschof, D. *et al.* (1992) Rapid Field Assessment of Antifouling and Foul-Release Coatings. *Biofouling*, 6(2), 181-192.
102. Brady, R. F., & Singer, I. L. (2000) Mechanical Factors Favouring Release from Fouling Release Coatings. *Biofouling*, 15(1-3), 73-81.

103. Lindner, E. (1992) A Low Surface Free Energy Approach in the Control of Marine Biofouling. *Biofouling*, 6(2), 193-205.
104. Kobayashi, H., Owen, M. J. (1995) Surface Properties of Fluorosilicones. *Trends in Polymer Science*, 3(10), 330-335.
105. Tsibouklis, J. *et al.* (1999) Preventing bacterial adhesion onto surfaces: the low-surface-energy approach. *Biomaterials*, 20(13), 1229–35.
106. Kingshott, P., Thissen, H., & Griesser, H. J. (2002) Effects of Cloud-Point Grafting, Chain Length and Density of PEG Layers on Competitive Adsorption of Ocular Proteins. *Biomaterials*, 23(9), 2043-2056.
107. Hentzer, M. *et al.* (2002) Inhibition of Quorum Sensing in *Pseudomonas aeruginosa* Biofilm Bacteria by a Halogenated Furanone Compound. *Microbiology*, 148(Pt 1), 87-102.
108. Manny, A. J. *et al.* (1997) Reinvestigation of the Sulfuric Acid-Catalysed Cyclisation of Brominated 2-alkyllevulinic Acids to 3-Alkyl-5-Methylene-2(5h)-Furanones. *Tetrahedron*, 53(46), 15813-15826.
109. Manefield, M. *et al.* (2002) Halogenated Furanones Inhibit Quorum Sensing Through Accelerated LuxR Turnover. *Microbiology*, 148(Pt 4), 1119-1127.
110. Costerton, J. W. *et al.* (1995) Microbial Biofilms. *Annual Review of Microbiology*, 49, 711-745.
111. Rasko, D. A. *et al.* (2008) Targeting QseC Signalling and Virulence for Antibiotic Development. *Science*, 321(5892), 1078-1080.
112. Geske, G. D. *et al.* (2008) Comparative Analyses of *N*-Acylated Homoserine Lactones Reveal Unique Structural Features that Dictate Their Ability to Activate or Inhibit Quorum Sensing. *Chembiochem*, 15(9), 389-400.
113. Geske, G. D., Wezeman, R. J., Siegel, A. P. & Blackwell, H. E. (2005) Small Molecule Inhibitors of Bacterial Quorum Sensing and Biofilm Formation. *Journal of the American Chemical Society*, 127(37), 12762-12763.
114. Rasch, M. *et al.* (2006) Well-known Quorum Sensing Inhibitors do not Affect Bacterial Quorum Sensing-Regulated Bean Sprout Spoilage. *Journal of Applied Microbiology*, 102(3), 826-837.
115. Janssens, J. C. A. *et al.* (2008) Brominated Furanones Inhibit Biofilm Formation by *Salmonella enterica* Serovar Typhimurium. *Applied Environmental Microbiology*, 74(21), 6639-6648.

116. Lönn-Stensrud, J., Petersen, F. C., Benneche, T., & Scheie, A. A. (2007) Synthetic Bromated Furanone Inhibits Autoinducer-2-mediated Communication and Biofilm Formation in Oral Streptococci. *Molecular Oral Microbiology*, 22(5), 340-346.

117. Martín-Rodríguez, A. J. *et al.* (2015) From Broad-Spectrum Biocides to Quorum Sensing Disruptors and Mussel Repellents: Antifouling Profile of Alkyl Triphenylphosphonium Salts. *Public Library of Science One*, 10(4), E0123652.

118. Choo, J. H., Rukayadi, Y. & Hwang, J-K. (2006) Inhibition of Bacterial Quorum Sensing by Vanilla Extract. *Letters in Applied Microbiology*, 42(6), 637-641.

119. Ponnusamy, K., Paul, D., & Kweon, J. H. (2009) Inhibition of Quorum Sensing Mechanism and *Aeromonas hydrophila* Biofilm Formation by Vanillin. *Environmental Engineering Science*, 26(8), 1359-1363.

120. Rasmussen, T. B. *et al.* (2005) Screening for Quorum-Sensing Inhibitors (QSI) by Use of a Novel Genetic System, the QSI Selector. *Journal of Bacteriology*, 187(5), 1799-1814.

121. Niu, C., Afre, S., & Gilbert, E. S. (2006) Subinhibitory Concentrations of Cinnamaldehyde Interfere with Quorum Sensing. *Letters in Applied Microbiology*, 43(5), 489-494.

122. Kalia, V. C., Raju, S. C., & Purohit, H. J. (2011) Genomic Analysis Reveals Versatile Organisms for Quorum Quenching Lactone-Acylase and –Lactonase. *Open Microbiology Journal*, 5, 1-13.

123. Niu, C., & Gilbert, E. S. (2004) Colorimetric Method for Identifying Plant Essential Oil Components That Affect Biofilm Formation and Structure. *Applied Environmental Microbiology*, 70(12), 6951-6956.

124. Nakajima, A., Hashimoto, K., & Watanabe, T. (2000) Transparent Superhydrophobic Thin Films with Self-Cleaning Properties. *Langmuir*, 16(17), 7044–7047.

125.Tan, S. P. *et al.* (2013) Development of a Novel Antimicrobial Seaweed Extract-Based Wound Dressing. *International Journal of Pharmaceutics*, 456(1), 10-20.

126. Wang, X., Wang, H., & Brown, H. R. (2011) Jellyfish Gel and its Hybrid Hydrogels with High Mechanical Strength. *Soft Matter*, 7, 211-219.

127. Annabi, N. *et al*. (2015) Highly Elastic and Conductive Human-Based Protein Hybrid Hydrogels. *Advanced Materials*, 28(1), 40-49.

128. Katsuyama, Y. *et al.* (2002) Inhibitory Effects of Hydrogels on the Adhesion, Germination, and Development of Zoospores Originating from Laminaria angustata. *Macromolecular Bioscience*, 2(4), 163-169.

129. Yin, H. *et al.*(2013) Double Network hydrogels from Polyzwitterions: High Mechanical Strength and Excellent Anti-Biofouling Properties. *RSC Journal of Materials Chemistry B*, 1(30), 3685-3693.

130. Brushan, B. (2009) Biomimetics: Lessons from Nature – an Overview. *Philosophical Transactions. Series A, Mathematical, Physical and Engineering Sciences*, 367(1893), 1445-1486.

131. Chen, K., Zhou, S., & Wu, L. (2016) Self-Healing Underwater Superoleophobic and Antibiofouling Coatings Based on the Assembly of Hierarchical Microgel Spheres. *ACS Nano*, 10(1), 1386-1394.

132. Wang, J. *et al.* (2009) Artificial Fish Flocked Surface as a Possible Anti-Biofoulant. *Nano/Micro Engineered and Molecular Systems 4th IEEE International Conference*.

133. Reddy, S. T. *et al.* (2011) Micropatterend Surfaces for Reducing the Risk of Catheter-Associated Urinary Tract Infection: An *In Vitro* Study in the Effect of Sharklet Micropatterend Surfaces to Inhibit Bacterial Colonization and Migration of Uropathogenic *Escherichia Coli*. *Journal of Endochrinology*, 25(9), 1547-1552.

134. Ralston, R., & Swain, G. (2009) Bioinspiration-The Solution for Biofouling Control. *Bioinspiration & Biomimetics*, 4(1), 015007.

135. Kesel, A., & Liedert, R. (2007) Learning From Nature: Non-Toxic Biofouling Control by Shark Skin Effect. *Comparitive Biochemistry and Physiology Par A: Molecular & Integrative Physiology*, 146(4), S130.

136. Ng, E. Y. K., & Luo, Y. (2016) Bio-Inspired Surface and Applications. *World Scientific Publishing Company*.

137. Chung, K. K. *et al.* (2007) Impact of Engineered Surface Microtopography on Biofilm Formation of *Staphylococcus aureus*. *Biointerphases*, 2(2), 89-94.

138. Asmathunisha, N. & Kathiresan, K. (2013) A review on Biosynthesis of Nanoparticles by Marine Organisms. *Colloids and Surfaces B: Biointerfaces*, 103, 283-287.

139. Baum, C. *et al*. (2001) A Zymogel Enhances the Self-Cleaning Abilities of the Skin of the Pilot Whale (*Globicephala melas*). *Comparative Biochemistry and Physiology Part A: Molecular & Integrative Physiology*, 130(4), 835-847.

140. Baum, C. *et al*. (2003) Surface Properties of the Skin of the Pilot Whale *Globicephala melas*. *Biofouling*, 19, 181-186.

141. Kohli, N. (2007) Biofouling and Design of a Biomimetic Hull-Grooming Tool. Ship Systems Integration & Design Department Technical Report, *Naval Surface Warfare Centre, Maryland*.

142. Zhang, H., & Chiao, Mu. (2015) Anti-fouling Coatings of Poly(dimethylsiloxane) Devices for Biological and Biomedical Applications. *Journal of Medical and Biological Engineering*, 35(2), 143-155.

143. Amiji, M., & Park, K. (1993) Surface Modification of Polymeric Biomaterials with Poly(ethylene oxide), Albumin and Heparin for Reduced Thrombogenicity. *Journal of Biomaterials Science, Polymer Edition*, 4(3), 217-234.

144. Krishnan, S., Weinman, C. J., & Ober, C. K. (2008) Advances in Polymers for Anti-Biofouling Surfaces. *Journal of Materials Chemistry*, 18(29), 3405-3413.

145. Hamming, L. M. & Messersmith, P. B. (2008) Fouling Resistant Biomimetic Poly(Ethylene Glycol) Based Grafted Polymer Coatings. *Material Matters*, 3.3, 52.

146. Liu, Q., Singh, A., & Liu, L. (2013) Amino Acid-Based Zwitterionic Poly(serine methacrylate) as an Antifouling Material. *Biomacromolecules*, 14(1), 226-231.

147. Sharma, S., Johnson, R. W., & Desai, T. A. (2004) Evaluation of the Stability of Nonfouling Ultrathin Poly(ethylene glycol) Films for Silicon-Based Microdevices. *Langmuir*, 20(2), 348-356.

148. Lee, J. H., Lee, H. B., & Andrade, J. D. (1995) Blood Compatibility of Polyethylene Oxide Surfaces. *Progress in Polymer Science*, 20(6), 1043-1079.

149. Lee, K. C. *et al*. (1999) Isolation, Characterization and Stability of Positional Isomers of Mono-PEGylated Salmon Calcitonins. *Pharmaceutical Research*, 16(6), 813-818.

150. Gudipati, C. S. *et al.* (2004) Hyperbranched Fluoropolymer and Linear poly-ethylene glycol) based Amphiphilic Crosslinked Networks as Efficient Antifouling Coatings: An Insight into the Surface Compositions, Topographies and Morphologies. *Journal of Polymer Science Part A: Polymer Chemistry,* 42(24), 6193-6208.

151. Statz, A. *et al.* (2006) Algal Antifouling and Fouling-release Properties of Metal Surfaces Coated with a Polymer Inspired by Marine Mussels. *Biofouling*, 22(6), 391–399.

152. Krishnan, S. *et al*. (2006) Anti-Biofouling Properties of Comblike Block Copolymers with Amphiphilic Side Chains. *Langmuir*, 22(11), 5076-5086.

153. Zhao, Y-H,. Zhu, B-K., Kong, L., & Xu, Y-Y. (2007) Improving Hydrophilicity and Protein Resistance of Poly(vinyledene fluoride) Membranes by Blending with Amphiphilic Hyperbranched-Star Polymer. *Langmuir*, 23(10), 5779-5786.

154. Ekblad, T. *et al*. (2008) Poly(ethylene glycol)-Containing Hydrogel Surfaces for Antifouling Applications in Marine and Freshwater Environments. *Biomacromolecules*, 9(10), 2775-2783.

155. Lee, S., Tong, X., & Yang, F. (2016) Effects of the Poly(ethylene glycol) Hydrogel Crosslinking Mechanism on Protein Release. *Biomaterials Science*, 4(3), 405-411.

156. Heath, D. E. *et al.* (2015) Regenerating the Cell Resistance of Micromolded PEG Hydrogels. *Lab on a Chip*, 15(9), 2073-2089.

157. Yeh, C-C., Venault, A., & Chang, Y. (2016) Structural Effect of Poly(ethylene glycol) Segmental Length on Biofouling and Hemocompatibility. *Polymer Journal*, 48, 551-558.

158. Lundberg, P. *et al.* (2010) Poly(ethylene glycol)-Based Thiol-ene Hydrogel Coatings-Curing Chemistry, Aqueous Stability and Potential Marine Antifouling Applications. *ACS Applied Materials & Interfaces*, 2(3), 903-912.

159. Schlip, S. *et al.* (2007) Settlement and Adhesion of Algal Cells to Hexa(ethylene glycol)-Containing Self-Assembled Monolayers with Systematically Changed Wetting Properties. *Biointerphases*, 2(4), 143-150.

160. Meyer, A., Baier R. E., Forsberg R. L. (1995) Degradation of Nontoxic Fouling-release Coatings as a Result of Abrasion and Long-term Exposure. *Proclamations of the 5th International Zebra Mussel and Other Aquatic Nuisance Organisms Conference*, 337-342.

161. Electrical Power Research Institute (1989) Non-toxic foul release coatings. EPRI Report GS-6566.

162. Cassé, F., & Swain, G. W. (2006) The Development of Microfouling on Four Commercial Antifouling Coatings under Static and Dynamic Immersion. *International Biodeterioration & Biodegradation*, 57(3), 179–185.

163. Terlizzi, A., Conte, E., Zupo, V., & Mazzella, L. (2000) Biological Succession on Silicone Fouling-release Surfaces: Long-term Exposure Tests in the Harbour of Ischia, Italy. *Biofouling*, 15(4), 327-342.

164. Brady, R. F. (2005) Fouling-release Coatings for Warships. *Defence Science Journal*, 55(1), 75–81.

165. Beigbeder, A., *et al.* (2008) Preparation and Characterisation of silicone-based Coatings Filled with Carbon Nanotubes and Natural Sepiolite and Their Application as Marine Fouling-release Coatings. *Biofouling*, 24(4), 291–302.

166. Beigbeder, A. *et al.* (2011) Surface and Fouling-Release Properties of Silicone/Organomodified Montmorillonite Coatings. *Journal of Adhesion Science and Technology*, 25(14), 1689–1700.

167. Truby, K. *et al.* (2000) Evaluation of the Performance Enhancement of Biofouling-release Coatings by Silicone Biofouling-release Oil Incorporation. *Biofouling*, 15(1-3), 141–150.

168. Barrios, C. A., Xu, Q., Cutright, T., & Newby, B. Z. (2005) Incorporating Zosteric Acid into Silicone Coatings to Achieve its Slow Release While Reducing Fresh Water Bacterial Attachment. *Colloids and surfaces B, Biointerfaces*, 41(2-3), 83–93.

169. Stein, J. K. *et al.* (2003). Structure-Property Relationships of Silicone Biofouling-Release Coatings: Effect of Silicone Network Architecture on Pseudobarnacle Attachment Strengths. *Biofouling*, 19(2), 87-94.

170. Holland, R. *et al.* (2004) Adhesion and Motility of Fouling Diatoms on a Silicone Elastomer. Biofouling, 20(6), 323–9.

171. Schumacher, J. F. *et al.* (2007) Engineered Antifouling Microtopographies – Effect of Feature Size, Geometry and Roughness on Settlement of Zoospores of the Green Alga Ulva. *Biofouling*, 23(1), 55-62.

172. Shivapooja, P. *et al.* (2015) Dynamic Surface Deformation of Silicone Elastomers for Management of Marine Biofouling: Laboratory and Field Studies Using Pneumatic Actuation. *Biofouling*, 31(3), 265-274.

173. Jiang, S., & Cao, Z. (2010) Ultralow-Fouling, Functionalizable AND Hydrolyzable Zwitterionic Materials and Their Derivatives for Biological Applications. *Advanced Materials*, 22(9), 920-932.

174. Nagarajan, R. (2011) Amphiphilic Surfactants and Ampiphilic Polymers: Principles of Molecular Assembly. Amphiphiles: Molecular Assembly and Applications, Chapter 1, *American Chemical Society*.

175. Leslie, D. C. *et al.* (2014) A Bioinspired Surface Coating That Prevents Thrombosis and Biofouling. *18th International Conference on Miniaturized Systems for Chemistry and Life Sciences*.

176. Kim, S.M. *et al.* (2015) Anti-Biofouling Effect of PEG-Grafted Block Copolymer Synthesized by RAFT Polymerization. *Journal of Nanoscience and Nanotechnology*, 15(10), 7866-7870.

177. Bianco, M. *et al.* (2015) Non-Biofouling Fluorinated Block Copolymer Coatings for Contact Lenses. *Science of Advanced Materials*, 7(7), 1387-1394.

178. Berndt, E. *et al.* (2010) Functional Coatings for Anti-Biofouling Applications by Surface Segregation of Block Copolymer Additives. *Polymer*, 51(25), 5910-5920.

179. Ye, G. *et al.* (2015) Controlled Architecture of Dual-Functional Block Copolymer Brushes on Thin-Film Composite Membranes for Integrated "Defending" and "Attacking" Strategies Against Biofouling. *ACS Applied Materials and Interfaces*, 7(41), 23069-79.

180. Yang, Y. *et al.* (2013) Adsorption of a PEO-PPO-PEO Triblock Copolymer on Metal Oxide Surfaces with a View to Reducing Protein Adsorption and Further Biofouling. *Biofouling*, 29(9), 1123-37.

181. Amadei, C. A. *et al.*(2014) Revealing Amphiphilic Nanodomains of Anti-Biofouling Polymers. *ACS Applied Materials and Interfaces*, 6(7), 4705-4712.

182. Feng, S. *et al*. (2009) Synthesis and Characterization of a Novel Amphiphilic Copolymer Capable as Anti-Biofouling Coating Material. *Journal of Applied Polymer Science*, 114(4), 2071-2078.

183. Weinman, C. J. *et al.* (2010) Protein Adsorption Resistance of Anti-Biofouling Block Copoymers Containing Amphiphilic Side Chains. *RSC Soft Matter*, 6(14), 3237-3243.

184. Olsen, G. W. *et al.* (2005) Historical Comparison of Perfluorooctanesulfonate, Perfluorooctanoate and Other Fluorochemicals in Human Blood. *Environmental Health Perspectives*, 113(5), 539-545.

185. Kim, S-M., *et al.* (2015) Amphiphilic Random Copolymers Consisting of Styrene, EGMA and HEMA for Anti-Biofouling Coatings. *Molecular Crystals and Liquid Crystals*, 622(1), 151-157.

186. Majumdar, P. (2011) Combinatorial Materials Research Applied to the Development of Surface Coatings XV: An Investigation of Polysiloxane Anti-Fouling/Fouling-Release Coatings Containing Tethered Quaternary Ammonium Salt Groups. *ASC Combinatorial Sciences*, 13(3), 298-309.

187. Gudipati, C. S. *et al.* (2005) The Antifouling and Fouling-Release Perfomance of Hyperbranched Fluoropolymer (HBFP)-Poly (ethylene glycol) (PEG) Composite Coatings Evaluated by Adsorption of Biomacromolecules and the Green Fouling Alga Ulva. *Langmuir*, 21(7), 3044–3053.

188. Pollack K. A. *et al.* (2014) Hyperbranched Fluoropolymer-Polydimethylsiloxane-Poly(ethylene glycol) Cross-Linked Terpolymer Networks Designed for Marine and Biomedical Applications: Heterogenous Nontoxic Antibiofouling Surfaces. *ACS Applied Materials and Interfaces*, 6(21), 19265-19274.

189. Kumar, V., Pulpytel, J., Giudetti, G., Rauscher, H., & Rossi, F. (2011) Amphiphilic Copolymer Coatings via Plasma Polymerisation Process: Switching and Anti-Biofouling Characteristics. *Plasma Processes and Polymers*, 8(5), 373-385.

190. Sidorenko, A., Minko, S., Schenk-Meuser, K., Duschner, H., & Stamm, Manfred. (1999) Switching of Polymer Brushes. *Langmuir*, 15(24), 8349-8355.

191. Da Silva, R. M. P., Mano, J. F., & Reis, R. L. (2007) Smart Thermoresponsive Coatings and Surfaces for Tissue Engineering: Switching Cell-Material Boundaries. *Trends in Biotechnology*, 25(12), 577-583.

192. Goswani, S., Klaus, S., & Benziger, J. (2008) Wetting and Absorption of Water Drops on Nafion Films. *Langmuir*, 24(16), 8627-8633.

193. Verplanck, N., Coffinier, Y., Thomy, V., & Boukherroub, R. (2007) Wettability Switching Technique of Superhydrophobic Surfaces. *Nano Review*, 2(12), 577-596.

194. Wang, Y. *et al.* (2011) Photocurable Amphiphilic Perfluoropolyether/Poly(ethylene glycol) Networks for Fouling-Release Coatings. *Macromolecules*, 44(4), 878-885.

195. Martinelli, E. *et al.* (2011) Amphiphilic Block Copolymer/Poly(dimethylsiloxane)(PDMS) Blends and Nanocomposites for Improved Fouling-Release. *Biofouling*, 27(5), 529-541.

196. Callow J. A., & Callow, M. E. (2011) Trends in the Development of Environmentally Friendly Fouling-Resistant Marine Coatings. *Nature Communications*, 2, Article 244.

197. Binnig, G., Quate, C. F., & Gerber, C. (1986) Atomic Force Microscope. *Physical Review Letters*, 56(9), 930-933.

198. Bruker. (2012) Fundamentals of Contact Mode and Tapping Mode Atomic Force Microscopy. *Azo Nano*.

199. Dokukin, M. E., & Sokolov, I. (2012) Quantitative Mapping of the Elastic Modulus of Soft Materials with HarmoniX and Peakforce QNM AFM Modes. *Langmuir*, 28(46), 16060-16071.

200. Alsteens, D. *et al.* High-Resolution Imaging of Chemical and Biological Sites on Living Cells Using Peak Force Tapping Atomic Force Microscopy. *Langmuir*, 28(49), 16738-16744.

201. Young, T. J. *et al.* (2011) The Use of the PeakForce^{TM} Quantitative Nanomechanical Mapping AFM-Based Method for High-Resolution Young's Modulus Measurement of Polymers. *Measurement Science and Technology*, 22(12), 125703 (6pp).

202. Magonov, S.N. & Whangbo, M-H (1996) Surface Analysis with STM and AFM. Verlagsgesellschaft mbH.

203. Crowell, C. (2006) Vibrations and Waves from the Light Matter Online Text Series.

204. Han, W., & Serry, F. M. (2008) Force Spectroscopy with the Atomic Force Microscope; Application Note; Agilent Technologies: Palo Alto, CA.

205. Vickerman, J.C. & Gilmore, I.S. (2009) Surface Analysis: The Principal Techniques. *John Wiley and Sons, Ltd*.

206. Szynkowska, M. I. *et al.* (2010) Detection of Exogenous Contaminants of Fingerprints using ToF-SIMS. *Surface Science Applications in Forensic Analysis*, 42(5), 393-397.

207. Van Nuffel, S. *et al.* (2016) Multivariate Analysis of 3D ToF-SIMS Images: Method Validation and Application to Cultured Neuronal Networks. *Analyst*, 141(1), 90-95.

208. Musat, N., *et al.* (2012) Detecting Metabolic Activities in Single Cells with Emphasis on nanoSIMS. *FEMS Microbiology Reviews*, 36(2), 486-511.

209. Bulle-Lieuwma, C.W.T. *et al.* (2003) Characterization of Polymer Solar Cells by TOF-SIMS Depth Profiling. *Applied Surface Science*, 203-204, 547-550.

210. Feldman, L.C. & Mayer, J.W. (1986) Fundamentals of Surface and Thin Film Analysis. New York: *Elsevier Science Publishing Co*.

211. Briggs, D. (1986) Surface Analysis of Polymers by XPS and Statics SIMS. New York: *Elsevier Science Publishing Co*.

212. Zhang, H., Lamb, R., & Lewis, J. (2005) Engineering Nanoscale Roughness on Hydrophobic Surface-Preliminary Assessment of Fouling Behaviour. *Science and Technology of Advanced Materials*, 6(3-4), 236-239.

213. Faille, C. *et al.* (2002) Adhesion of Bacillus Spores and *Escherichia coli* Cells to Inert Surfaces: Role of Surface Hydrophobicity. *Canadian Journal of Microbiology*, 48(8), 728-738.

214. Semwogerere, D. & Weeks, E.R. (2005) Encyclopaedia of Biomaterials and Biomedical Engineering. Taylor & Francis.

215. Fellers, T.J. & Davidson, M.W. Introduction to Confocal Microscopy. http://olympus.magnet.fsu.edu/primer/techniques/confocal/confocalintro.html

216. Bucher, D. http://www.bio.brandeis.edu/marderlab/microscopyB.html.

217. Ruzin, S. E. (1999) Plant Microtechnique and Microscopy. Oxford University Press.

218. Murphy D. B. et al.
http://www.olympusmicro.com/primer/techniques/dic/dicintro.html

219. Warner, J. C., Rothwell, S. D., Keevil, C.W. (2008) Use of Episcopic Differential Interference Contrast Microscopy to Identify Bacterial Biofilms on

Salad Leaves and Track Colonization by Salmonella Thompson. *Environmental Microbiology*, 10(4), 918-925.

220. Turner, L., Ryu, W. S., Berg, H, C. (2000) Real-time Imaging of Fluorescent Flagellar Filaments. *Journal of Bacteriology*, 182(10), 2793-2801.

221. Sader, J. E., Chon, J. W. M., Mulvaney, P. (1999) Calibration of Rectangular Atomic Force Microscope Cantilevers. Review of Scientific Instruments, 70, 3967-3969.

222. Sader, J. E. (1998) Frequency Response of Cantilever Beams Immersed in Viscous Fluids with Applications to the Atomic Force Microscope. *Journal of Applied Physics*, 84, 64-76.

223. Clifford, C. A., & Seah, M. P. (2005) Quantification Issues in the Identification of Nanoscale Region of Homopolymers Using Modulus Measurements via AFM Nanoidentation. *Applied Surface Science*, 252(5), 1915-1933.

224. Derjaguin B.V., Muller V.M., Toropov Yu.P. (1975) Effect of Contact Deformations on the Adhesion of Particles. *Journal of Colloidal Interface Science*, 53, 314-326.

225. Beamson, G., Briggs, D. (1993) High Resolution XPS of Organic Polymers: The Scienta ESCA300 Database. *Journal of Chemical Education*, 70, 84-85 & 269-269.

226. Beamson G., Briggs, D. (2000) The XPS of Polymers Database. Surface Spectra Ltd, Appendix 1.

227. Briggs, D. (1983) Analysis of Polymer Surface by SIMS. *Surface and Interface Analysis*, 5, 113-118.

228. Briggs, D., Brown, A., Vickerman, J. C. (1989) Handbook of Static Secondary Ion Mass Spectrometry (SIMS). Wiley and Sons, 28-29.

229. Hobbs, C., Taylor, J., Hong, S. (2006) Effect of Surface Roughness on Fouling of RO and NF Membranes During Filtration of a High Organic Surficial Groundwater. *Journal of Water Supply: Research and Technology*, 55(7-8), 559-570.

230. Wenzel, R. N. (1936) Resistance of Solid Surfaces to Wetting by Water. *Industrial and Engineering Chemistry*, 28, 988-994.

231. Patanker. N. A. (2003) On the Modelling of Hydrophobic Contact Angles on Rough Surfaces. *Langmuir*, 19(4), 1249-1253.

232. Ko, Y. C., Ratner, B. D., Hoffman, A. S. (1981) Characterization of Hydrophilic-Hydrophobic Polymeric Surfaces by Contact Angle Measurements. *Journal of Colloid and Interface Science*, 82(1), 25-37.

233. Owen, M. J. (2014) Silicone Hydrophobicity and Oleophilicity. *Silicon*, 1-5.

234. Volynskii, A. L., Bondarev, V. V., & Bakeev, N. F. (2002) Emergence of Helical Cracks Upon Swelling of a Polyamide Fiber with a Thin Hard Coating. *Polymer Science Series B*, 44(11-12), 299-300.

235. Sundaram, H. S., *et al.* (2011) Fluorine-free Mixed Amphiphilic Polymers Based on PDMS and PEG Side Chains for Fouling Release Applications. *Biofouling*, 27, 589–602.

236. Mera, A. E. *et al.* (1997) Toward Minimally Adhesive Surfaces Utilizing Siloxanes. *Naval Research Reviews*, 4(69), 4-8.

237. Berglin, M., Wynne, K. J., Gatenholm, P. (2003) Fouling-release Coatings Prepared from α,ω-dihydroxypoly(dimethylsiloxane) cross-linked with (heptadecafluoro-1, 1, 2, 2-tetrahydrodecyl)triethoxysilane. *Journal of Colloid and Interface Science*, 2(257), 383-391.

238. Arce, F. T. *et al.* (2006) Modification of Surface Properties of a Poly(dimethylsiloxane)-Based Elastomer, RTV11, upon Exposure to Seawater. *Langmuir*, 22(17), 7217-7225.

239. Schön, P. *et al.* (2013) Probing Biofouling Resistant Polymer Brush Surfaces by Atomic Force Microscopy based Force Spectroscopy. *Colloids and Surfaces B:* Biointerfaces, 102, 923-930.

240. Cho. Y. *et al.* (2012) Reconstruction of Surfaces from Mixed Hydrocarbon and PEG Components in Water: Responsive Surfaces Aid Fouling Release. *Biomacromolecules*, 13(6), 1864-1874.

241. Yang, S. *et al.* (2008) Group Reorientation and Migration of Amphiphilic Polymer Bearing Phosphorylcholine Functionalities on Surface of Cellular Membrane Mimicking Coating. *Journal of Biomedical Materials Research Part A*, 3(84a), 837-841.

242. Lukáš, J., Sodhi, R. N. S., Sefton, M. V. (1995) An XPS Study of the Surface Reorientation of Statistical Methacrylate Copolymers. *Journal of Colloid and Interface Science*, 174(2), 421-427.

243. Yasuda, H., Sharma, A. K., Yasuda, T. (1981) Effect of Orientation and Mobility of Polymer Molecules at Surfaces on Contact Angle and its Hysteresis. *Journal of Polymer Science Part B: Polymer Physics,* 19(9), 1285-1291.

244. Fu, Y. *et al.* (2014) Detection of Surface Mobility of poly(2, 3, 4, 5, 6-pentafluorostyrene) Films by in situ Variable-Temperature ToF-SIMS and Contact Angle Measurements. *Journal of Colloid and Interface Science,* 431, 180-186.

245. Taylor, M., *et al.* (2015) 3D Chemical Characterisation of Frozen-Hydrated Hydrogels using ToF-SIMS with Argon Clusters Sputter Depth Profiling. *Biointerphases*, 11, 02A301.

246. Khorasani, M. T., Mirzadeh, H. (2003) *In vitro* Blood Compatibility of Modified PDMS surfaces as Superhydrophobic and Superhydrophilic Materials. *Journal of Applied Polymer Science*, 91, 2042-2047.

247. Sundaram, H. S., *et al.* (2011) Fluorine-free Mixed Amphiphilic Polymers Based on PDMS and PEG Side Chains for Fouling Release Applications. *Biofouling*, 27, 589–602.

248. Lötters, J. C. *et al.* (1997) The Mechanical Properties of the Rubber Elastic Polymer Polydimethylsiloxane for Sensor Applications. *Journal of Micromechanical Microengineering*, 7, 145-147.

249. Shard, G. A. *et al.* (2015) Matrix Effect in Organic Secondary Ion Mass Spectrometry. *International Journal of Mass Spectrometry*, 377, 599-609.

250. Wagner, M. S., Castner, D.G. (2001). Characterization of Adsorbed Protein Films by Time-of-Flight Secondary Ion Mass Spectrometry with Principal Component Analysis. *Langmuir*, 17(15), 4649-4660.

251. Hook, A. *et al.* (2013) Discovery of Novel Materials with Broad Resistance to Bacterial Attachment Using Combinatorial Polymer Microarrays. *Advanced Materials*, 14;25(18), 2542-2547.

252. Jagani, S., Chelikani, R., Kim D. S. (2009) Effects of Phenol and Natural Phenolic Compounds on Biofilm Formation by Pseudomonas aerugoniosa. *Biofouling*, 25(4), 321-324.

253. Smith, K., Hunter, I. S. (2008) Efficacy of Common Hospital Biocides with Biofilms of Multi-Drug Resistance. *Journal of Medical* Microbiology, 57(Pt 8), 966-973.

254. Neu, T. R., Lawrence, J. R. (1997) Development and Structure of Microbial Biofilms in River Water Studied by Confocal Laser Scanning Microscopy. *Microbiology Ecology*, 24(1), 11-25.

255. Stewart, P. S., Franklin, M. J. (2008) Physiological Heterogeneity in Biofilms. *Nature Reviews Microbiology*, 6(3), 199-210.

256. Conrad, J. C. *et al.* (2011) Flagella and Pili-Mediated Near-Surface Single-Cell Motility Mechanisms in *P. aeruginosa*. *Biophysical Journal*, 100(7), 1608-1616.

257. Jin, F. *et al.* (2011) Bacteria use Type-IV Pili to Slingshot on Surfaces. *Proceedings of the National Academy of Sciences of the United States of America*, 108(31), 12617-12622.

258. Vater, S. M. *et al.* (2014) Swimming Behaviour of *Pseudomonas aeruginosa* Studied by Holographic 3D Tracking. *Public Library of Science ONE*, 9(1), e87765.

259. Maleschlijski, S. e*t al.* (2012) Three Dimensional Tracking of Exploratory Behaviour of Barnacle Cyprids Using Stereoscopy. *Biointerphases*, 7(1-4), 50.

260. Lecuyer, S. *et al.* (2011) Shear Stress Increases the Residence Time of Adhesion of *Pseudomonas aeruginosa. Biophysical Journal*, 100(2), 341-350.

261. Arpa-Sancet, M. P., Christophis, C., Rosenhahn, A. (2012) Microfluidic Assay to Quantify the Adhesion of Marine Bacteria. *Biointerphases*, 7, 26.

262. Alles, M., Rosenhahn, A. (2015) Microfluidic Detachment Assay to Probe the Adhesion Strength of Diatoms. *Biofouling*, 31(5), 469-480.

263. Christophis, C. *et al.* (2011) Shear Stress Regulates Adhesion and Rolling of CD44+ and Hematopoietic Progenitor Cells on Hyaluronan. *Biophysical Journal*, 101(3), 585-593.

264. Deen, W. M. (1998) Analysis of Transport Phenomena. *Oxford University Press, New York.*

265. Zhang, R. *et al.* (2014) Bacteria Slingshot More on Soft Surfaces. *Nature Communications*, 5, 5541.

266. Lovewell, R. R. *et al.* (2011) Step-Wise Loss of Bacterial Flagellar Torsion Confers Progressive Phagocytic Evasion. *Public Library of Science Pathogens*, 7(9), e1002253.

267. Halldorsson, S., Lucimi, E., Gómez-Sjöberg R., & Fleming, R. M. (2015) Advantages and Challenges of Microfluidic Cell Culture in Polydimethylsiloxane Devices. *Biosensors & Bioelectronics,* 63, 218-231.

268. Berntsson. K. M. *et al.* (2000) Analysis of Behavioural Rejection of Micro-textured Surfaces and Implications for recruitment by the Barnacle *Balanus improvises*. *Journal of Experimental Marine Biology and Ecology*, 251(1), 59-83.

269. Pelletier, E., Bonnet, C., Lemarchand, K. (2009) Biofouling Growth in Cold Estuarine Waters and Evaluation of Some Chitosan and Copper Anti-Fouling Paints. *International Journal of Molecular Sciences*, 10(7), 3209-3223.

270. Trees, C.C., *et al.* (2000) Fluorimetric Chlorophyll α: Sampling Laboratory Methods and Data Analysis Protocols. *NASA Technological Memo*; NASA: Washington, DC.

271. Artham, T., Doble, M. (2009) Fouling and Degradation of Polycarbonate in Seawater: Field and Lab Studies. *Journal of Polymers and the Environment*, 17(3), 170-180.

272. Brydon, H. L. *et al.* (1998) Protein Adsorption to Hydrocephalus Shunt Catheters: CSF Protein Adsorption. *Journal of Neurology, Neurosurgery & Psychiatry*, 64(5), 643-647.

273. Hirsh, S. L. (2013) The Vroman Effect: Competitive Protein Exchange with Dynamic Multilayer Protein Aggregates. *Colloids and Surfaces B: Biointerfaces*, 103, 395-404.

274. Chapman, J., Regan, F. (2012) Nanofunctionalized Superhydrophobic Antifouling Coatings for Environmental Sensor Applications-Advancing Deployment with Answers from Nature. *Advanced Engineering Materials*, 14(4), B175-B184.

275. Peterson, G. L. (1977) A Simplification of the Protein Assay Method of Lowry *et al.* which is More Generally Applicable. *Analytical Biochemistry*, 83(2), 346-356.

276. Dubois, M. *et al.* (1956) Colorimetric Method for Determination of Sugars and Related Substances. *Analytical Chemistry*, 28(3), 350-356.

277. Chapman, J. *et al*. (2014) Bioinspired Prosthetic Macroalgae: Examples from Nature for Antifouling Applications. *International Biodeterioration & Biodegradation,* 86(A), 6-13.

278. Stein, J. *et al.* (2003) Silicone Foul Release Coatings: Effect of the Interaction of Oil and Coating Functionalities on the Magnitude of Macrofouling Attachment Strengths. *Biofouling*, 19(1), 71-82.
279. Swain, G. *et al*. (2000) Biofouling and Barnacle Adhesion Data for Fouling-release Coatings Subjected to Static Immersion at Seven Marine Sites. *Biofouling*, 16(2-4), 331-344.
280. Bressy, C., Briand, J-F., Compere, C., & Rehel, K. (2014) Efficacy Testing of Biocides and Biocidal Coatings. In: Dobretsov, S., Thomason, J. C., & Williams, D. N. *Biofouling Methods*. New Jersey: Wiley & Sons, 332-345.
281. ASTM Standard D3623 − 78a. (2004) Standard Test Method for Testing Antifouling Panels in Shallow Submergence. ASTM International, West Conshohocken, PA.
282. D6990 – 05 (2011) Standard Practice for Evaluating Biofouling Resistance and Physical Performance of Marine Coating Systems. ASTM International, West Conshohocken, PA.
283. Heydt, M. *et al.* (2007) Digital In-Line Holography as a Three-Dimensional Tool to Study Motile Marine Organisms During Their Exploration of Surfaces. *The Journal of Adhesion*, 83(5), 417-430.
284. Chen, L., Hook, D. J., Valint Jr, P. L., & Gardella Jr, J. A. (2008) X-Ray Photoelectron Spectroscopy Studies of Water-Induced Surface Reorganization of Amphiphilic poly(2-hydroxyethyl methacrylate-g-dimethylsiloxane) Copolymers Using Cryogenic Sample Handling Techniques. *Journal of Vacuum Technology*, 26(4), 616-623.

Chapter 9

Appendixes

9.1. Appendix 1: Scanning Electron Microscopy

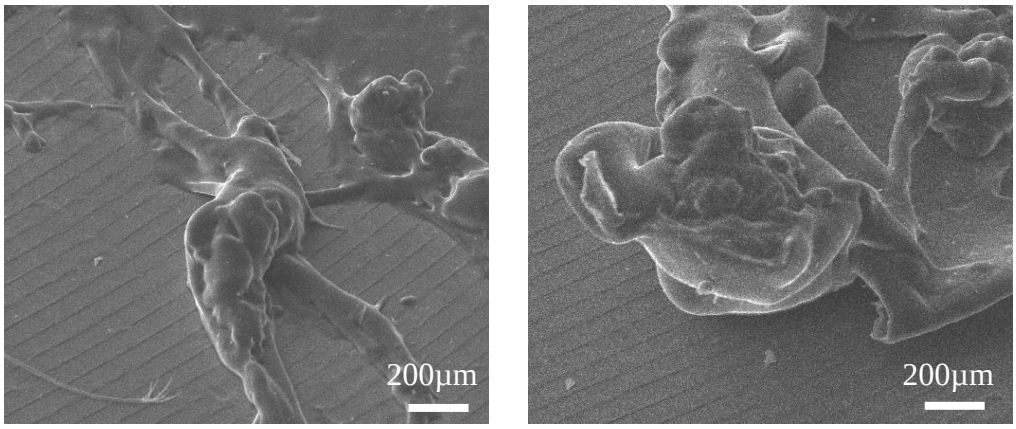

Figure 9.1. SEM images of examples of non-standard drying defects in the coating cross-linked using TnBT. These demonstrate that the catalyst concentration must be low enough to ensure drying does not occur too quickly**.**

9.2. Appendix 2: Atomic Force Microscopy

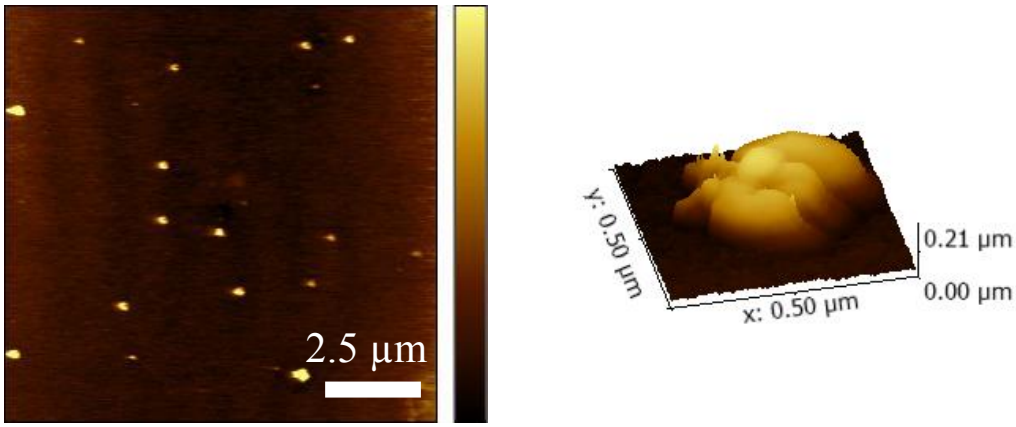

Figure 9.2. (*Left*) 10 micron image displaying aggregates across the surface of a coating cross linked using 900c. (*Right*) 500nm higher magnification 3D image of an example of these defects. The image shows these features are of an amorphous shape and are roughly 200nm tall.

9.3. Appendix 3: Water Contact Angle

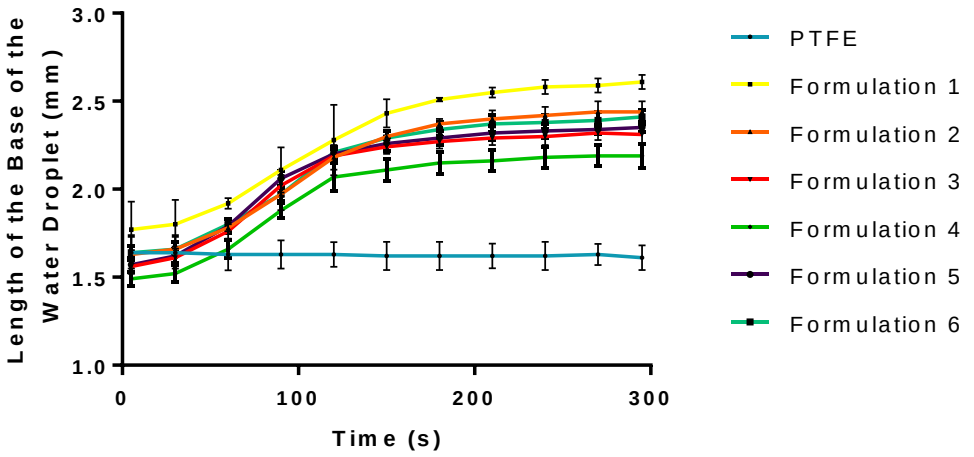

Figure 9.3. Graph demonstrating the length of the base of the water droplet used to determine the contact angle over a period of five minutes. Due to the increase of wettability of the coating there is an increase in the length of this droplet across the surface.

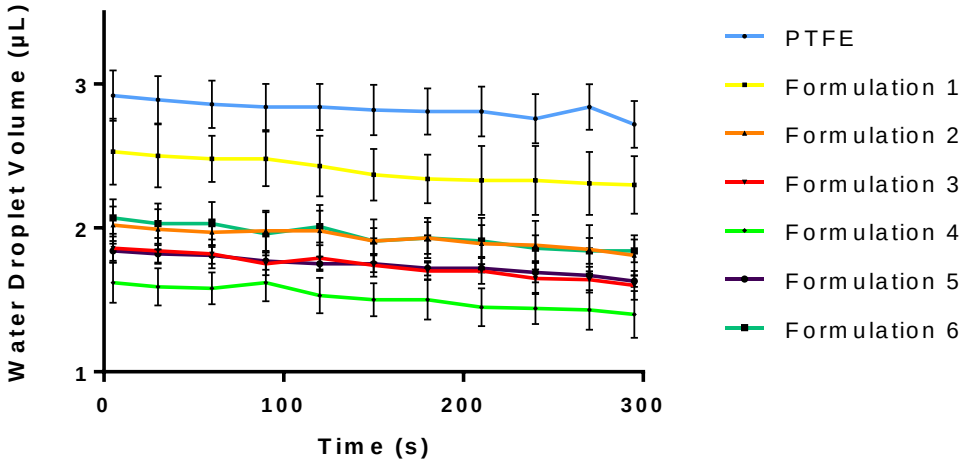

Figure 9.4. Graph depicting the volume of the water droplet used to determine the contact angle of the surface over five minutes. Shows a minor decrease in volume over the duration due to evaporation but unlikely to be so significant as to be affecting the measured contact angle.

9.4. Appendix 4: Optical Microscopy

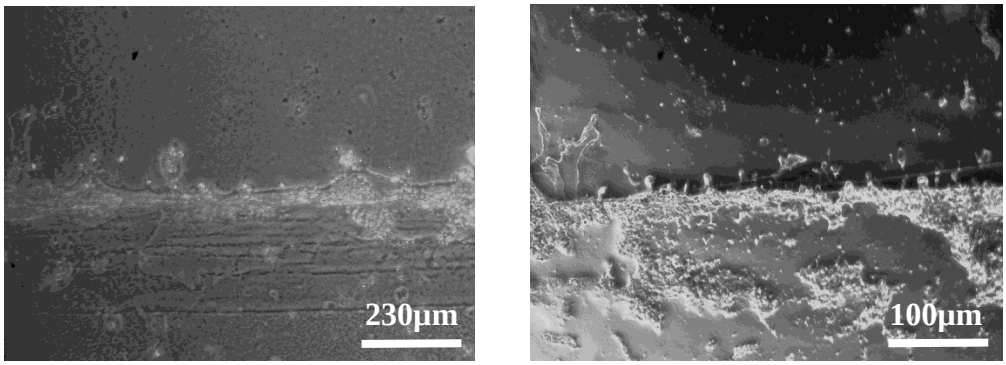

Figure 9.5. Phase contrast images of coating formulation 2 after 3 months in Pembrokeshire sea water. Both images are taken at the interface where the upper point of the water meets the coating. (Left) 4x magnification shows a distinct change in surface features after immersion. These features are a combination of salts and short and long chain proteins and potentially bacteria. (Right) 20x magnification image which more distinctly displays the difference in the coating after it has been immersed in sea water with clear aggregations and features seen in the lower part of the image.

9.5. Appendix 5: Time-of-Flight Mass Spectrometry

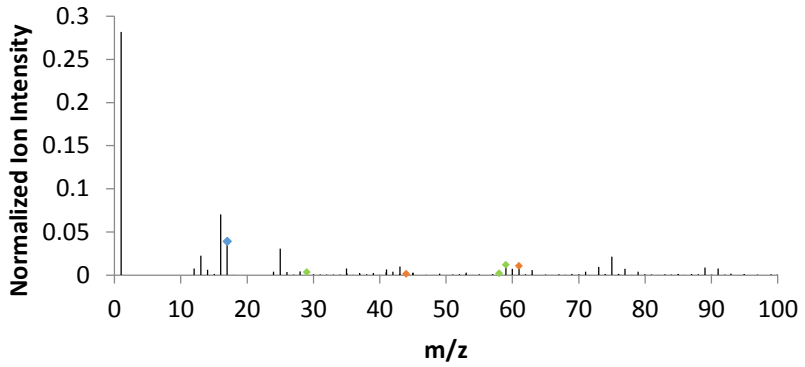

Figure 9.6. Negative polarity surface spectrum of coating formulation 2. Intense hydrogen ion peak presence due to hydration. PDMS and PEG peaks are more equal in intensity due to chemical reorientation of the surface.

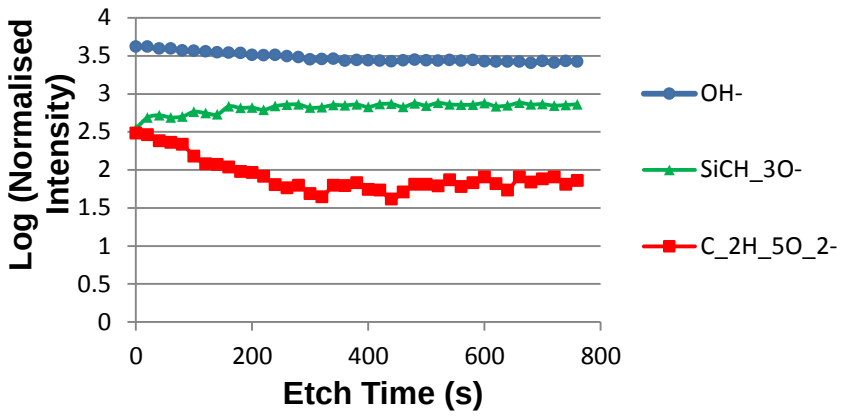

Figure 9.7. Negative polarity depth profile of formulation 2. Equal intensity of PDMS and PEG ions at the surface. $SiCH_3O^-$ increases in intensity through the bulk as representative water and PEG ions decrease before levelling at around 300s etch time.

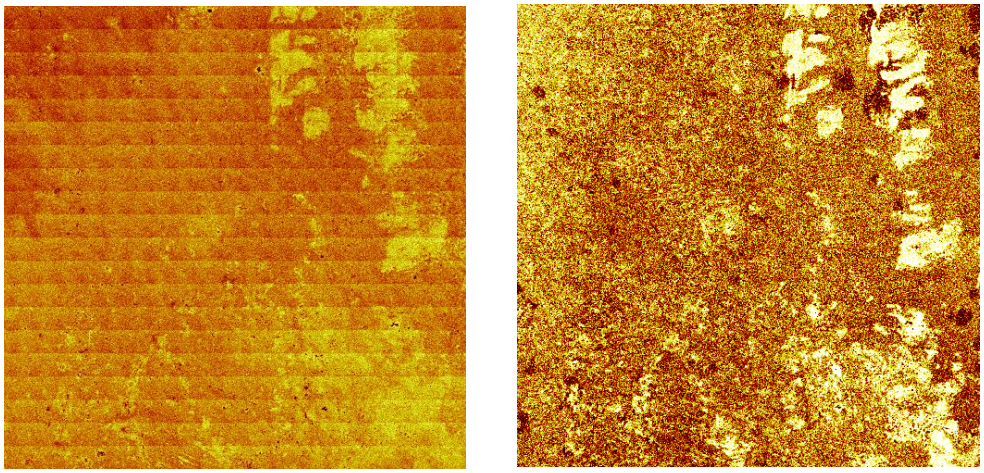

Figure 9.8. (*Left*) 10 x 10mm ToF-SIMS combined ion image of a glass slide which was rinsed but left naturally to dry. There are clear patches on the left hand side demonstrating salt deposits. (*Right*) 10 x 10mm ToF-SIMS Na^+ ion image of the same surface. High intensity features on the right hand side line up with those in the total ion image. This demonstrates that salt ions are the major contributor to these regions.

9.6. Appendix 6: Confocal Microscopy

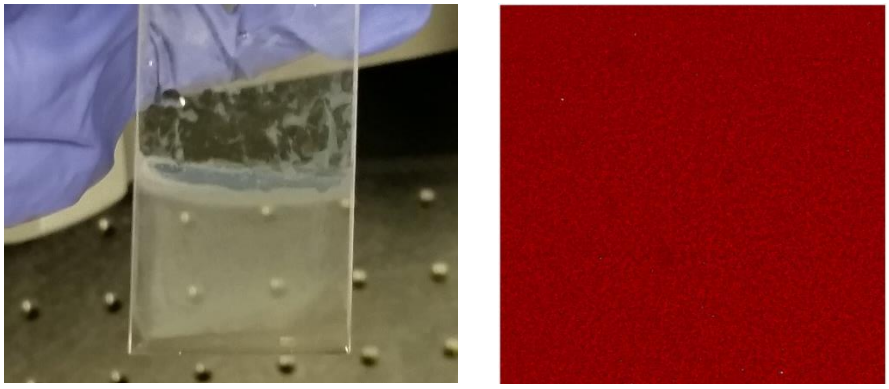

Figure 9.9. (*Left*) Picture of a glass slide after being subjected to PA01 bacterial solution for 72 hours. Shows accumulation of bacteria at the point of the meniscus. Demonstrative of all the samples which were deposited onto slides. All confocal images were taken below the mark. (*Right*) Confocal microscopy image of a 560 x 560µm region from the slide at the meniscus line. Demonstrates a total saturation of bacteria at this region. This was the same for all samples on glass slides.

9.6. Appendix 7: Protein and Carbohydrate Calibration Curves

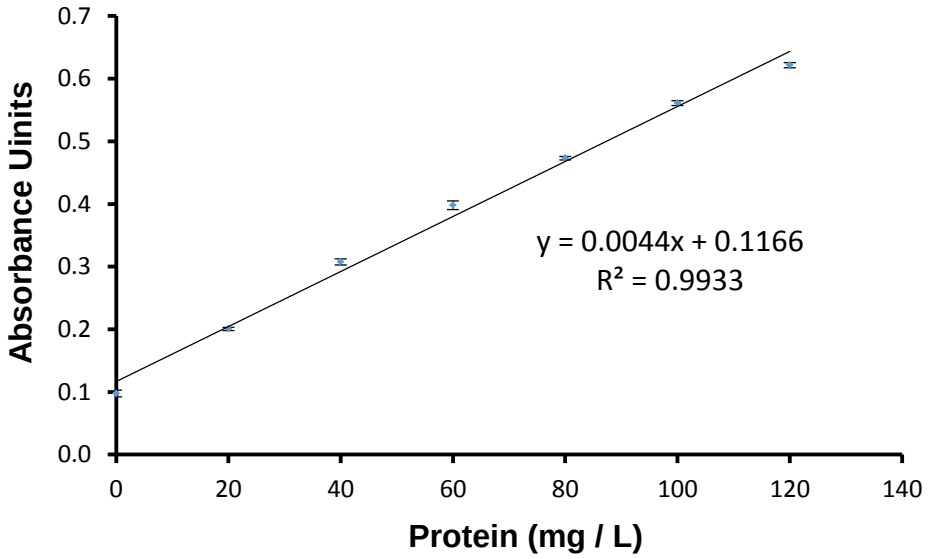

Figure 9.10. Calibration curve for protein adhesion assay.

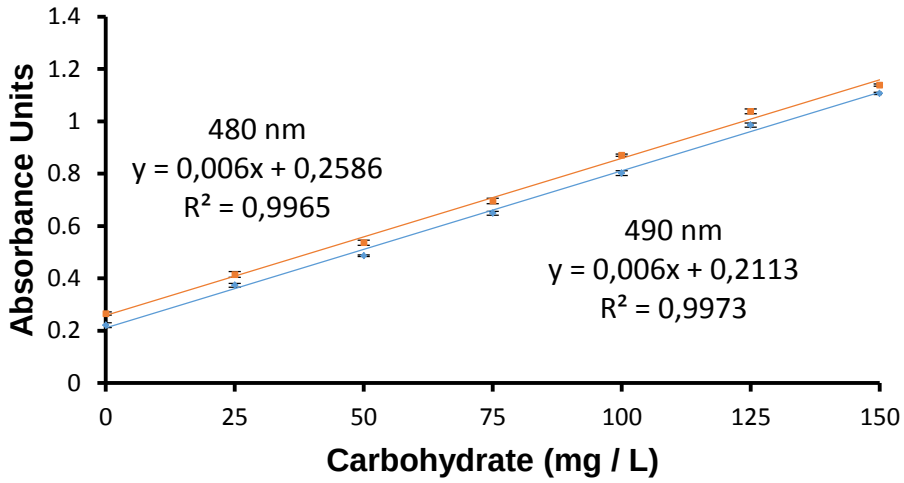

Figure 9.11. Calibration curve for carbohydrate adhesion assay.